

Study of Peristaltic Transport of Multiphase Fluids



By


Nouman Ijaz

41-FBAS/PHDMA/F-13

**Department of Mathematics and Statistics
Faculty of Basic and Applied Sciences
International Islamic University, Islamabad
Pakistan**

2017




Accession No TH:1896-11/21

PhD
532.051
NOS

Flow-fluid mechanics.

Multiphase flow

Non-Newtonian fluid

Study of Peristaltic Transport of Multiphase Fluids



By
Nouman Ijaz

Supervised by
Dr. Ahmad Zeeshan

**Department of Mathematics and Statistics
Faculty of Basic and Applied Sciences
International Islamic University, Islamabad
Pakistan
2017**

Study of Peristaltic Transport of Multiphase Fluids

By

Nouman Ijaz

A Thesis

Submitted in the Partial Fulfillment of the

Requirements for the Degree of

DOCTOR OF PHILOSOPHY

IN

MATHEMATICS

Supervised by

Dr. Ahmad Zeeshan

Department of Mathematics and Statistics

Faculty of Basic and Applied Sciences

International Islamic University, Islamabad

Pakistan

2017

Author's Declaration

I, **Nouman Ijaz** Reg. No. **41-FBAS/PHDMA/F13** hereby state that my Ph.D. thesis titled: **Study of Peristaltic Transport of Multiphase Fluids** is my own work and has not been submitted previously by my for taking any degree from this university, **International Islamic University, Sector H-10, Islamabad, Pakistan** or anywhere else in the country/world.

At any time if my statement is found to be incorrect even after my Graduate the university has the right to withdraw my Ph.D. degree.



Name of Student: (*Nouman Ijaz*)
Reg. No. **41-FBAS/PHDMA/F13**
Dated: **19/12/2017**

Plagiarism Undertaking

I solemnly declare that research work presented in the thesis titled: **Study of Peristaltic Transport of Multiphase Fluids** is solely my research work with no significant contribution from any other person. Small contribution/help wherever taken has been duly acknowledged and that complete thesis has been written by me.

I understand the zero tolerance policy of the HEC and University, **International Islamic University, Sector H-10, Islamabad, Pakistan** towards plagiarism. Therefore, I as an Author of the above titled thesis declare that no portion of my thesis has been plagiarized and any material used as reference is properly referred/cited.

I undertake that if I am found guilty of any formal plagiarism in the above titled thesis even after award of Ph.D. degree, the university reserves the rights to withdraw/revoke my Ph.D. degree and that HEC and the University has the right to publish my name on the HEC/University Website on which names of students are placed who submitted plagiarized thesis.

Student/Author Signature: _____


Name: (Nouman Ijaz)

Certificate of Approval

This is to certify that the research work presented in this thesis, entitled: **Study of Peristaltic Transport of Multiphase Fluids** was conducted by **Mr. Nouman Ijaz**, Reg. No. **41-FBAS/PHDMA/F13** under the supervision of **Dr. Ahmed Zeeshan** no part of this thesis has been submitted anywhere else for any other degree. This thesis is submitted to the **Department of Mathematics & Statistics, FBAS, IIU, Islamabad** in partial fulfillment of the requirements for the degree of **Doctor of Philosophy in Mathematics, Department of Mathematics & Statistics, Faculty of Basic & Applied Science, International Islamic University, Sector H-10, Islamabad, Pakistan.**

Student Name: Nouman Ijaz

Signatures: 

Examination Committee:

a) **External Examiner 1:**
Name/Designation/Office Address

Prof. Dr. Tasawar Hayat
Department of Mathematics,
QAU, Islamabad.

Signatures: 

b) **External Examiner 2:**
Name/Designation/Office Address)

Prof. Dr. Saleem Asghar
Department of Mathematics,
COMSATS. IIT. Islamabad.

Signatures: Saleem Asghar

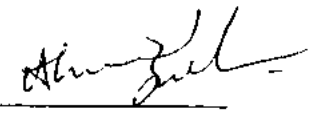
c) **Internal Examiner:**
Name/Designation/Office Address)

Dr. Tariq Javed,
Associate professor

Signatures: 

Supervisor Name:

Dr. Ahmed Zeeshan

Signatures: 

Name of Dean/HOD

Prof. Dr. Muhammad Sajid, T.I

Signatures: 

DEDICATION

This thesis is dedicated to:

My beloved *Father, Mother, Brother, Sisters, Wife, Daughters* and
my honorable teacher

MUHAMMAD NAEEM KHALID.

Acknowledgements

First and foremost, I am thankful to Almighty Allah, who created us, taught us everything we know, provided us with the health, knowledge and Intelligence to explore this world. I am reminded of the verse *قَبِيْأَيَّ ءَالَآءِ رَبِّكُمَا تُكَذِّبَتَانِ* when I reflect on the graces that Allah has showered upon us. I thank the lord Almighty with whose will and help I have achieved this very important goal in my life. I send Salutations upon the last Messenger of Allah, Hazrat Muhammad (*SALLAH O ALI WALI WASALAM*) who is forever a torch of guidance, a source of knowledge and blessings for the entire creation. His teachings show us to ponder and to keep our mind open.

I express my profound gratitude to my respectable supervisor **Dr. Ahmad Zeeshan**, who helped me through my PHD with his cooperative guidance. His many valuable comments and suggestions put me on the straight path when I was led astray.

I would like to pay thank to all my friends specially *M.M. Bhatti, Imtiaz Ahmed, Ch.Sagheer Saeed, Wasif Raza Khan, Touqeer Anjum, Danish Niaz, Abid Hussain, Nasir Shahzad Lohdi, Arshad Siddiqui, Arshad Riaz, Shafiq-ur-Rehman, Aqib Majeed, Muhammad Mudassar Maskeen, Nasir Shahzad, Farooq Hussain, Bilal Aryan, Shahid Nadeem* and all of those who directly or indirectly have helped influencing this work.

I am indebted to my father **Ijaz Ahmed Malik** for his continuous persuasion, encouragement, moral and academic support his kind, eminent, affectionate nature and encouraging behavior enlightened me to work in this field and to achieve what is a distant dream for most. I cannot express enough love and appreciation to my mother who showered her everlasting love, care and support throughout her life trying to make me easier. I also express my gratitude to my beloved brother **Imran Ejaz**, my sweet sisters who are always there-fore encouragement and support my wife and my sweet daughters *Abeeha* and *Minahil*, even in the gloomiest time of life they were always encouraging me and showered their everlasting love, care and support throughout my life. Their humble prayers have always been a source of success for me and whose sustained hope led myself to where, I am today.

Nouman Ijaz

Preface

The multiphase flow usually has complex flow pattern, which brings many difficulties in measuring. In recent years, researchers have been doing numerous research in two and three-phase flow, and many new measurement methods and theoretical models are proposed. Also, lots of instruments and tremendous milestones have been achieved in these research works. Peristaltic flow are physiological flows existing naturally in animal body and many industrial devices in medical science and fluid transport are inspired by these flow phenomenon. Due to such importance, it grabs the attention of different researchers. Peristaltic is continuous process of compressing and relaxation of smooth muscles in a living body in digestive system and blood flow etc. Moreover, this phenomenon is keenly observed in a motion of cilia, a motion of urine from the kidney to the bladder and a motion of Chyme in the gastrointestinal tract work on the principle of peristalsis. Peristalsis has also shown a significant role in biomechanical and mechanical instruments such as, finger pumps, heart-lung machine and roller pumps. Such kinds of applications opened a new way for physicians and scientist to manipulate their equipment for analyzing better results. The motivation of this thesis is to study multiphase fluid in variety of geometries in which flow is induced by peristaltic movement. To observe the various aspect of these flows formulated for flow situation and mathematical equations are non-dimensionalized. The exact and numerical solution are obtained and plotted.

This thesis consist of nine chapters. Chapter one provides literature review and some preliminary discussion about peristalsis, its phenomenon and constitutive relation for Newtonian and non-Newtonian fluids. Also, a section is delighted for Multiphase fluids.

In chapter two, the peristaltic movement of particle-liquid suspension with slip effect and endoscopy through a non-uniform annulus is discussed. The equations for the flow problem of

particle fluid suspension comprises of continuity and momentum equation for both particle and fluid phase. The particles are consider light and suspended uniform in base fluid. The fluid in this case assumed to be Jeffrey fluid. **The Results are published in Journal of Molecular Liquids, 218 (2016): 240-245.**

Chapter three, studies the peristaltic transport of MHD dusty three-dimensional Biorheological Non-Newtonian fluid in a rectangular duct is investigated. The base fluid is taken as Casson and Ree-Eyring fluids separately. The governing flow problem is based on law of conservation of mass and momentum. Numerical integration has been used to determine the pumping characteristics. Trapping phenomena are also discussed and sketched by drawing streamlines. **This study is published in Chinese Journal of Physics, (2017).**

Chapter four to nine focus on the flow of multiphase fluid through different channels.

Chapter four, illustrates the flow of suspension of small particles in non-Newtonian Ree-Eyring base fluid in a channel. The effects of transverse magnetic field is also observed. The problem is modeled using law of conservation of mass, momentum and energy. Under the assumption of creeping flow and long wave length the governing equations of solid and liquid phases are reduced. The exact solutions have been obtained by solving the formulated model. **This article is published online in Thermal Science (accepted June 8, 2017).**

Chapter five, explores the simultaneous effects of heat transfer and inclined magnetic field on peristaltically induced motion of particles through a uniform inclined channel. Asymmetric channel waves are accounted. The problem formulated contains continuity equation, momentum equation and energy equation. **This analysis is published in the Brazilian Society of Mechanical Sciences and Engineering (2017): 1-9.**

Chapter six, investigates the heat and mass transfer with the transverse magnetic field on peristaltic flow of particle-fluid suspension through a planar channel with peristaltic wave has

been examined. The flow is observed under the influence of electroosmosis and chemical reaction. The present flow problem is modelled using equation of continuity, momentum, heat and diffusion equations, lubrication theory approximation in combination with long wavelength and creeping flow assumptions is used to simplify the problem. Moreover, the electric effects are simplified using Debye linearization. Analytical solutions are obtained for the resulting differential equations. **The problem is published in the Journal of Molecular Liquids 230 (2017): 237-246.**

Chapter seven, devoted to discuss the peristaltic flow of two phase fluid in a rotating channel with wall properties in the presence of magnetic field. Law of conservation of mass and momentum is used to formulate the problem. The governing equations subject to the conditions of low Reynolds number and long wavelength and solved analytically. **This analysis is submitted in Chinese Journal of Physics.**

Chapter eight, addresses the influence of particulate-fluid suspension on asymmetric peristaltic motion through a curved channel with heat and mass transfer. To examine the two-phase peristaltic motion between small muscles for different biological fluids this study is useful. The mathematical formulation of problem includes continuity, momentum, energy and mass transfer equations. Exact solutions are presented for velocity, temperature and concentration distributions with help of MATHEMATICA. **The Results are submitted in Journal of Bionics for possible publications.**

Chapter nine, established the theoretical and analytical analysis of a unidirectional laminar bubbly two-phase flow in a symmetric channel with flexible wall. The two-phase model uses water as base fluid and hydrogen bubble suspended in it. Rayleigh-Plesset equation in term of volume fraction is used to model void produce due to presence of hydrogen. The flow is driven by symmetric peristaltic movement of the wall. A uniform magnetic field in the transverse

direction to peristaltic motion is applied. Homotopy perturbation Method (HPM) is utilized to get the series solution, after simplifying the differential governing equations under the influence of long wave length and low Reynolds number. The volume of the void and radius of the bubble is analyzed graphically. **The problem is accepted at International journal of hydrogen energy.**

NOMENCLATURE

b_1	Radius of endoscope	\tilde{b}	Width of the channel
b_0	Radius of outer tube	\tilde{c}	Wave velocity
U, V, W	Velocity components	\tilde{a}	Wave amplitude
u, v, w	Dimensionless velocity components	b	Duct height
X, Y, Z	Coordinate axis	d	Duct width
x, y, z	Dimensionless coordinate axis	B_0	Magnetic field strength
t	Time	h	Non-Dimensional wave
V_0	Boundary velocity	Re	Reynolds number
C	Concentration of particle	c_p	Effective heat capacity
Q	Volume flow rate	Sc	Schmidt number
P	Fluid pressure	Pr	Prandtl number
S	Stress tensor	Ec	Eckert number
U_{HS}	electrical field parameter	T_m	Mean temperature
S'	Drag force	M_1	Suspension parameter
J	Current density	W_0	Weber number
$d_1 + d_2$	Curve channel width	B	Magnetic field
k_p	Thermal conductivity		
\bar{K}_c	Chemical reaction parameter		
D_m	Mass diffusivity		
R^*	Radius of curvature		
Sr	Soret number		
k	Curvature parameter		

T_m	Mean temperature
k_T	Thermal diffusivity
m	electro-osmotic parameter
U_{HS}	electrical field parameter
k^*	Behaviour index
M	Hartmann number
Fr	Froude number
S^*	Surface tension
\tilde{K}	spring stiffness
R	Upstream bubble radius
\tilde{m}	mass per unit area
\tilde{B}	flexural rigidity
\tilde{D}	coefficient of the viscous damping membrane
\tilde{T}	elastic tension in the membrane

Greek symbols

λ_1	Jeffery parameter	λ_2	Retardation time
μ_s	viscosity of the fluid	τ'	Cavitation number
Θ	Angle of inclination	γ^*	Rotation parameter
κ	Slope of outer tube	γ	Chemical reaction parameter
$\phi_{f,p}$	Concentration	η	Bubble population per unit liquid volume
β	Slip parameter	ρ_{G_0}	Density of the gas
ρ_L	Density of the liquid	Φ	Dimensionless concentration
Θ^*	Phase difference	α, θ	Inclined angles
σ	Electric conductivity of the fluid	ρ	Fluid density
θ	Dimensionless temperature	ν	Volume of the void
α'	Ree-Eyring parameter	ϕ	Amplitude ratio
ζ	Casson parameter	Ψ	Stream function
λ	Wavelength	μ_0	Constant fluid viscosity

Subscripts

p	particulate phase
f	fluid phase

Contents

Preliminarily	4
1.1 Literature review	4
1.1.1 Peristaltic movement and pumping.....	4
1.1.2 Multiphase flow	6
1.2 Peristaltic flow.....	9
1.2.1 Pumping phenomena	9
1.2.2 Trapping phenomena.....	9
1.3 Multiphase fluid	10
1.3.1 Solid liquid flow	10
1.3.2 Gas liquid flow.....	10
1.4 Non-Newtonian fluid models.....	10
1.4.1 Jeffrey fluid.....	11
1.4.2 Casson fluid	11
1.4.3 Ree-Eyring fluid.....	12
Flow of particulate fluid through an annulus with endoscopy and slip effects.....	13
2.1 Geometry of the problem	13
2.2 Mathematical formulation.....	14
2.3 Solution of the problem	16
2.4 Illustrations and discussion	17
2.5 Conclusion	22
Flow of particulate non-Newtonian fluid through a duct with magnetic field	23
3.1 Geometry of the problem	23
3.2 Mathematical formulation.....	24
3.3 Solution of the problem	25
3.4 Illustrations and discussion	27

3.5 Conclusion	33
Flow of particulate fluid through a channel with heat transfer	35
4.1 Geometry of the problem	35
4.2 Mathematical formulation.....	36
4.3 Solution of the problem	37
4.4 Illustrations and discussion	39
4.5 Conclusion	43
Flow of particulate fluid in a channel with inclined magnetic field and heat transfer... ..	44
5.1 Geometry of the problem	44
5.2 Mathematical formulation.....	45
5.3 Solution of the problem	46
5.4 Illustrations and discussion	48
5.5 Conclusion	55
Flow of particulate fluid in a channel with electric double layer effects along with heat and mass transfer.....	56
6.1 Geometry of the problem	56
6.2 Mathematical formulation.....	57
6.3 Solution of the problem	59
6.4 Illustrations and discussion	64
6.5 Conclusion	72
Flow of particulate fluid in a rotating channel with wall properties and magnetic field	74
7.1 Geometry of the problem	74
7.2 Mathematical formulation.....	75
7.3 Solution of the problem	77
7.4 Illustrations and discussion	78
7.5 Concluding remarks.....	84
Flow of particulate fluid in a curved configuration with heat and mass transfer	85

8.1 Geometry of the problem.....	85
8.2 Mathematical formulation.....	86
8.3 Solution of the problem	88
8.4 Illustrations and discussion	91
8.5 Conclusion	97
Flow of bubbly fluid in water with magnetic field.....	99
9.1 Geometry of the problem.....	99
9.2 Mathematical formulation.....	100
9.3 Solution of the problem	102
9.4 Illustrations and discussion	103
9.5 Concluding remarks.....	107
References	109

Chapter 1

Preliminarily

The chapter is divided into two parts. In first part, a comprehensive review of the literature present on the topic is presented. Whereas, in second part basic introduction of all the component of the topic and related material is presented.

1.1 Literature review

1.1.1 Peristaltic movement and pumping

Peristaltic transport is an important biotic mechanism which is produced through the contraction and extension of a stretchable boundary e.g. human digestive tract peristaltic flow with different reactions are also found in the physiological study and due to such importance, it grabs the attention of different researchers. Peristaltic is the continuous process of compressing and clasping of smooth muscles in a living body such as digestive system or digestive tract. Moreover, this phenomenon is keenly observed in a motion of cilia, a motion of vasomotion of small blood vessels and Chyme in the gastrointestinal tract i.e. Venues, capillaries and arterioles exertion on the principle of peristalsis. Moreover, peristalsis has also shown a significant role in physiological sciences by formulation biomechanical and mechanical instruments such finger pumps, heat-lung machine and roller pumps that work on the mechanism of peristalsis. Such kinds of applications opened a new way for physicians and mathematicians to manipulate their equipment for analyzing better results. For instance, Mekheimer [1] considered the peristaltic motion of blood under the effects of a magnetic field through a channel. He obtained the exact solution for both Uniform and non-uniform channel. Haroun [2] considered the nonlinear peristaltic movement of further grade fluid through an inclined asymmetric channel. Hayat et al. [3] also investigated the nonlinear peristaltic motion

through a planar channel. He also measured the effects of magnetic with non-Newtonian fluid model. The peristaltic movement of Carreau nanofluid through an asymmetric channel numerically simulated by Akbar et al. [4]. Khan et al. [5] examined analytically the peristaltic transport of non-Newtonian Jeffrey fluid. He also considered the fluid with variable viscosity through a porous asymmetric channel. Maraj et al. [6] presented Williamson fluid model mathematically the peristaltic motion through a curved channel. The particles in a fluid flow is a branch of multiphase and multicomponent flows. The flow of multiphase and multicomponent mixtures involves an enormous range of applications and flow conditions. Such kinds of study are important in various physical problems such as sedimentation, atmospheric fallout, powder technology, aerosol filtration, fluidization [7], ash and lunar flows etc. Moreover, with the help of continuum theory of mixtures, it is easy to examine various diverse subjects [8], disposition of particles in a respiratory tract and swimming of microorganisms [9]. Furthermore, particle characterization is also an important part in a production of particle, processing, handling, and manufacturing and in various industrial applications [10]. Particle characterization is a necessary and initial step that helps in a process including solid particles. Such kind of characterization not only involves the intrinsic static parameters i.e. density, morphology, shape and size etc. also their dynamic attitude associated with fluid flow i.e. terminal velocity and drag coefficient. Yao et al. [11] studied the multiphase flow through the permeable porous channel with wall effect. He considered the Beavers and Joseph slip boundary conditions and using perturbation method to obtained the series solution. He observed that slip boundary condition significantly enhance the velocity of the fluid a decrement of slip parameter tends to rise the magnitude of velocity through a channel. Furthermore, he also observed that increase in volume fraction density, fluid phase axial velocity rises. Mekheimer [12] considered peristaltic motion of Newtonian solid-liquid suspension through an annulus. Kamel et al. [13] investigated the slip effects on the peristaltic

flow through a planar channel of particle-fluid suspension and using perturbation method to calculate the series solution. Bhatti and Zeeshan [14] studied analytically the heat transfer on non-Newtonian Jeffrey fluid having variable viscosity through a planar channel. Bhatti et al. [15] investigated very recently the effects of Magnetic field on a metachronal wave of solid-liquid suspension induced by cilia motion. Javed et al. [16] analyzed the velocity and thermal slip effects on the peristaltic motion of a non-Newtonian Walters-B fluid model. Bhatti et al. [17] studied the three- dimensional peristaltic motion of a Jeffrey fluid model in the existence of magnetic field with compliant walls. He attained exact solution for the velocity function, and found that influence of magnetic field significantly which opposes fluid velocity. Ellahi et al. [18] also determined the three-dimensional peristaltic flow with compliant walls. Ellahi et al. [19] discuss the peristaltic movement of a non-Newtonian Carreau fluid through a rectangular duct having porous walls. They applied homotopy perturbation method to obtain series solution. Kothandapani et al. [20] discussed the peristaltic flow through an asymmetric permeable channel in the presence of a magnetic field. Some more pertinent studies can be found from the Refs. [21–30] and several works cited therein.

1.1.2 Multiphase flow

Multiphase flow means a flow which contains more than one fluid phase or a mixture of gases, liquids and/or solid particles flowing simultaneously in the same enclosure. Multiphase flow and heat transport has gained out class attention of scientists and engineers due to their application in chemical and petrochemical engineering, power generation, mineral engineering, food production, nuclear reactor technology, chemical process, aerospace and automotive industries in complex field, material engineering, information technology, micro and nano-technologies, microelectronics engineering, space technology, biomedicine and life sciences. The equation for the motion of multiphase fluids are proposed by the Navier-stokes equations. The major difficulty as said by researcher that modeling of turbulence flow and its impact on

momentum and mass transport. The governing equations for multiphase flows with correct formulation is still the area to debate. Multiphase flow further classify into the following sub categories. Magnetohydrodynamics incompressible flow towards a porous media through dilating and squeezing permeable walls. Zaidi and Mohyud-din [31] addressed the heat transfer and Magnetohydrodynamics impact on two dimensional wall nanofluid wall jet flow using passive control flow model. Khan et al. [32] simultaneously examined the thermo-diffusion and diffusion thermo impact on second grade fluid towards two inclined plane walls. The influence of Magnetohydrodynamics on peristaltic flow have significant importance in arterial flow, hyperthermia, magneto therapy, and compressor etc. Furthermore, Magnetohydrodynamics is very helpful to analyses various kinds of electrically conducting fluids such as electrolytes, plasmas, and liquid metals. Some more pertinent on the said topic can be found from references [34-40]. The model of non-Newtonian is most useful to understand various physical problems. Also, the investigation on the flow of combinations is useful to understand different physical problems in various area of technical significance. Fetecau et al. [41] observed that the Newtonian and non-Newtonian solutions contributions. Maxwell and Newtonian fluids having the similar solutions, execution the equal motion, are gained as limiting cases of our common results. Fetecau et al. [42] presented the unsteady flow of an incompressible generalized Oldroyd-B fluid induced by a constantly accelerating plate between two side walls perpendicular to the plate has been considered by Fourier sine and Laplace transforms. Fetecau et al. [43] analyzed the simpler exact solutions corresponding to the second problem of Stokes for Newtonian fluids are established by the Laplace transform method. Khalique et al. [44] examined the stationary solution of the nonlinear Schrödinger's equation in non-Kerr law media. The types of nonlinearity that are measured are Kerr law, power law, parabolic law and the dual-power law. Khalique et al. [45] illustrated the solution of the three dimensional Zakharov–Kuznetsov modified equal width equation. The Lie group

analysis is used to carry out the integration of this equation. Khalique et al. [46] discussed the integrals of the various cases, which admit Noether point symmetries, and reduction to quadratures for these cases are obtained. Gazanfer et al. [47] devoted the symmetries of Stratonovich dynamical system is given. Determining systems of symmetries for Stratonovich systems have been obtained, and their relation has been discussed. Gazanfer et al. [48] discussed the exact and quasi symmetries of Stratonovich dynamical control systems. Determining systems of symmetries for these systems have been obtained and their relation is discussed. Nazar et al. [49] devoted the micro polar fluid for steady two-dimensional stagnation point flow of an incompressible over a stretching sheet. Nazar et al. [50] investigates the incompressible viscous fluid in two-dimensional unsteady stagnation point flow over a flat sheet. Nazar et al. [51] reported the induced unsteady flow due to a stretching surface in a rotating fluid, where the unsteadiness is caused by the suddenly stretched surface. Ishak et al. [52] derived the solution to the unsteady mixed convection boundary layer flow and heat transfer problem due to a stretching vertical surface. Ishak et al. [53] published the heat transfer over a stretching surface with uniform or variable heat flux in micro polar fluids. Ishak et al. [54] investigated the unsteady laminar boundary layer flow over a continuously stretching permeable surface. Turkyilmazoglu et al. [55] reported that the viscous compressible boundary layer flow in three-dimensional direct resonance instability in rotating disk. Turkyilmazoglu et al. [56] examined the exact solutions to the steady Navier-Stokes equations for the incompressible Newtonian viscous fluid flow motion due to a disk rotating with constant angular speed. Vieru et al. [57] studied the unsteady flow of the fractional Maxwell and a viscoelastic fluid with model between two side walls perpendicular to a plate. Exact solutions for the velocity field are established by means of the Fourier and Laplace transforms. Nazar et al. [58] derived the exact solutions for second grade fluids using Laplace transform method.

1.2 Peristaltic flow

The mechanism of peristaltic movement fluids in channel or ducts under progressive wave of range expansion or contraction propagates of a distensible tube having fluid. It investigates, mixing and propulsive movement the fluids against pressure rise. Peristaltic movements in physiology is an intestine leverage of smooth muscle contraction. It contains the transport food through the digestive tract, urine from the kidney to the bladder, chyme motion in the gastrointestinal tracts, vasomotion of small blood vessels, movement of ovum in fallopian tube, bile from the gall-bladder into the duodenum, swallowing food through the esophagus, movement of Spermatozoa and the human reproductive tract, etc. Peristaltic flows is quite valuable in physiology and industry because enormous of applications and in mathematics and complex geometries and results of nonlinear equations. Also, in industry, this mechanism is widely used in roller and finger pumps and in blood filtration devices. Latham et al. [61] is the first introduced the mechanism of peristaltic pumping fluid motion.

1.2.1 Pumping phenomena

The peristaltic transport has been enticing devotion of biomechanical engineers. The importance of mechanical and physiological situations. In physiological applications it is motivating to deliberate the peristaltic movement of a bio fluid with suction and injection. Peristaltic pumping are distributed into four regions i.e. ($Q > 0, \Delta p > 0$), retrograde pumping ($Q < 0, \Delta p > 0$), augmented pumping region ($Q > 0, \Delta p < 0$) and free pumping region.

1.2.2 Trapping phenomena

Another most engrossing phenomena of this study is trapping viewed of streamlines. Physically, this mechanism is very favorable for the preparation of thrombus in blood and the propagation of food bolus i.e. in a gastrointestinal tract. The stream function (Ψ) satisfying

equation of continuity is described as

$$v_{f,p} = -\frac{\partial \hat{\Psi}_{f,p}}{\partial x}, u_{f,p} = \frac{\partial \hat{\Psi}_{f,p}}{\partial y}. \quad (1.1)$$

1.3 Multiphase fluid

Almost all the said studies have invariably measured single-phase systems. Most of the technological applications having combustion, lunar ash flow, micro-propulsion, vapor deposition and aerosol filtration, multi-phase suspensions ascend. Systems are mentioned to as “dusty” fluids and the solid particle flow in these fluid-particulate suspensions has a significant influence on thermo fluid characteristics. Thermal conductivity of occupied fluids in industrial strategies may be enhanced via the cautious introduction of small solid particles in the fluids to form slurries.

1.3.1 Solid liquid flow

The flow of this nature represent the liquid continuum transport a dispersed solid particles suspended under the impact of drag and pressure forces of liquid act on particles, also arises in crystallization systems, in hydro-cyclones and in china clay extraction.

1.3.2 Gas liquid flow

It is surely most imperative type of two-phase flow in which gas-liquid are enforced to move together and have many practical applications in pipeline systems for carrying gas-oil mixtures, sewerage treatment plants, submerged combustion systems, evaporators, boilers, condensers, refrigeration plants and air-conditioning, cryogenic plants. Additional combination of gas and liquid schemes are also useful in weathercasting and other natural wonders.

1.4 Non-Newtonian fluid models

Non-Newtonian fluids deviate from Newton's law of viscosity, and exhibit variable viscosity. The behavior of non-Newtonian fluids is generally represented by a rheological model, or

correlation of shear stress and shear rate. Examples of substances which exhibit non-Newtonian behavior include solutions and melts of high molecular weight polymers, suspensions of solids in liquids, emulsions, and materials possessing both viscous and elastic properties.

1.4.1 Jeffrey fluid

The Jeffrey fluid with Cauchy stress tensor is described as [59]

$$S = \frac{\mu}{1 + \lambda} (\dot{\gamma} + \lambda_2 \ddot{\gamma}). \quad (1.2)$$

Here μ is the viscosity, λ_1 is the retardation time, $\dot{\gamma}$ is the velocity gradient, λ_2 is the delay time and $\ddot{\gamma}$ is the second derivative with respect to time.

1.4.2 Casson fluid

Stress tensor for Casson fluid which is presented as [60]

$$S = -p\delta_y + 2\mu(J_2)V_y, \quad (1.3)$$

$$\mu(J_2) = \left[(\eta^2 J_2)^{1/4} + 2^{-1/2} \tau_y^{1/2} \right]^2 J_2^{-1/2} = \left[\eta^{1/2} + 2^{-1/2} \tau_y^{1/2} J_2^{-1/4} \right]^2 = \left[\alpha + \beta J_2^{-1/4} \right]^2 = \mu \quad (1.4)$$

$$\alpha = \eta^{1/2} : \beta = 2^{-1/2} \tau_y^{1/2}, \quad (1.5)$$

$$V_y = \frac{1}{2} \left(\frac{\partial u_i}{\partial x_i} + \frac{\partial u_j}{\partial x_j} \right) \quad (1.6)$$

Where η is the Casson coefficient of viscosity, and τ_y is the yield stress.

$$J_2 = \frac{1}{2} V_y V_y = \frac{1}{2} (V_{11}^2 + V_{22}^2 + 2V_{12}^2), \quad (1.7)$$

$$V_{11} = \frac{\partial u}{\partial x}, \quad (1.8)$$

$$V_{22} = \frac{\partial v}{\partial y}, \quad (1.9)$$

$$V_{12} = V_{21} = \frac{1}{2} \left(\frac{\partial u}{\partial y} + \frac{\partial v}{\partial x} \right), \quad (1.10)$$

1.4.3 Ree-Eyring fluid

Stress tensor for Ree-Eyring fluid model is presented as

$$S = \mu_s \frac{\partial V_i}{\partial x_j} + \frac{1}{B} \text{Sinh}^{-1} \left(\frac{1}{C} \frac{\partial V_i}{\partial x_j} \right), \quad (1.11)$$

Since $\sinh^{-1} x \approx x$ of $|x| \leq 1$, then

$$\tau_{ij} = \mu_s \frac{\partial V_i}{\partial x_j} + \frac{1}{B} \left(\frac{1}{C} \frac{\partial V_i}{\partial x_j} \right), \quad (1.12)$$

Chapter 2

Flow of particulate fluid through an annulus with endoscopy and slip effects

This chapter peristaltic movement of particle-liquid suspension discussed analytically with slip effect and endoscopy through a non-uniform annulus. The equations of the flow problem of particle fluid suspension comprise of continuity and momentum equations for both fluid and particulate phase. The particles are considered light and suspended uniformly in base fluid. The fluid, in this case, assumed to be Non-Newtonian (Jeffrey) fluid. Partial differential equation is non-dimensions and reduced with the long wavelength and low Reynolds number assumptions. The pressure rise is obtained by using numerical integration. The results are displayed graphically.

2.1 Geometry of the problem

In this problem, a non-uniform annulus whose radius increase linearly is considered. An Endoscope of radius b_1 is placed such that both annulus and Endoscope is co-centric as shown in Fig. (2.1).

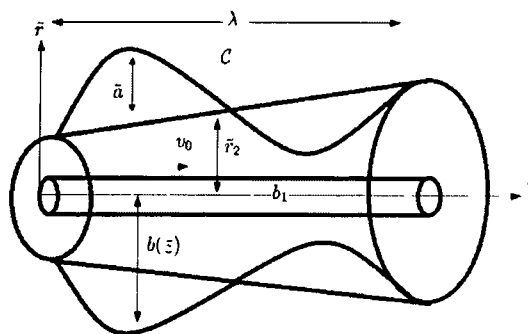


Figure 2.1: Geometry of the flow problem

A sinusoidal wave travels on the walls of external tube. The equation describes boundaries are given mathematically as,

$$\tilde{r}_1 = b_1, \quad \tilde{r}_2 = b(Z) + \tilde{a} \sin \frac{2\pi}{\lambda} (Z - ct), \quad (2.1)$$

Where,

$$b(Z) = b_0 + \kappa Z. \quad (2.2)$$

Radius of outer tube at any point Z is $b(Z)$, where Z is axial distance, at inlet radius of the outer tube is b_0 . Velocity of wave propagation, wavelength, wave amplitude, radius of the endoscope and time is represented by c, λ, a, b_1, t . $\kappa (\ll 1)$ is a constant.

2.2 Mathematical formulation

Consider incompressible, laminar flow of particles in Jeffery fluid. It is assumed that the particles are small and uniformly distributed and transmitted in base fluid. The equation of fluid phase and particle phase in an annulus is given by

$$(1-C) \frac{\partial V_f}{\partial R} + (1-C) \frac{\partial U_f}{\partial Z} + (1-C) \frac{V_f}{R} = 0, \quad (2.3)$$

$$(1-C) \frac{\partial P}{\partial R} = (1-C) \mu_s \left(\frac{1}{R} \frac{\partial}{\partial R} R \mathbf{S}_{rr} + \frac{\partial}{\partial Z} \mathbf{S}_{rz} - \frac{\mathbf{S}_{\theta\theta}}{R} \right) + CS'(V_p - V_f), \quad (2.4)$$

$$(1-C) \frac{\partial P}{\partial Z} = (1-C) \mu_s \left(\frac{1}{R} \frac{\partial}{\partial R} R \mathbf{S}_{rz} + \frac{\partial}{\partial Z} \mathbf{S}_{zz} \right) + CS'(U_p - U_f), \quad (2.5)$$

$$C \frac{\partial V_p}{\partial R} + C \frac{\partial U_p}{\partial Z} + C \frac{V_p}{R} = 0, \quad (2.6)$$

$$C \frac{\partial P}{\partial R} = CS'(V_f - V_p), \quad (2.7)$$

$$C \frac{\partial P}{\partial Z} = CS'(U_f - U_p). \quad (2.8)$$

Here $S_{rr}, S_{rz}, S_{\theta\theta}$ are components of stress tensor S for Jeffrey fluid defined in Eq. (1.2), C is the concentration of particles, U and V velocity components, P is pressure, suspension viscosity and drag force is given by μ_s and S' . The equations are transforming from the laboratory frame to wave frame using.

$$V_{p,f} = \tilde{V}_{p,f}, U_{p,f} + c = \tilde{U}_{p,f}, R - ct = \tilde{R}, Z = \tilde{Z}, P = \tilde{P}. \quad (2.9)$$

Non-dimensional parameter are describe as

$$\begin{aligned} r = \frac{\tilde{R}}{b_0}, z = \frac{\tilde{Z}}{\lambda}, u_{f,p} = \frac{\tilde{U}_{f,p}}{c}, v_{f,p} = \frac{\lambda \tilde{V}_{f,p}}{b_0 c}, t = \frac{\tilde{t} c}{\lambda}, p = \frac{b_0^2}{\lambda \mu_0 c} \tilde{P}, \bar{\mu} = \frac{\tilde{\mu}_s}{\mu_0}, v_0 = \frac{V_0}{c}, \\ r_1 = \epsilon = \frac{\tilde{r}_1}{b_0}, r_2 = \frac{\tilde{r}_2}{b_0}, \varphi = \frac{\tilde{a}}{b_0}, \delta = \frac{b_0}{\lambda}, M_1 = \frac{S b_0^2}{\mu_0}, \beta = \frac{\tilde{\beta}}{\lambda}. \end{aligned} \quad (2.10)$$

Using transformation Eq. (2.9) and non-dimensional parameters defined in Eq. (2.10) the governing equations are simplified as,

$$\frac{\partial p}{\partial r} = 0, \quad (2.11)$$

$$\frac{\partial p}{\partial z} = \frac{\bar{\mu}}{r(1 + \lambda_1)} \frac{\partial}{\partial r} \left(r \frac{\partial u_f}{\partial r} \right) + \frac{M_1}{(1 - C)} (u_p - u_f), \quad (2.12)$$

$$\frac{\partial p}{\partial z} = M_1 (u_f - u_p). \quad (2.13)$$

Boundary conditions in dimensionless form are

$$u_f(r) = v_0, \quad r = r_1 = \epsilon, \quad (2.14)$$

$$u_f(r) = -\beta \frac{\partial u_f}{\partial r}, \quad r = r_2 = 1 + \frac{\lambda \kappa z}{b_0} + \varphi \sin 2\pi(x - t). \quad (2.15)$$

Where β is slip parameter and ϵ is radius of endoscope.

2.3 Solution of the problem

Fluid and particulate velocities are obtained in terms of $\frac{dp}{dz}$, given as

$$u_f = \frac{(1 + \lambda_1)(r^2 - r_1^2)}{4\bar{\mu}(1-C)} \frac{dp}{dz} + \frac{r_2((1 + \lambda_1) \frac{dp}{dz} (r_1^2 - r_2^2 - 2r_2\beta) - 4(1-C)v_0\bar{\mu}) \ln(r)}{4(1-C)\bar{\mu} \left(\beta - r_2 \ln \left(\frac{r_1}{r_2} \right) \right)} \quad (2.16)$$

$$+ \frac{r_2((1 + \lambda_1) \frac{dp}{dz} (r_1^2 - r_2^2 - 2r_2\beta) - 4(1-C)v_0\bar{\mu}) \ln(r_1)}{4(1-C)\bar{\mu} \left(\beta - r_2 \ln \left(\frac{r_1}{r_2} \right) \right)} + v_0,$$

$$u_p = \frac{(1 + \lambda_1)(r^2 - r_1^2)}{4\bar{\mu}(1-C)} \frac{dp}{dz} + \frac{r_2((1 + \lambda_1) \frac{dp}{dz} (r_1^2 - r_2^2 - 2r_2\beta) - 4(1-C)v_0\bar{\mu}) \ln(r)}{4(1-C)\bar{\mu} \left(\beta - r_2 \ln \left(\frac{r_1}{r_2} \right) \right)} \quad (2.17)$$

$$+ \frac{r_2((1 + \lambda_1) \frac{dp}{dz} (r_1^2 - r_2^2 - 2r_2\beta) - 4(1-C)v_0\bar{\mu}) \ln(r_1)}{4(1-C)\bar{\mu} \left(\beta - r_2 \ln \left(\frac{r_1}{r_2} \right) \right)} - \frac{1}{M_1} \frac{dp}{dz} + v_0.$$

The volume flow rate is described as

$$Q(z, t) = Q_f(z, t) + Q_p(z, t), \quad (2.18)$$

Where

$$Q_f = 2\pi(1-C) \int_{r_1}^{r_2} r u_f dr, \quad (2.19)$$

$$Q_p = 2\pi C \int_{r_1}^{r_2} r u_p dr. \quad (2.20)$$

Integrating and replaced in Eq. (2.18)

$$\begin{aligned}
Q(z, t) = & \frac{\pi}{8(1-C)M_1\bar{\mu} \left(\beta - r_2 \ln \left(\frac{r_1}{r_2} \right) \right)} \left((r_1^2 - r_2^2) \left((1 + \lambda_1) M_1 \frac{dp}{dz} (r_1^2 (r_2 + \beta)) \right. \right. \\
& - r_2^2 (r_2 + 3\beta) \left. \left. + 4(-1 + C) \left(-C \frac{dp}{dz} \beta + M_1 v_0 (r_2 + 2\beta) \right) \bar{\mu} \right) + r_2 (-1 + \lambda_1) M_1 \right. \\
& \left. \frac{dp}{dz} (r_1^4 - r_2^3 (r_2 + 4\beta)) + 4(-1 + C) \left(C \frac{dp}{dz} (r_1^2 - r_2^2) - 2M_1 r_1^2 v_0 \right) \bar{\mu} \right) \ln \left(\frac{r_1}{r_2} \right). \tag{2.21}
\end{aligned}$$

Simplifying Eq. (2.20) to get pressure gradient in terms of Q

$$\begin{aligned}
\frac{dp}{dz} = & -4(-1 + C)M_1\bar{\mu}(-2Q\beta - \pi(r_1^2 - r_2^2)v_0(r_2 + 2\beta) + 2r_2(Q + \pi r_1^2 v_0)) \\
& \ln \left(\frac{r_1}{r_2} \right) / \left(\pi((r_1^2 - r_2^2)(-1 + \lambda_1)M_1(r_1^2(r_2 + \beta) - r_2^2(r_2 + 3\beta)) + 4(-1 + C)C\bar{\mu}) \right. \\
& \left. + r_2(-1 + \lambda_1)M_1(r_1^4 - r_2^3(r_2 + 4\beta)) + 4(-1 + C)C(r_1^2 - r_2^2)\bar{\mu} \right) \ln \left(\frac{r_1}{r_2} \right). \tag{2.22}
\end{aligned}$$

Pressure rise and the wall friction force for the outer tube and inner tube is calculated numerically using MATHEMATICA

$$\Delta p_L(t) = \int_0^{L/\lambda} \frac{dp}{dz} dz, \tag{2.23}$$

$$\Delta F_L^o(t) = \int_0^{L/\lambda} r_2^2 \left(-\frac{dp}{dz} \right) dz, \tag{2.24}$$

$$\Delta F_L'(t) = \int_0^{L/\lambda} r_1^2 \left(-\frac{dp}{dz} \right) dz. \tag{2.25}$$

2.4 Illustrations and discussion

To examine the impacts of several parameters i.e., slip parameters (β), Jeffrey fluid parameter (λ_1) and particle volume fraction (C) on velocity profile, pressure rise and wall frictions graphs are plotted from Fig. (2.2) - (2.12).

Fig. (2.2) indicates the variations in velocity for fluid for particle volume fraction C and Jeffery parameter λ_1 . It is observed that the velocity decreases with an increase of both C and λ_1 .

Physically, when the particle volume fraction rises, it tends to enhance the viscosity of the fluid which reduces the velocity profile. Also at $\lambda_1 = 0$ fluid reduces to Newtonian fluid case. It is clear that Newtonian fluids flows faster than Jeffery fluid. Fig. (2.3) is plotted to see the influence of velocity of endoscope v_0 and slip parameter β for non-Newtonian case. On the wall no slip condition is observed in the figure. Whereas, also increasing value of β shows an increase in velocity on the channel wall. In stationary endoscope case maximum fluid velocity was achieve for $\beta = 0$ and a slightly greater value of velocity is observed on the wall when $v_0 = 0$. it is observed that in Fig. (2.4) particle velocity is greater in Non-Newtonian fluid then in Newtonian fluid also velocity of particle decrease with in values of C because of the collision increases and particles accumulates and started to get heavy. It can be seen that in Fig. (2.5) particle velocity is increasing with the increasing values of slip parameter and endoscope velocity. Fig. (2.6) - (2.8) are sketched to see the variation on pressure rise. From Fig. (2.6) it is examine that with the slip parameter increase pressure rise tends to decreased. It is observed that the pressure rise decreases for the different values endoscope velocity and particle volume fraction. The effects of Newtonian and non-Newtonian fluid is discussed in Fig. (2.7) and (2.8) in which the value of Jeffrey parameter is not zero then the pressure rise is minimized. On the other hand Jeffrey parameter is equal to zero fluid become Newtonian then pressure rise increases.

The numerical results of the friction forces for outer tube are examined in Fig. (2.9) and (2.10) for different physical parameters. Fig. (2.9) indicates that friction force increase with the increasing value of slip parameter. It is clear from Fig. (2.10) with the increase of Jeffrey parameter friction force increases.

Fig. (2.11) and (2.12) is plotted for the friction forces on an inner tube. It is observed that the behavior of the inner tube is the similar to the outer tube.

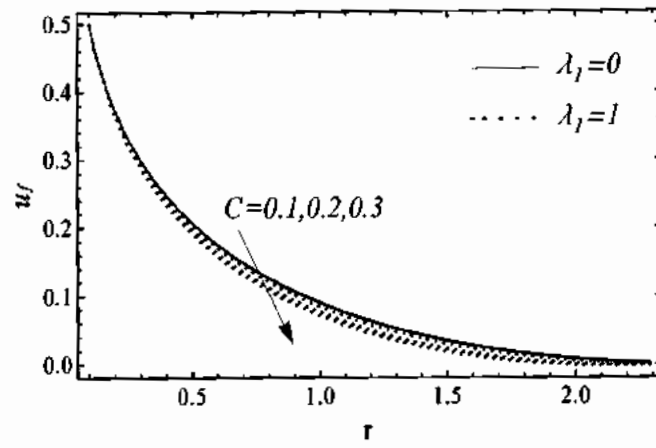


Figure 2.2: Fluid velocity for different values of C and λ_1 .

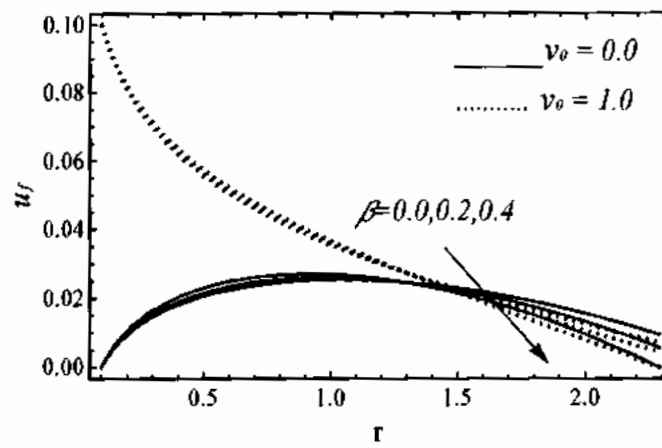


Figure 2.3: Fluid velocity for different values of β and v_0 .

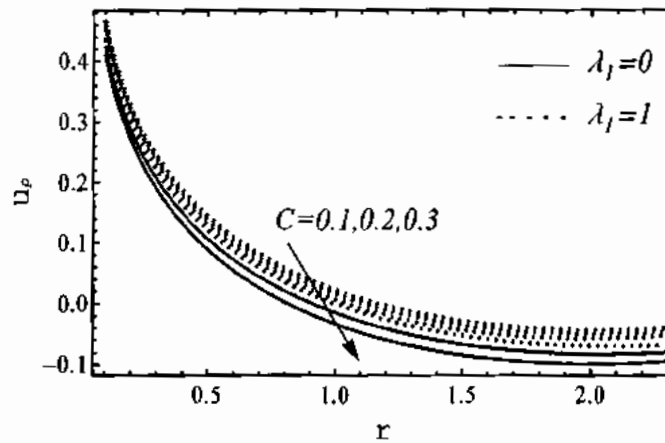


Figure 2.4: Particle velocity for different values of C and λ_1 .

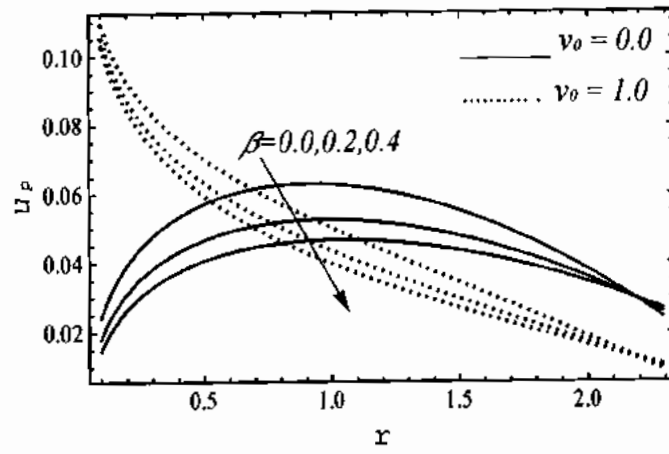


Figure 2.5: Particle velocity for different values of β and v_0 .

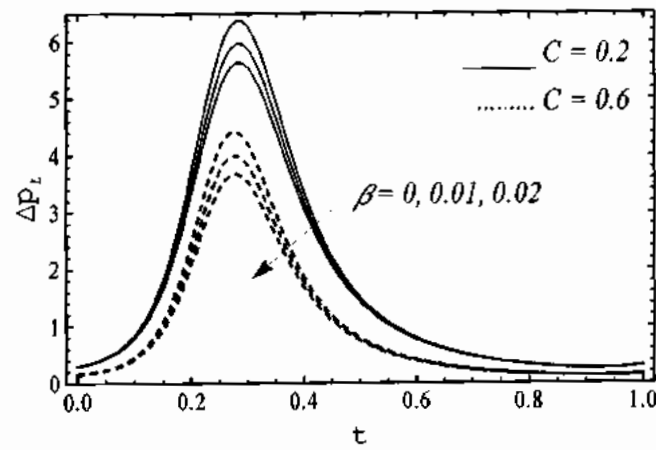


Figure 2.6: Pressure profile for different values of β and C .

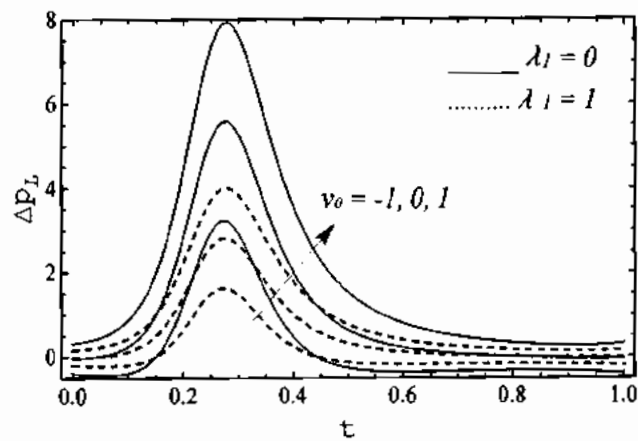


Figure 2.7: Pressure profile for different values of v_0 and λ_1 .

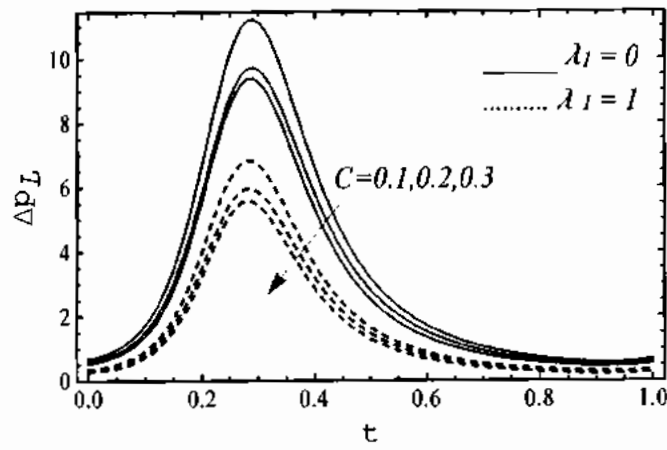


Figure 2.8: Pressure profile for different values of λ_1 and C .

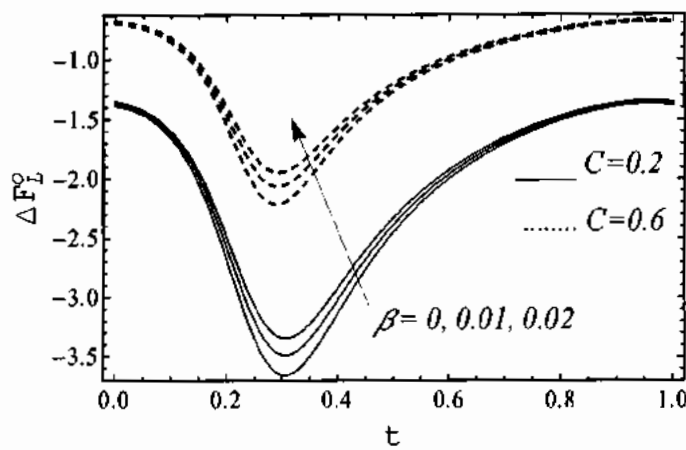


Figure 2.9: Friction forces on outer tube for various of C and β .

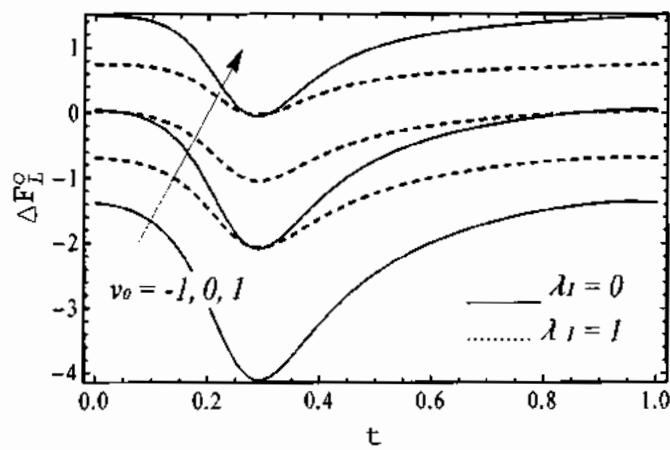


Figure 2.10: Friction forces on outer tube for various values of ν_0 and λ_1 .

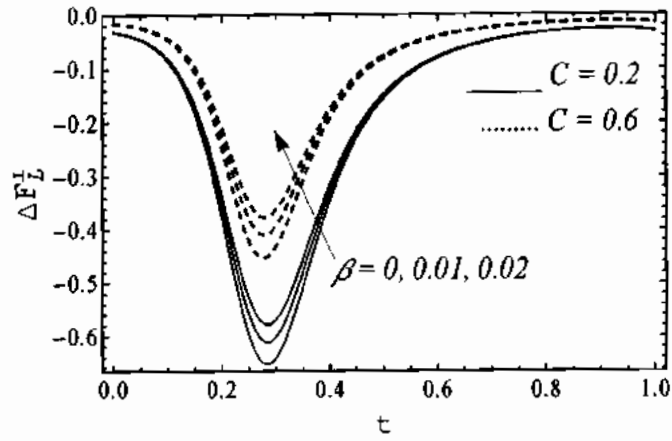


Figure 2.11: Inner tube friction forces for different values of C and β .

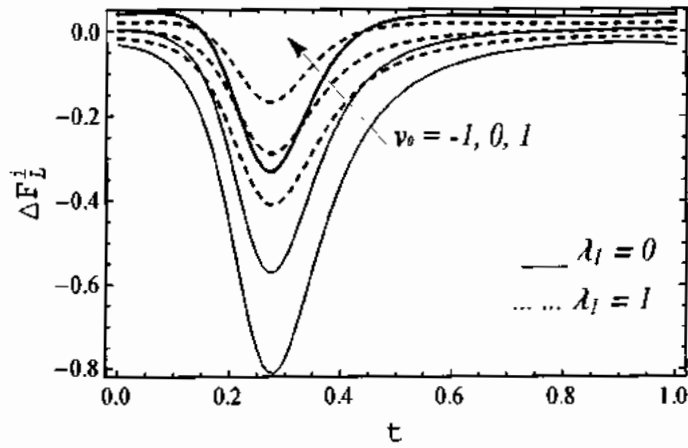


Figure 2.12: Inner tube friction forces for various values of v_0 and λ_1 .

2.5 Conclusion

In this chapter, the effect of endoscope and slip on peristaltic flow of particulate fluid in non-uniform annulus. By the assumption of low Reynolds number and long wavelength obtaining the governing equations for both fluid and particulate phase. Following are some main finding of the study.

- Increase in particle volume fraction shows a decrease in pressure rise and fluid velocity.
- When fluid represents non-Newtonian behavior minimum pressure rise can be achieved.
- Greater value of Jeffery fluid parameter velocity fluid decrease.
- Due to slip effects, friction forces for inner and outer tube also rise.

Chapter 3

Flow of particulate non-Newtonian fluid through a duct with magnetic field

In this chapter, peristaltic transport of MHD dusty three-dimensional Bio rheological Non-Newtonian (Casson and Ree-Eyring) fluid in a rectangular duct is investigated. The governing flow problem is based on law of conservation of mass and momentum. These equations are modelled for fluid-particle phase along with the assumptions of a creeping regime and wave travelling along the wall has long wavelength as compare to amplitude of wave. The exact solution has been obtained from the resulting partial differential equation by means of Eigen function expansion method. Graphical results are discussed against all emerging parameters such as Hartmann number, particle volume fraction, Casson and Ree-Eyring fluid parameter etc. Numerical integration has been used to determine the pumping characteristics. Trapping phenomena are also discussed and sketched by drawing streamlines.

3.1 Geometry of the problem

A rectangular duct is assumed with flexible walls at $Z = \pm H$. the peristaltic wave propagates parallel to X -axis as illustrated in schematic diagram in Fig. (3.1). Wave is travelling with a speed c , an amplitude of \bar{a} units and wave length λ . the dimensions of duct in the absence of wave is $b \times d$.

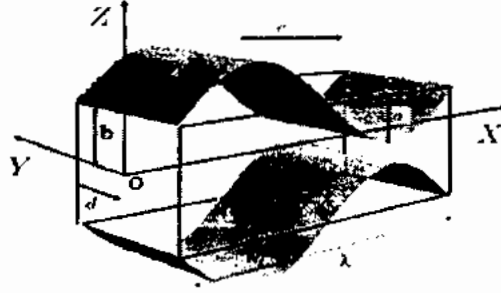


Fig. 3.1: Geometry of the problem

Rectangular coordinate system is assumed with O as origin. The mathematical relation for geometry of the wall is presented as

$$Z = H(X, T) = \pm b \pm a \cos\left[\frac{2\pi}{\lambda}(X - ct)\right], \quad y = \pm d. \quad (3.1)$$

3.2 Mathematical formulation

The flow of solid particles in a two Non-Newtonian i.e. Casson and Ree-Eyring fluid through a duct driven by a symmetric peristaltic wave. The flow is described using continuity and momentum equations for both fluid and particle phases using continuum approach. A transverse magnetic field is applied to the flow. The equations describing the flow are

$$\frac{\partial U_f}{\partial X} + \frac{\partial W_f}{\partial Z} = 0, \quad (3.2)$$

$$(1-C)\rho_f \left(\frac{\partial U_f}{\partial t} + U_f \frac{\partial U_f}{\partial X} + W_f \frac{\partial U_f}{\partial Z} \right) = -(1-C) \frac{\partial P}{\partial X} + (1-C) \left(\frac{\partial}{\partial X} S_{xx} + \frac{\partial}{\partial Y} S_{xy} + \frac{\partial}{\partial Z} S_{xz} \right) + CS'(U_p - U_f) - \sigma B_0^2 U_f, \quad (3.3)$$

$$(1-C)\rho_f \left(\frac{\partial W_f}{\partial t} + U_f \frac{\partial W_f}{\partial X} + W_f \frac{\partial W_f}{\partial Z} \right) = -(1-C) \frac{\partial P}{\partial Z} + (1-C) \left(\frac{\partial}{\partial X} S_{zx} + \frac{\partial}{\partial Y} S_{zy} + \frac{\partial}{\partial Z} S_{zz} \right) + CS'(W_p - W_f), \quad (3.4)$$

$$\frac{\partial U_p}{\partial X} + \frac{\partial W_p}{\partial Z} = 0, \quad (3.5)$$

$$C\rho_p \left(\frac{\partial U_p}{\partial t} + U_p \frac{\partial U_p}{\partial X} + W_p \frac{\partial U_p}{\partial Z} \right) = -C \frac{\partial P}{\partial X} + CS'(U_f - U_p), \quad (3.6)$$

$$C\rho_p \left(\frac{\partial W_p}{\partial t} + U_p \frac{\partial W_p}{\partial X} + W_p \frac{\partial W_p}{\partial Z} \right) = -C \frac{\partial P}{\partial Z} + CS'(W_f - W_p). \quad (3.7)$$

The stress tensor of Casson fluid and Ree-Eyring fluid is describe in Eq. (1.3) and (1.11) respectively. The equations are transform in wave frame using Eq. (3.8).

$$\tilde{X} = X - ct, \tilde{Y} = Y, \tilde{Z} = Z, U_{f,p} = U_{f,p} - c, \tilde{W}_{f,p} = W_{f,p}, P(x,t) = P(X, Z, t). \quad (3.8)$$

Non-dimensional parameter are describe as

$$x = \frac{\tilde{X}}{\lambda}, y = \frac{\tilde{Y}}{d}, w_{f,p} = \frac{\tilde{W}_{f,p}}{c\delta}, h = \frac{\tilde{H}}{a}, \delta = \frac{a}{\lambda}, \beta^* = \frac{a}{d}, Re = \frac{\rho a c \delta}{\mu}, \alpha' = \frac{1}{\mu_s B C}. \quad (3.9)$$

Using non-dimensional parameters defined in Eq. (3.9) and (2.10) and assuming that δ and $Re \rightarrow 0$ the governing equation for Casson fluid becomes

$$\left(1 + \frac{1}{\zeta} \right) \beta^{*2} \frac{\partial^2 u_f}{\partial y^2} + \left(1 + \frac{1}{\zeta} \right) \frac{\partial^2 u_f}{\partial z^2} - M^2 (u_f + 1) = \frac{1}{(1-C)} \frac{dp}{dx}, \quad (3.10)$$

and for Ree-Eyring fluid

$$(1 + \alpha') \left(\beta^{*2} \frac{\partial^2 u}{\partial y^2} + \frac{\partial^2 u}{\partial z^2} \right) - M^2 (u_f + 1) = \frac{1}{(1-C)} \frac{dp}{dx}. \quad (3.11)$$

Equation of motion for particulate phase is

$$\frac{dp}{dx} = M_1 (u_f - u_p), \quad (3.12)$$

along with corresponding dimensionless boundary conditions

$$u_f(\pm 1, z) = -1, \text{ and } u_f(y, \pm h) = -1. \quad (3.13)$$

3.3 Solution of the problem

Using Eigen function expansion method, Non-homogenous partial differential equations are

solved. The exact solution for Casson fluid is represented as

$$u_f = C_1 - \frac{4 \cos(C_4 z) \cosh(y C_2) \operatorname{sech}(C_3) ((1 + C_1) \sin(-C_4))}{(\pi - 2n\pi) \left(h + \frac{\sin(h(1-2n)\pi)}{\pi - 2n\pi} \right)}, \quad (3.14)$$

$$u_p = -(1-C)M_1 \left[C_1 - \frac{4 \cos(C_4 z) \cosh(y C_2) \operatorname{sech}(C_3) ((1 + C_1) \sin(-C_4))}{(\pi - 2n\pi) \left(h + \frac{\sin(h(1-2n)\pi)}{\pi - 2n\pi} \right)} \right], \quad (3.15)$$

and the exact solution for Ree-Eyring fluid case is

$$u_f = C_1 - \frac{4 \cos(C_4 z) \cosh(y C_5) \operatorname{sech}(C_3) ((1 + C_1) \sin(-C_4))}{(\pi - 2n\pi) \left(h + \frac{\sin(h(1-2n)\pi)}{\pi - 2n\pi} \right)}, \quad (3.16)$$

$$u_p = -(1-C)M_1 \left[C_1 - \frac{4 \cos(C_4 z) \cosh(y C_5) \operatorname{sech}(C_3) ((1 + C_1) \sin(-C_4))}{(\pi - 2n\pi) \left(h + \frac{\sin(h(1-2n)\pi)}{\pi - 2n\pi} \right)} \right], \quad (3.17)$$

Where

$$C_1 = \frac{\left(\frac{dp}{dx} - ((-1+C)(1+M^2) + \frac{dp}{dx}) \cosh(C_2 z) \operatorname{sech}(h C_3) \right)}{((-1+C)(1+M^2))},$$

$$C_2 = \frac{\sqrt{1+M^2}}{\sqrt{1+\zeta}},$$

$$C_3 = \sqrt{\frac{M^2 + \frac{1}{4}(-1+2n)^2 \pi^2 \left(1 + \frac{1}{2}(-1+2n)\pi \right)}{\left(1 + \frac{1}{2}(-1+2n)\pi \right) \beta^{**}}},$$

$$C_4 = \frac{1}{2}(2n-1)\pi z,$$

$$C_5 = \frac{\sqrt{1+M^2}}{\sqrt{1+\alpha'}},$$

The relation for flow rate in duct is defined as

$$Q_f = (1-C) \int_0^h \int_0^1 (u_f + 1) dy dz, \quad (3.18)$$

$$Q_p = (C) \int_0^h \int_0^1 u_p dy dz, \quad (3.19)$$

and hence

$$Q = Q_f + Q_p. \quad (3.20)$$

The pressure rise Δp is calculated numerically with the help of following expression

$$\Delta p = \int_0^l \frac{dp}{dx} dx. \quad (3.21)$$

3.4 Illustrations and discussion

The graphical results of emerging parameters involved in the governing flow problem. To determine the impact of these parameters on the flow, computational software “*MATHEMATICA*” used. Particularly, the behaviour of velocity profile for both fluid, and particle phase along peristaltic pumping, and trapping mechanism are sketched. For this purpose Fig. (3.2) - (3.13) have been sketched for the variation of particle volume fraction C , Hartmann number M and fluid parameter Casson ζ and Ree-Eyring α' . Fig. (3.2) and (3.3) indicate the velocity variations of particle volume fraction C for both particle and fluid (Casson and Ree-Eyring) phase. The fluid velocity decreases because particle volume fraction rises then fluid becomes thicker which goes to oppose the flow and as a results velocity of the fluid decreases. Further it is seen that for both fluids particles flow slows down with an increase in particle concentration, whereas, in the middle of flow the velocity of particles increases. Fig. (3.4) and (3.5) are drawn to show the effects of Hartmann number M on flow. Both fluid (Casson and Ree-Eyring) and particles phase, velocity slows down for higher values of

Hartman number M when the magnetic field is applied, an opposite force generated known as Lorentz force which goes to oppose the velocity significantly. Since $M = B_0 \tilde{a} \sqrt{\frac{\sigma}{\mu_s}}$ which shows the influence of hydrodynamic body force and the magnetic body force, therefore it is found that the greater transverse magnetic field creates more Lorentz force M^2 which in results decelerates the flow more significantly. Fig. (3.6) - (3.9) displays the variation of Casson and Ree-Eyring fluid parameter ζ and α' on the velocity of a fluid and particles in respective solutions. The results for Newtonian fluid can be achieved by taking $\zeta \rightarrow \infty$ and $\alpha' \rightarrow 0$. It can be viewed from these figures that fluid parameter does not cause any major impact on particle velocity, however, the fluid velocity increases near the walls of the duct and converse behaviour has been observed in the middle of the duct the behaviour is opposite for Ree-Eyring fluid.

Fig. (3.10) - (3.11) are developed to analyse the pumping characteristics for both fluid Casson and Ree-Eyring under the effect of magnetic field and particle volume fraction. In Fig. (3.10) we can be seen that due to an increment in Hartmann number M tends to boost the pumping rate in retrograde and peristaltic pumping region whereas its behaviour is converse in augmented pumping region. However, it can be observed from Fig. (3.11) pumping rate tends to diminish in peristaltic and retrograde pumping region for particle volume fraction (C) greater values.

One of the most interesting features of peristaltic motion is trapping phenomena, which can be observed by drawing streamlines. The size of the bolus describes the volume of the fluid that is bounded by the closed streamlines. It is clear from Fig. (3.12) and (3.13) that when the Hartmann number M rises the number of bolus remains constant when the magnitude of the trapping bolus rises.

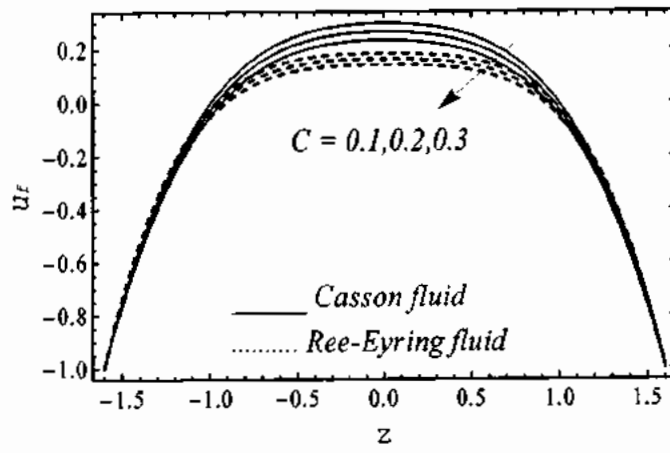


Fig. 3.2: Fluid velocity curves for various values of C .

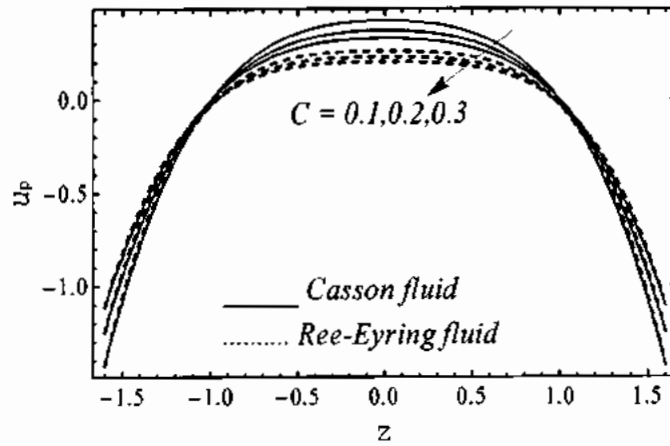


Fig. 3.3: Particulate velocity for various values of C .

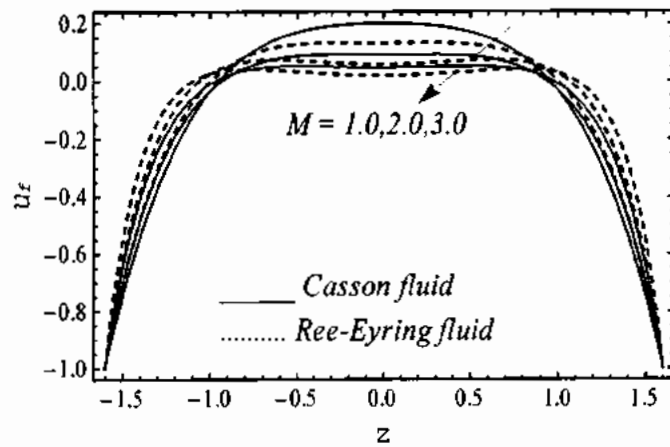


Fig. 3.4: Fluid velocity curves for various values of M .

TH: 15/10/16

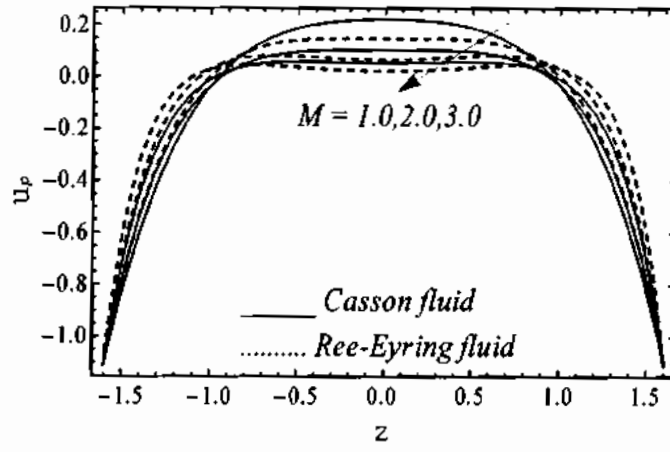


Fig. 3.5: Particulate velocity for various values of M .

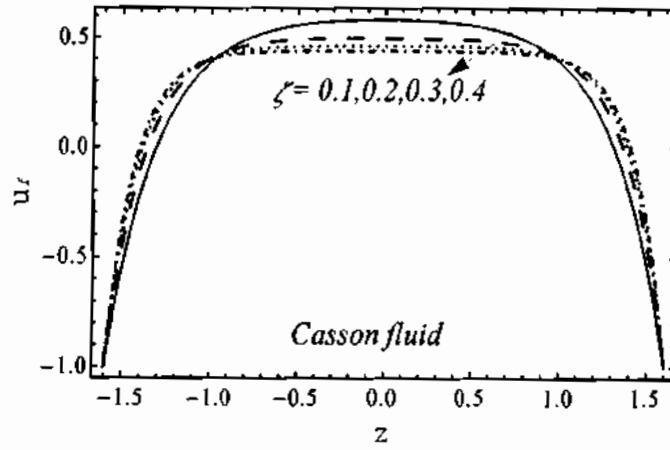


Fig. 3.6: Fluid velocity curves for various values of ζ .

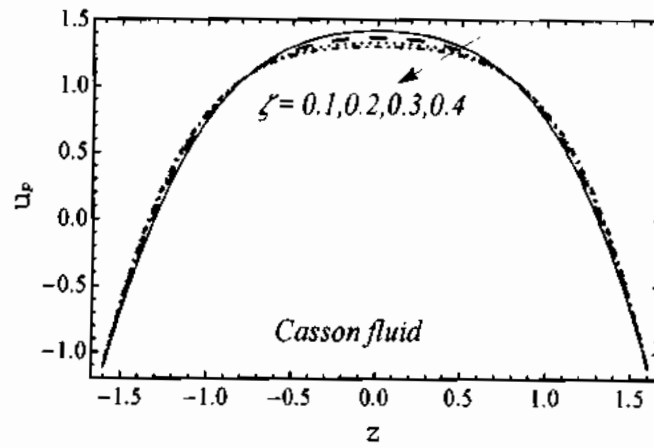


Fig. 3.7: Particulate velocity for various values of ζ .

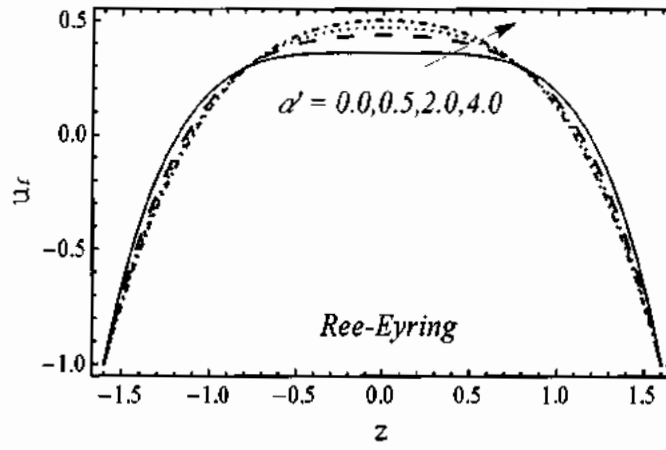


Fig. 3.8. Fluid velocity for various values of α' .

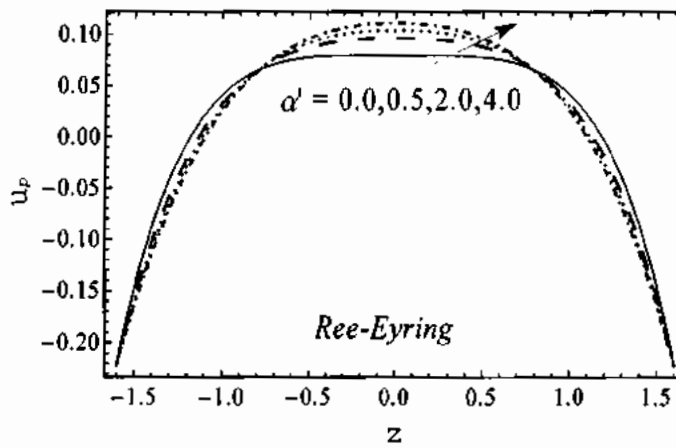


Fig. 3.9. Particulate velocity for various values of α' .

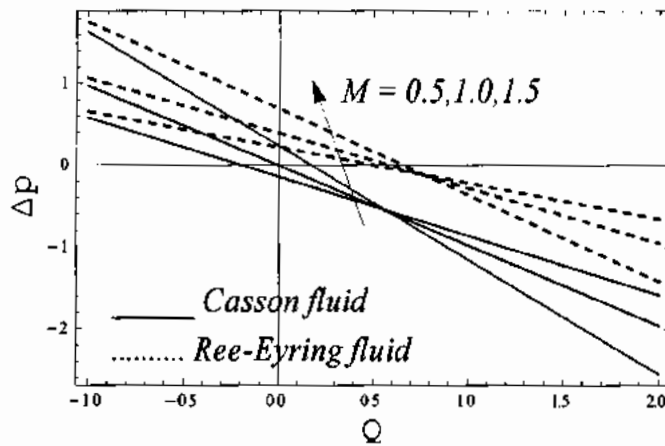


Fig. 3.10: Pressure rise vs. volume flow rate for various values of M .

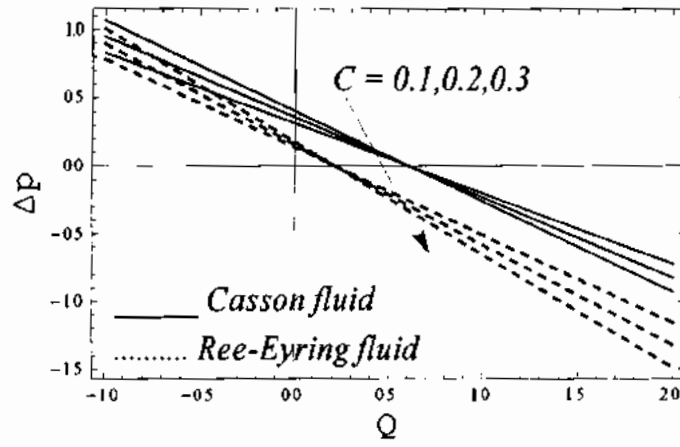


Fig. 3.11: Pressure rise vs. volume flow rate for various values of C .

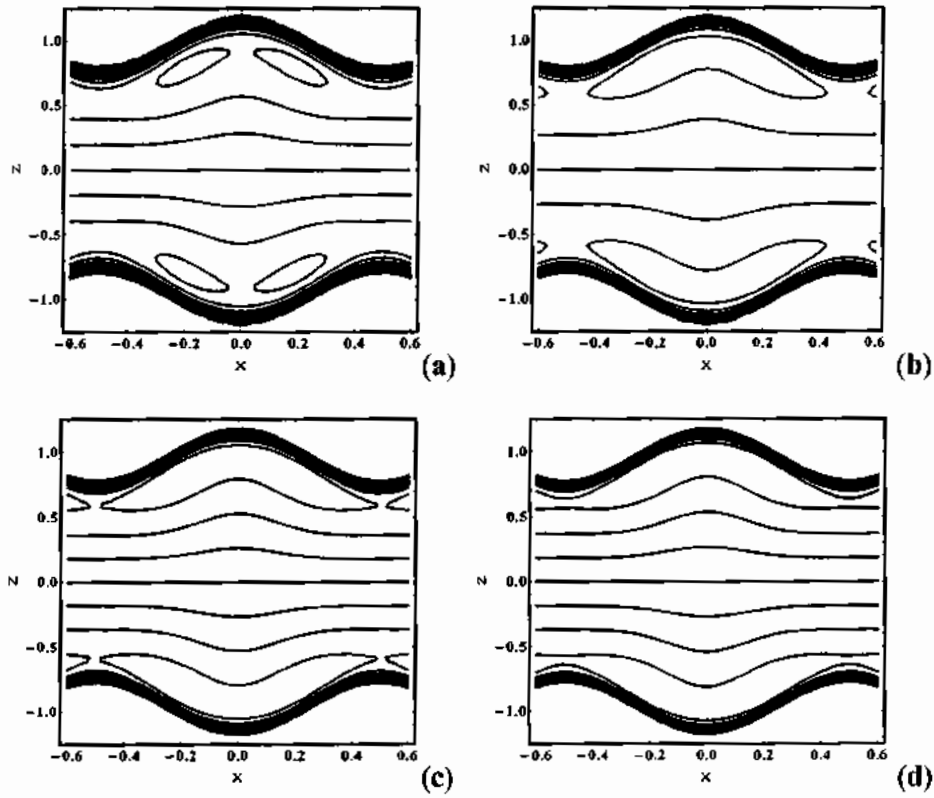


Fig. 3.12: Streamlines of Casson fluid for various values of M . (a) 1.5, (b) 2.0, (c) 2.5, (d) 3.0.

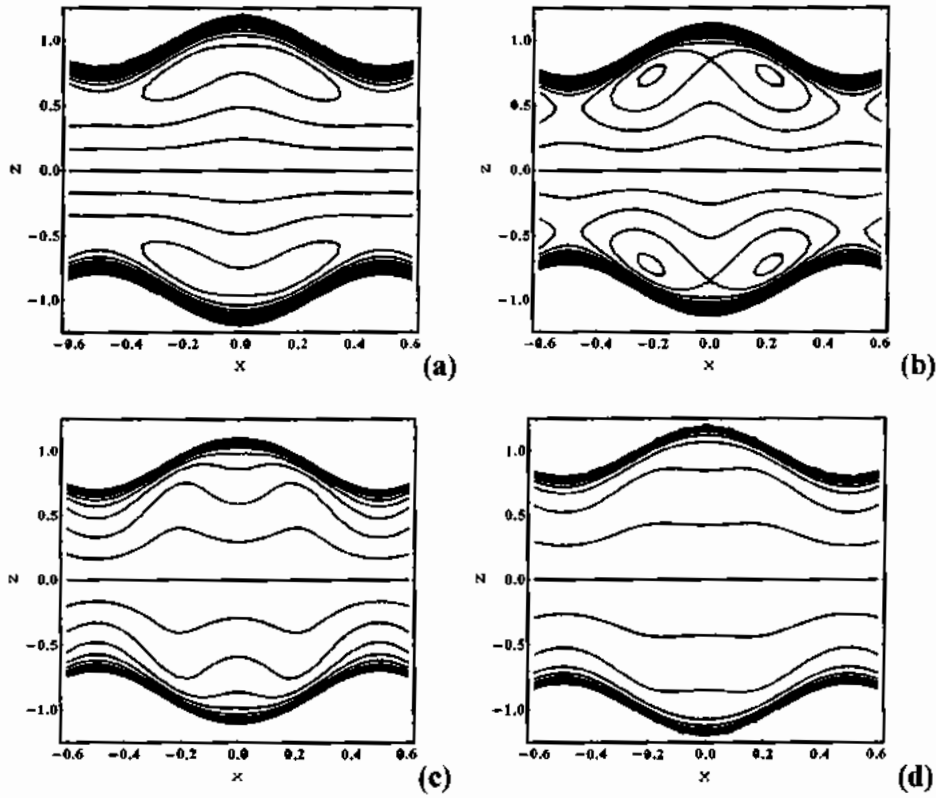


Fig. 3.13: Streamlines of Ree-Eyring fluid for various values of M . (a) 1.5, (b) 2.0, (c) 2.5, (d) 3.0.

3.5 Conclusion

This chapter addresses the peristaltic flow of bio rheological non-Newtonian (Casson and Ree-Eyring model) having small solid particles propagation through a rectangular duct. The flow is described by means of continuity and momentum equations for both fluid and particulate phase. The governing equation is solved with the assumption of low Reynolds number and long wavelength. The resulting partial differential equations are solved analytically with the help of Eigen function expansion method and exact solutions are presented. The major outcomes for the present analysis are summarized below:

- Velocity of the fluid reveals significant reduction due to greater influence of magnetic field.

- Higher values of particle volume fraction also provides a significant reduction in the transmission of fluid.
- Casson fluid parameter tends to enhance the velocity of the near the walls of the duct, however, it reveals converse behaviour in the middle of the duct. Opposite behaviour is observed for Ree-Eyring fluid.
- When the fluid is Newtonian pressure rise is increased.
- The magnitude of trapping bolus rises gradually due to an increase in the particle volume fraction and magnetic field.
- The present results reduces to Newtonian fluid and single phase flow by taking $\zeta \rightarrow \infty$ or $\alpha' \rightarrow 0$ and $C = 0$.

Chapter 4

Flow of particulate fluid through a channel with heat transfer

In this chapter, the flow of suspension of small particles in non-Newtonian Ree-Eyring fluid in a channel induced by peristaltic waves is described. The effects of transverse magnetic field is also observed. The problem is modeled using law of conservation of mass, momentum and energy. Under the assumption of creeping flow and long wave length the governing equations partial differential equations of solid and liquid phases are reduced to ordinary differential equations. The exact solutions have been obtained by solving the non-linear coupled differential equations analytically. The physical interpretation of emerging parameters for Newtonian and non-Newtonian case is displayed using graphs.

4.1 Geometry of the problem

Let the Cartesian coordinate system i.e. X –axis is along the direction of the flow and Y –axis is taken normal to the flow. Infinite plates parallel to X – axis bounds the fluid. A sinusoidal wave travel with the velocity c and amplitude a along the plate induces the flow Fig. (4.1). Mathematically, equation of wall is defined as

$$\tilde{H}(\tilde{X}, \tilde{t}) = b + a \sin \frac{2\pi}{\lambda}(\tilde{X} - ct), \quad (4.1)$$

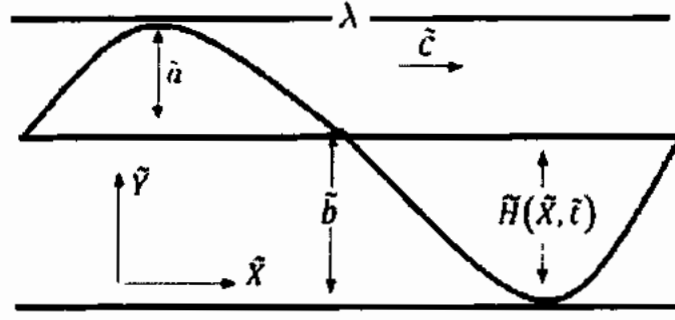


Fig. 4.1 Geometry of the problem.

4.2 Mathematical formulation

The void between the channels filled with incompressible, Ree-Eyring fluid with uniform distributed small solid particle. The flow is laminar and in creeping regime induced due to propagation of wave on the plate. The equation of fluid phase and particle phase is given by

$$\frac{\partial U_f}{\partial X} + \frac{\partial V_f}{\partial Y} = 0, \quad (4.2)$$

$$\rho_f(1-C) \left(\frac{\partial U_f}{\partial t} + U_f \frac{\partial U_f}{\partial X} + V_f \frac{\partial U_f}{\partial Y} \right) = -(1-C) \frac{\partial P}{\partial X} + (1-C) \left(\frac{\partial}{\partial X} S_{xx} + \frac{\partial}{\partial Y} S_{xy} \right) + CS'(U_p - U_f) - \sigma B_0^2 U_f, \quad (4.3)$$

$$(1-C) \rho_f \left(\frac{\partial V_f}{\partial t} + U_f \frac{\partial V_f}{\partial X} + V_f \frac{\partial V_f}{\partial Y} \right) = -(1-C) \frac{\partial P}{\partial Y} + (1-C) \left(\frac{\partial}{\partial X} S_{yx} + \frac{\partial}{\partial Y} S_{yy} \right) + CS'(V_p - V_f), \quad (4.4)$$

$$\rho_f c_p (1-C) \left(\frac{\partial T_f}{\partial t} + U_f \frac{\partial T_f}{\partial X} + V_f \frac{\partial T_f}{\partial Y} \right) = k_p (1-C) \frac{\partial^2 T_f}{\partial Y^2} + \rho_p c_p C (T_p - T_f) + CS'(U_p - U_f)^2 + S_{xy} (1-C) \left(\frac{\partial U_f}{\partial Y} \right), \quad (4.5)$$

$$\frac{\partial U_p}{\partial X} + \frac{\partial V_p}{\partial Y} = 0, \quad (4.6)$$

$$C\rho_p \left(\frac{\partial U_p}{\partial t} + U_p \frac{\partial U_p}{\partial X} + V_p \frac{\partial U_p}{\partial Y} \right) = -C \frac{\partial P}{\partial X} + CS'(U_f - U_p), \quad (4.7)$$

$$C\rho_p \left(\frac{\partial V_p}{\partial t} + U_p \frac{\partial V_p}{\partial X} + V_p \frac{\partial V_p}{\partial Y} \right) = -C \frac{\partial P}{\partial Y} + CS'(V_f - V_p), \quad (4.8)$$

$$\rho_p C c_p \left(\frac{\partial T_p}{\partial t} + U_p \frac{\partial T_p}{\partial X} + V_p \frac{\partial T_p}{\partial Y} \right) = \rho_p c_p C (T_f - T_p). \quad (4.9)$$

Here, S_{xx} and S_{xy} are components of stress tensor defined in Eq. (1.11). The equations are transform to wave frame using Eq. (3.8). Eq. (4.5) and Eq. (4.9) uses non-dimensional parameters.

$$\theta_{f,p} = \frac{T_{f,p} - T_0}{T_1 - T_0}, \text{Pr} = \frac{\mu_s c}{k}, \text{Ec} = \frac{c^2}{c_p (T_1 - T_0)}, \quad (4.10)$$

Using Eq. (2.10), (3.9) and Eq. (4.10). The governing flow Eq. (4.2) - (4.9) are simplified. Also, employing long wave length and creeping flow.

$$(1 + \alpha') \frac{\partial^2 u_f}{\partial y^2} - M^2 u_f - \frac{1}{1-C} \frac{dp}{dx} = M^2, \quad (4.11)$$

$$\frac{1}{\text{Pr}} \frac{\partial^2 \theta_f}{\partial y^2} + \text{Ec}(1 + \alpha') \left(\frac{\partial u_f}{\partial y} \right)^2 = -\frac{\text{Ec}}{M_1(1-C)} \left(\frac{dp}{dx} \right)^2, \quad (4.12)$$

$$\frac{dp}{dx} - M_1 (u_f - u_p) = 0, \quad (4.13)$$

$$\theta_f = \theta_p. \quad (4.14)$$

The corresponding non-dimensional boundary conditions are

$$u'_f = \theta'_f = 0, \text{ at } y = 0 \text{ and } u_f = -1, \theta_f = 1 \text{ at } y = h. \quad (4.15)$$

4.3 Solution of the problem

Solving the velocity and temperature profile, the exact solution is represented as

$$u_f = \frac{(1-C)M^2 - \frac{dp}{dx} + \frac{dp}{dx} \cosh \frac{yM}{\sqrt{1+\alpha'}} \operatorname{sech} \frac{hM}{\sqrt{1+\alpha'}}}{(1-C)M^2}, \quad (4.16)$$

$$u_p = \frac{(1-C)M^2 - \frac{dp}{dx} + \frac{dp}{dx} \cosh \frac{yM}{\sqrt{1+\alpha'}} \operatorname{sech} \frac{hM}{\sqrt{1+\alpha'}}}{(1-C)M^2} - \frac{1}{M_1} \frac{dp}{dx}, \quad (4.17)$$

$$\theta_{f,p} = C_6 y + C_7 y^2 - C_8 \operatorname{Cosh} \left(\frac{My}{\sqrt{1+\alpha'}} \right) \operatorname{Sech} \left(\frac{hM}{\sqrt{1+\alpha'}} \right)^2 - C_9 \operatorname{Cosh} \left(\frac{2My}{\sqrt{1+\alpha'}} \right) \operatorname{Sech} \left(\frac{hM}{\sqrt{1+\alpha'}} \right)^2. \quad (4.18)$$

Where

$$\begin{aligned} C_6 = & \frac{1}{8(-1+C)^2 hM^6 M_1} \left(-2((-1+C)^2 \operatorname{Ech}(1+\alpha')) M^6 M_1 \operatorname{Pr} \right. \\ & + 4(-1+C) \operatorname{Ech}(1+\alpha') M^4 M_1 \frac{dp}{dx} \operatorname{Pr} + 2(-1+C) \operatorname{Ech} M^6 \left(\frac{dp}{dx} \right)^2 \operatorname{Pr} \\ & - 4 \operatorname{Ech}(1+\alpha') M^2 M_1 \left(\frac{dp}{dx} \right)^2 \operatorname{Pr} + 2(-1+C) \operatorname{Ech} M^6 \left(\frac{dp}{dx} \right)^2 \operatorname{Pr} \operatorname{Cosh} \left(\frac{2hM}{\sqrt{1+\alpha'}} \right) \\ & \left. - 2 \operatorname{Ech}(1+\alpha') M^2 M_1 \left((1-C)M^2 + \frac{dp}{dx} \right)^2 \operatorname{Pr} \operatorname{Cosh} \left(\frac{2hM}{\sqrt{1+\alpha'}} \right) \operatorname{Sech} \left(\frac{hM}{\sqrt{1+\alpha'}} \right)^2 \right), \end{aligned}$$

$$\begin{aligned} C_7 = & \frac{1}{8(-1+C)^2 hM^6 M_1} 2(-1+C)^2 \operatorname{Ech}^2(1+\alpha') M^6 M_1 \operatorname{Pr} \\ & - 4(-1+C) \operatorname{Ech}^2(1+\alpha') M^4 M_1 \frac{dp}{dx} \operatorname{Pr} - 2(-1+C) \operatorname{Ech}^2 M^6 \left(\frac{dp}{dx} \right)^2 \operatorname{Pr} \\ & - \operatorname{Ec}(1+\alpha') M_1 \left(\frac{dp}{dx} \right)^2 \operatorname{Pr} - \operatorname{Ec} \alpha'(1+\alpha') M_1 \left(\frac{dp}{dx} \right)^2 \operatorname{Pr} \\ & + 4 \operatorname{Ech}^2(1+\alpha') M^2 M_1 \left(\frac{dp}{dx} \right)^2 \operatorname{Pr} - 16 \operatorname{Ec}(1+\alpha')^2 M_1 \left((-1+C)M^2 - \frac{dp}{dx} \right) \\ & \frac{dp}{dx} \operatorname{Pr} \operatorname{Cosh} \left(\frac{hM}{\sqrt{1+\alpha'}} \right) + 8 M_1 ((-1+C)^2 M^6 + 2 \operatorname{Ec}(1+\alpha')^2 \\ & \left((-1+C)M^2 - \frac{dp}{dx} \right) \frac{dp}{dx} \operatorname{Pr} \operatorname{Cosh} \left(\frac{hM}{\sqrt{1+\alpha'}} \right)^2, \end{aligned}$$

$$\begin{aligned} C_8 = & \frac{1}{8(-1+C)^2 hM^6 M_1} \operatorname{Ech}(1+\alpha') M_1 \left(\frac{dp}{dx} \right)^2 \operatorname{Pr} + \operatorname{Ech} \alpha'(1+\alpha') M_1 \left(\frac{dp}{dx} \right)^2 \operatorname{Pr} \\ & + 16 \operatorname{Ech}(1+\alpha')^2 M_1 \left((-1+C)M^2 - \frac{dp}{dx} \right) \frac{dp}{dx} \operatorname{Pr} \operatorname{Cosh} \left(\frac{hM}{\sqrt{1+\alpha'}} \right) \\ & - 16 \operatorname{Ech}(1+\alpha')^2 M_1 \left((-1+C)M^2 - \frac{dp}{dx} \right) \frac{dp}{dx} \operatorname{Pr} \operatorname{Cosh} \left(\frac{hM}{\sqrt{1+\alpha'}} \right), \end{aligned}$$

$$C_9 = Ech(1 + \alpha')^2 M_1 \left(\frac{dp}{dx} \right)^2 Pr.$$

The volume flow rate is specified by

$$Q = \frac{hM \left(M_1 \frac{dp}{dx} + (1-C)M^2 \left(M_1 + C \frac{dp}{dx} \right) \right) - \sqrt{1+\alpha'} M_1 \frac{dp}{dx} \tanh \left(\frac{hM}{\sqrt{1+\alpha'}} \right)}{(-1+C)M^3 M_1} \quad (4.19)$$

To obtain dp/dx after solving Eq. (4.19)

$$\frac{dp}{dx} = - \frac{(-1+C)M^3 M_1 (h+Q)}{(-1+C)ChM^3 - hMM_1 + \sqrt{1+\alpha'} M_1 \tanh \left(\frac{hM}{\sqrt{1+\alpha'}} \right)} \quad (4.20)$$

The pressure rise Δp is calculated numerically with the help of MATHEMATICA using Eq. (3.18).

4.4 Illustrations and discussion

To examine the impacts of several parameters Prandtl number(Pr), particles volume fraction(C), Hartmann number (M) and Eckert number (Ec) solution are plotted for both Newtonian and non-Newtonian fluid cases in Fig. (4.2) - (4.9).

The transvers magnetic field parameter M effects on the fluid velocity, negatively due to Lorentz opposing forces as shown in Fig. (4.2). From Fig. (4.3) it is notice that the decelerate the velocity profile when increasing the values of particle volume fraction it indicates increase in fluid viscosity.

From Fig. (4.4) it is examined that the values of Prandtl number rises temperature profile.

Prandtl number $Pr = \frac{\mu_s c}{k}$ is the ratio between thermal diffusivity and momentum diffusivity.

The Prandtl number also described by the specific heat capacity and dynamic viscosity divided by a thermal conductivity of the fluid. Prandtl number $Pr < 1$ are associated to rheological

propellants and shows that thermal diffusivity governs more as compared to momentum diffusivity. When the fluid is Newtonian the temperature profile is lower for the Eckert number whereas when values of Eckert number increases a rise in the temperature profile is seen (Fig. (4.5)). Eckert number $E_c = \frac{c^2}{c(\bar{T}_1 - \bar{T}_o)}$ is the relationship between boundary layer enthalpy difference and kinetic energy of the flow and is used to analyse the heat dissipation effects. It is observed through Fig. (4.6) when the value of particle volume fraction reduces the temperature profile. The value of Hartman number effects the temperature profile positively as investigated in Fig. (4.7).

Fig. (4.8) and (4.9) are discussed for pressure rise which is helpful in biological fluid. From Fig. (4.8) the pumping rate rises ($\Delta p < 0, Q > 0$) in co-pumping region and free pumping region ($\Delta p < 0, Q < 0$) when increases the value of particle volume fraction but in retrograde pumping region ($\Delta p > 0, Q < 0$) behavior is opposite. From Fig. (4.9) it is seen that when increase in the value of Hartmann number is observed the decrease in pumping rate in co-pumping region ($\Delta p < 0, Q > 0$) and free pumping region ($\Delta p < 0, Q < 0$) is noted and increases in retrograde pumping region ($\Delta p > 0, Q < 0$) is seen.

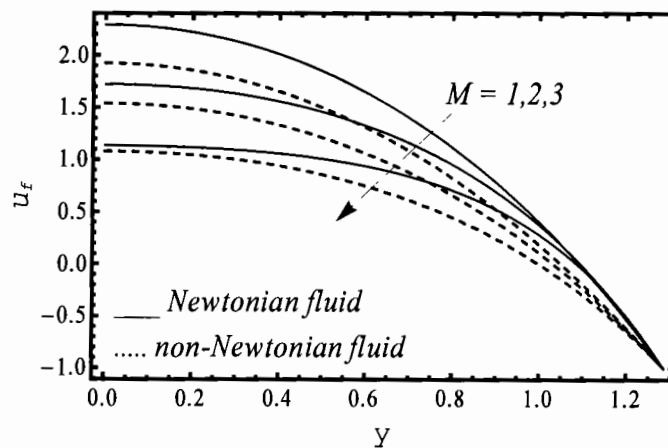


Fig. 4.2 Velocity field for different values of M .

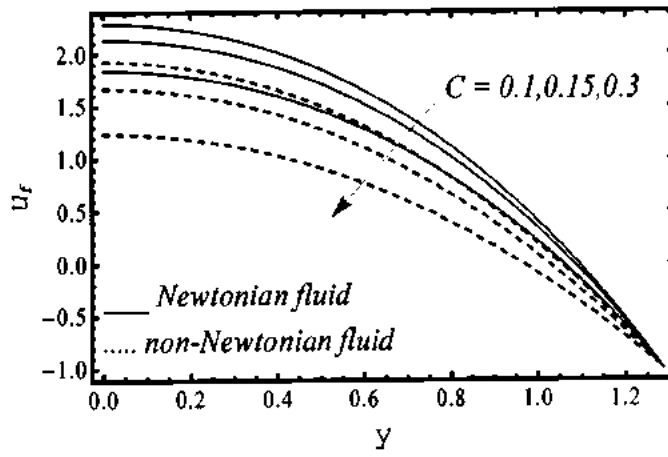


Fig. 4.3 Velocity field for different values of C .

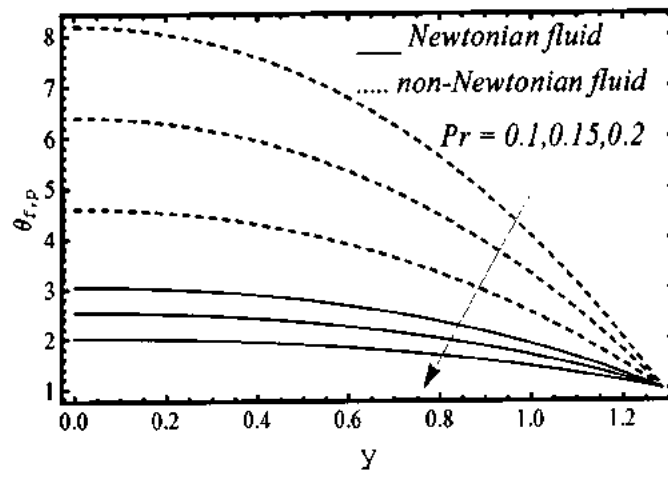


Fig. 4.4 Temperature field for different values of Pr .

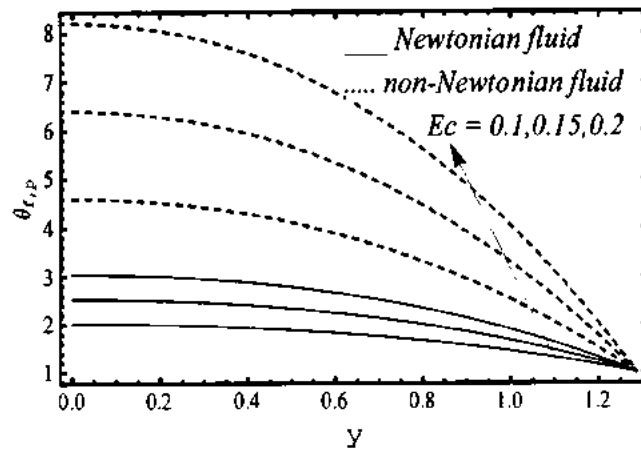


Fig. 4.5 Temperature field for different values of Ec .

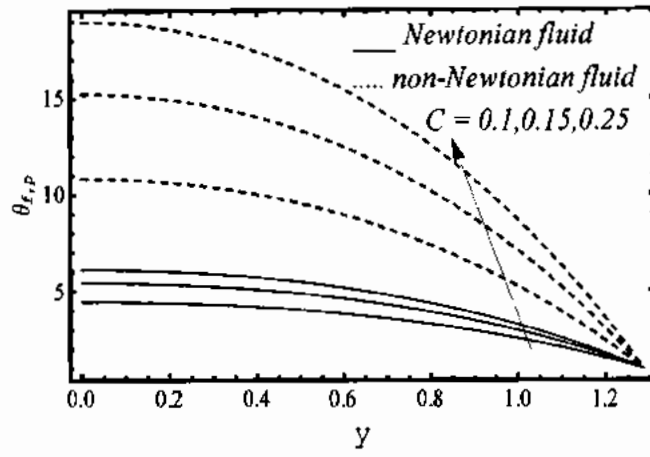


Fig. 4.6 Temperature field for different values of C .

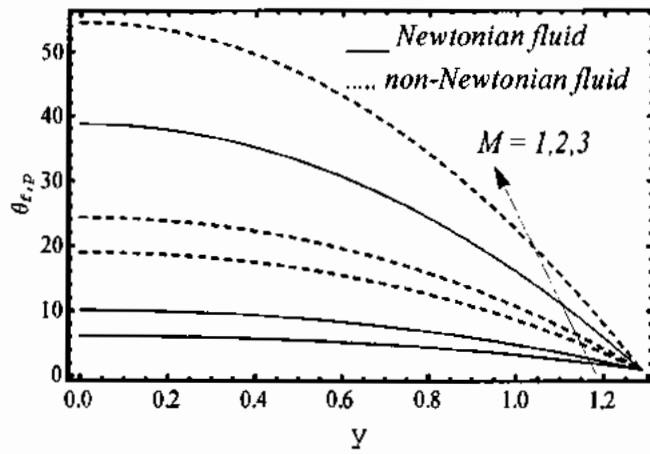


Fig. 4.7 Temperature field for different values of M .

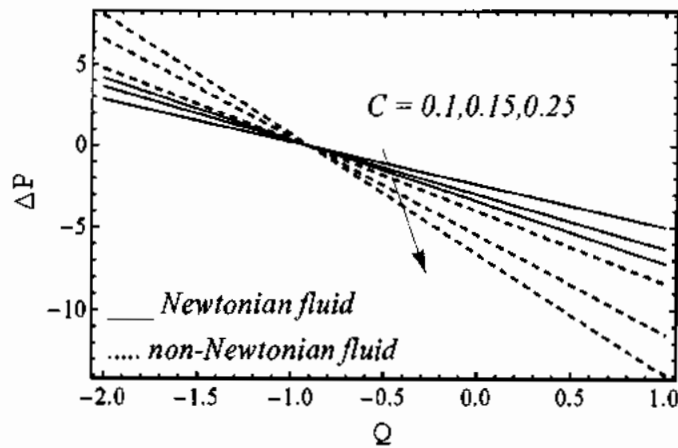


Fig. 4.8 Pressure field for different values of C .

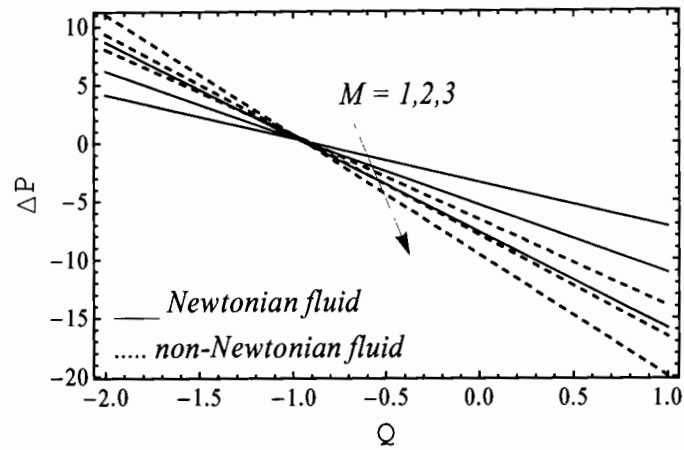


Fig. 4.9 Pressure field for different values of M .

4.5 Conclusion

In this chapter, the effect of heat transfer examined on peristaltic wave with Ree-Eyring fluid and magnetic field. The governing equations are solved with the assumption of low Reynolds number and long wave length. The analytical solution is obtained by solving the coupled ordinary differential equations. The main points are summarized below.

- The magnitude of velocity distribution for non-Newtonian fluid is larger than that of Newtonian fluid.
- The effect of Hartman number and particle volume fraction velocity distribution reduces.
- The behaviour is opposite for the temperature profile for particle and volume fraction Hartmann number whereas temperature rises for Prandtl number.
- When the fluid is non-Newtonian pressure rise is greater.
- The present analysis is reduced to Newtonian fluid by taking $\alpha=0$, and single phase when $C=0$ as a special case of this study.

Chapter 5

Flow of particulate fluid in a channel with inclined magnetic field and heat transfer

In this Chapter, the heat transfer of peristaltic movement of particles with uniform inclined magnetic field has been examined over a uniform inclined channel. The problem modelled use of momentum equations along with the energy equations in wave frame, with the assumption of long wavelength, Problem are solved for both fluid and particle phase. The exact solution is obtained by solving coupled ordinary differential equations for fluid and particulate phase. The effect of different physical parameters is discussed graphically. Also, numerical manipulation used to observe the pumping character.

5.1 Geometry of the problem

Consider the peristaltic (“*sinusoidal*”) wave is moving with wave velocity c on the wall of the channel having a wave length λ . The equation of wave propagation is described in Eq. (4.1).

The channel is inclined at a small angle α with X – axis as shown in Fig. (5.1)

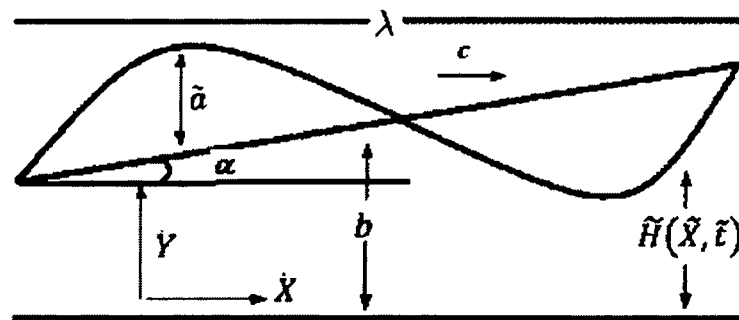


Fig. (5.1) Geometry of problem

5.2 Mathematical formulation

The fluid bounded by the channel has structures of incompressibility, irrotational, constant density contain uniformly distributive small particles. The existence of magnetic field $\mathbf{B} = \{B_0 \sin \Theta, B_0 \cos \Theta, 0\}$ is applied at an angle Θ with the flow. The magnetic field is precise small, hence induced magnetic field considered negligible. The equations governs the flow are

$$\frac{\partial U_f}{\partial X} + \frac{\partial V_f}{\partial Y} = 0, \quad (5.1)$$

$$(1-C)\rho_f \left(\frac{\partial U_f}{\partial t} + U_f \frac{\partial U_f}{\partial X} + V_f \frac{\partial U_f}{\partial Y} \right) = -(1-C) \frac{\partial P}{\partial X} + (1-C) \left(\frac{\partial^2 U_f}{\partial X^2} + \frac{\partial^2 U_f}{\partial Y^2} \right) - CS'(U_f - U_p) - \sigma B_0^2 \left[(U_f + 1)(\cos \Theta)^2 - V_f \cos \Theta \sin \Theta \right] + \rho_f g \sin \alpha, \quad (5.2)$$

$$(1-C)\rho_f \left(\frac{\partial V_f}{\partial t} + U_f \frac{\partial V_f}{\partial X} + V_f \frac{\partial V_f}{\partial Y} \right) = -(1-C) \frac{\partial P}{\partial Y} + (1-C) \left(\frac{\partial^2 V_f}{\partial X^2} + \frac{\partial^2 V_f}{\partial Y^2} \right) + CS'(V_p - V_f) - \sigma B_0^2 \left[(U_f \cos \Theta + \cos \Theta) \sin \Theta - V_f (\sin \Theta)^2 \right] - \rho_f g \cos \alpha, \quad (5.3)$$

$$(1-C)\rho_f c \left(\frac{\partial T_f}{\partial t} + U_f \frac{\partial T_f}{\partial X} + V_f \frac{\partial T_f}{\partial Y} \right) = k_p (1-C) \frac{\partial^2 T_f}{\partial Y^2} + \rho_p c_p C (T_p - T_f) + CS'(U_f - U_p)^2 + \mu_s (1-C) \left(\frac{\partial U_f}{\partial Y} \right)^2 + \sigma B_0^2 \cos \Theta \left((U_f + 1) \cos \Theta - V_f \sin \Theta \right)^2, \quad (5.4)$$

$$\frac{\partial U_p}{\partial X} + \frac{\partial V_p}{\partial Y} = 0, \quad (5.5)$$

$$C\rho_p \left(\frac{\partial U_p}{\partial t} + U_p \frac{\partial U_p}{\partial X} + V_p \frac{\partial U_p}{\partial Y} \right) + C \frac{\partial P}{\partial X} = -CS'(U_p - U_f), \quad (5.6)$$

$$C\rho_p \left(\frac{\partial V_p}{\partial t} + U_p \frac{\partial V_p}{\partial X} + V_p \frac{\partial V_p}{\partial Y} \right) + C \frac{\partial P}{\partial Y} = -CS'(V_p - V_f), \quad (5.7)$$

$$\rho_p C c \left(\frac{\partial T_p}{\partial t} + U_p \frac{\partial T_p}{\partial X} + V_p \frac{\partial T_p}{\partial Y} \right) = \rho_p C c_p (T_f - T_p). \quad (5.8)$$

The equations are transform in wave frame using Eq. (3.8).

Using non-dimensional parameters defined in Eq. (2.10), (3.9) and (4.10) and resultant equations are simplified using long wavelength and creeping flow assumption, the governing equations become

$$\frac{\partial^2 u_f}{\partial y^2} - M^2(1+u_f)\cos^2 \Theta + \frac{Re}{Fr} \sin \alpha - \frac{1}{1-C} \frac{dp}{dx} = 0, \quad (5.9)$$

$$\frac{1}{Pr} \frac{\partial^2 \theta_f}{\partial y^2} + Ec \left(\frac{\partial u_f}{\partial y} \right)^2 + \frac{Ec}{M_1(1-C)} \left(\frac{dp}{dx} \right)^2 + EcM^2(u_f+1)^2 \cos^2 \Theta = 0, \quad (5.10)$$

$$M_1(u_f - u_p) = \frac{dp}{dx}, \quad (5.11)$$

$$\theta_p = \theta_f. \quad (5.12)$$

Boundary conditions are presented as

$$u'_f(0) = 0, \quad \theta'_f(0) = 0, \quad \text{and} \quad u_f(h) = -1, \quad \theta_f(h) = 1. \quad (5.13)$$

5.3 Solution of the problem

Solving the velocity and temperature profile, the exact solution is represented as

$$u_f = \frac{\sec^2 \Theta (C_{10} - C_{11} \cosh My \cos \Theta)}{2(-1+C)FrM^2}, \quad (5.14)$$

$$u_p = \frac{\sec^2 \Theta (C_{10} - C_{11} \cosh My \cos \Theta)}{2(-1+C)FrM^2} - \frac{1}{M_1} \frac{dp}{dx}, \quad (5.15)$$

$$\theta = C_{12} + C_{13}y + C_{14}y^2 + C_{15} \cosh [My \cos \Theta] + C_{16} \cosh [2My \cos \Theta]. \quad (5.16)$$

Where

$$C_{10} = Fr \left(M^2 - CM^2 + 2 \frac{dp}{dx} \right) - (-1+C)FrM^2 \cos(2\theta) + 2(-1+C)Re \sin(\alpha),$$

$$C_{11} = 2 \operatorname{Sech}(hM \cos(\theta)) \left(Fr \frac{dp}{dx} + (-1+C) \operatorname{Re} \sin(\alpha) \right),$$

$$C_{12} = \operatorname{Sec}(\theta) \operatorname{Sech}(hM \cos(\theta)) \frac{\left(Fr \frac{dp}{dx} + (-1+C) \operatorname{Re} \sin(\alpha) \right)}{2(-1+C)FrM},$$

$$C_{13} = Fr \left(M^2 - CM^2 + 2 \frac{dp}{dx} \right) - (-1+C)FrM^2 \cos(2\theta) + 2(-1+C) \operatorname{Re} \sin(\alpha),$$

$$C_{14} = \operatorname{Sech}(hM \cos(\theta)) \left(Fr \frac{dp}{dx} + (-1+C) \operatorname{Re} \sin(\alpha) \right),$$

$$C_{15} = 2(-1+C)FrM^2,$$

$$C_{16} = \frac{Ec}{M_1 - M_1 C} \left(\frac{dp}{dx} \right)^2,$$

$$\begin{aligned} C_{17} = & \frac{C_{16} h \operatorname{Pr}}{2} - \frac{1}{4} C_{12}^2 Ec h \operatorname{Pr} + \frac{1}{4} Ec h M^2 \operatorname{Pr} + \frac{C_{13} Ec h M^2 \operatorname{Pr}}{C_{15}} \\ & + \frac{1}{4} Ec h M^2 \operatorname{Pr} \cos(2\theta) + \frac{4C_{14} Ec \operatorname{Pr} \operatorname{Sec}(\theta)^2}{C_{15} h} - \frac{C_{12}^2 Ec \operatorname{Pr} \operatorname{Sec}(\theta)^2}{8hM^2} \\ & + \frac{C_{13}^2 Ec h M^2 \operatorname{Pr} \operatorname{Sec}(\theta)^2}{2C_{15}^2} + \frac{C_{14}^2 Ec h M^2 \operatorname{Pr} \operatorname{Sec}(\theta)^2}{C_{15}^2} - \frac{4C_{14} Ec \operatorname{Pr} \operatorname{Cosh}(hM \cos(\theta)) \operatorname{Sec}(\theta)^2}{C_{15} h} \\ & + \frac{C_{12}^2 Ec \operatorname{Pr} \operatorname{Cosh}(2hM \cos(\theta)) \operatorname{Sec}(\theta)^2}{8h^2 M^2} + \frac{4C_{13} C_{14} Ec \operatorname{Pr} \operatorname{Sec}(\theta)^4}{C_{15}^2 h} - \frac{C_{14}^2 Ec \operatorname{Pr} \operatorname{Sec}(\theta)^4}{2C_{15}^2 h} \\ & - \frac{4C_{13} C_{14} Ec \operatorname{Pr} \operatorname{Cosh}(hM \cos(\theta)) \operatorname{Sec}(\theta)^4}{C_{15}^2 h} + \frac{C_{14}^2 Ec \operatorname{Pr} \operatorname{Cosh}(2hM \cos(\theta)) \operatorname{Sec}(\theta)^4}{2C_{15}^2 h}, \end{aligned}$$

$$\begin{aligned} C_{18} = & -\frac{C_{16} \operatorname{Pr}}{2} + \frac{1}{4} C_{12}^2 Ec \operatorname{Pr} - \frac{1}{4} Ec M^2 \operatorname{Pr} - \frac{C_{13} Ec M^2 \operatorname{Pr}}{C_{15}} - \frac{1}{4} Ec M^2 \operatorname{Pr} \cos(2\theta) \\ & - \frac{C_{13}^2 Ec M^2 \operatorname{Pr} \operatorname{Sec}(\theta)^2}{2C_{15}^2} - \frac{C_{14}^2 Ec M^2 \operatorname{Pr} \operatorname{Sec}(\theta)^2}{C_{15}^2}, \end{aligned}$$

$$C_{19} = -\frac{4C_{14} Ec \operatorname{Pr} \operatorname{Sec}(\theta)^2}{C_{15}} + \frac{C_{12}^2 Ec \operatorname{Pr} \operatorname{Sec}(\theta)^2}{8M^2} - \frac{4C_{13} C_{14} Ec \operatorname{Pr} \operatorname{Sec}(\theta)^4}{C_{15}^2} + \frac{C_{14}^2 Ec \operatorname{Pr} \operatorname{Sec}(\theta)^4}{2C_{15}^2},$$

$$C_{20} = \frac{4C_{14} Ec \operatorname{Pr} \operatorname{Sec}(\theta)^2}{C_{15}} + \frac{4C_{13} C_{14} Ec \operatorname{Pr} \operatorname{Sec}(\theta)^4}{C_{15}^2},$$

$$C_{21} = -\frac{C_{12}^2 Ec Pr Sec(\theta)^2}{8M^2} - \frac{C_{14}^2 Ec Pr Sec(\theta)^4}{2C_{15}^2}.$$

The volume flow rate is defined as

$$Q = \int_0^h (u_f - Cu_f) dy + \int_0^h Cu_p dy. \quad (5.17)$$

Simplifying Eq. (5.17) to get

$$\frac{dp}{dx} = -\frac{(-1 + C)M_1(2FrM^3Q + FrhM^3Sec[\theta]^2 + FrhM^3Cos[2\theta]Sec[\theta]^2 - 2hMReSec[\theta]^2Sin[\alpha] + 2ReSec[\theta]^3Sin[\alpha]Tanh[hMCos[\theta]])}{2Fr(-ChM^3 + C^2hM^3 - hMM_1Sec[\theta]^2 + M_1Sec[\theta]^3Tanh[hMCos[\theta]])} \quad (5.18)$$

The pressure rise Δp is defined in Eq. (3.18).

5.4 Illustrations and discussion

This section consist of graphical behavior of different parameters. Computational software MATHEMATICA has been used to conclude the novelties of inclined angles (α, θ), Froude number Fr , Hartmann number M , Reynolds number Re , Prandtl number Pr , Eckert number Ec , particle volume fraction C and volume flow rate Q respectively. In particular, the impacts on temperature profile $\theta_{f,p}$, velocity profiles u_f and u_p and pressure rise Δp are conferred. For this purpose Fig. (5.2) - (5.11) are sketched.

Fig. (5.2) - (5.4) shows the behavior of velocity profile that with multiple values of particle volume fraction C , Inclined angles (α, θ), Froude number Fr and Hartman number M . From Fig. (5.2) it can be notice that when particle volume fraction increases velocity profile decrease as it opposes the flow. Lorentz force is opposing the flow when magnetic field is applied as observed from Fig. (5.2) it is observed that when increasing the value of magnetic field the velocity profile of the fluid reduces. Fig. (5.3) explains the differences of u_f verses y

for different values of Q and α . Figure displays the velocity profile enhanced with increase in inclination angle α . Furthermore, it can be notice that the velocity profile also increases with the increasing the volume flow rate Q . In Fig. (5.4) it can be notice that velocity profile increasing with rising the inclination angle of magnetic field Θ . Froude number Fr goes to resist the flow, the velocity of the fluid has larger effect when $Fr < 1$ (subcritical flow) as associated to when $Fr = 1$ (critical) and $Fr > 1$.

Fig. (5.5) - (5.8) are drawn for temperature profile for different parameters. It shows from Fig. (5.5) inclination angle α rises then the temperature profile rises moderately, the temperature profile rising with the volume flow rate Q increase. It is clear that in Fig. (5.6) Hartmann number M rises with temperature profile increase. The same behavior of temperature profile examined with the particle volume fraction C rises. Fig. (5.7) shows the behavior of inclination angle Θ and Froude number Fr on temperature profile. From this figure Froude number Fr accelerate temperature profile is observed. Fig. (5.8) illustrates the behavior of Prandtl number Pr and Eckert number Ec on temperature profile. From this figure it is observed that Prandtl number Pr , increases the temperature profile.

Fig. (5.9) - (5.11) are discuss for pumping characteristics and pressure rise. Fig. (5.9) shows the behavior of Hartman number M and particle volume fraction C on pressure increase. When Hartman number M and particle volume fraction C increases the pressure rise increases. From Fig. (5.10) that pressure increase depicts similar behavior, by rising Reynolds. Whereas, for Front number pressure rise decrease. Fig. (5.11) is drawn for inclined angle α and amplitude ratio ϕ From this figure it is clear that the pumping rate rises in this region. The attitude of inclination angle α is reverse on pressure rise as related to the compoment of amplitude ratio.

Fig. (5.12) - (5.16) explains the streamlines (or “*Trapping*”) for different values of controlling parameters. Fig. (5.12) clarifies that the magnitude of trapped bolus decreases

slowly for values of angle α . From Fig. (5.13) the impact of particles shows similar performance whereas magnitude of trapped bolus decreases more expressively. From Fig. (5.14) it is notice that the increase in Froude number Fr effects the streamlines and causes the bolus size to decrement. In Fig. (5.15), it is observed that magnetic field influenced on streamlines trapped bolus vanishes. From Fig. (5.16) it can be seen that reduction of angle Θ goes to contract the trapping bolus.

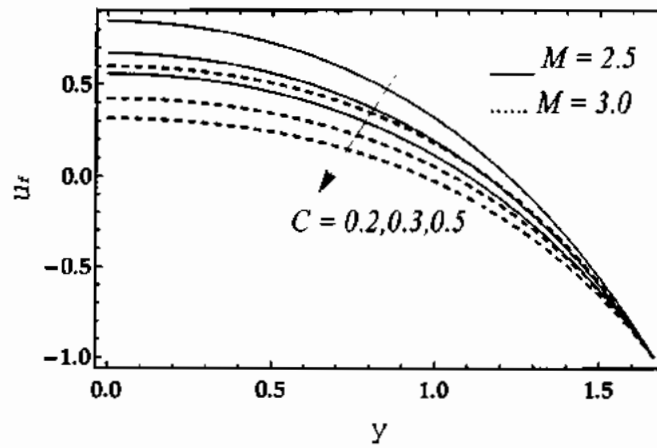


Fig. 5.2 Velocity field for different values of M and C .

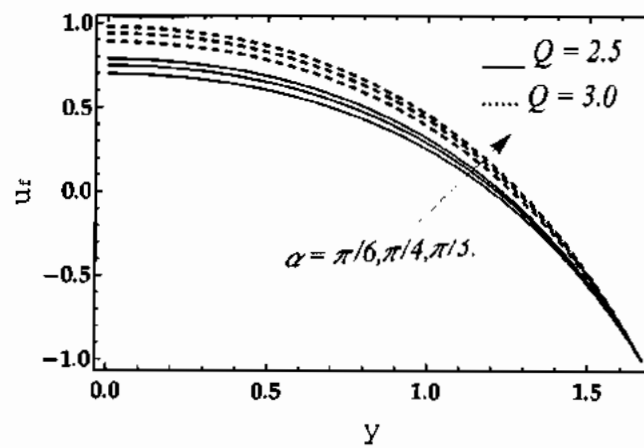


Fig. 5.3 Velocity field for different values of Q and α .

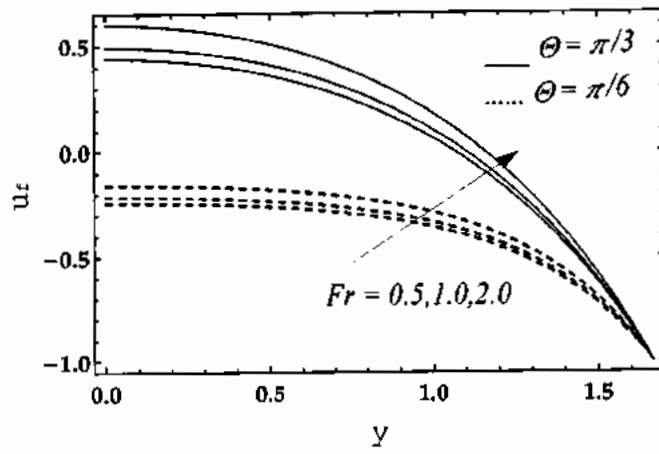


Fig. 5.4 Velocity field for different values of Θ and Fr .

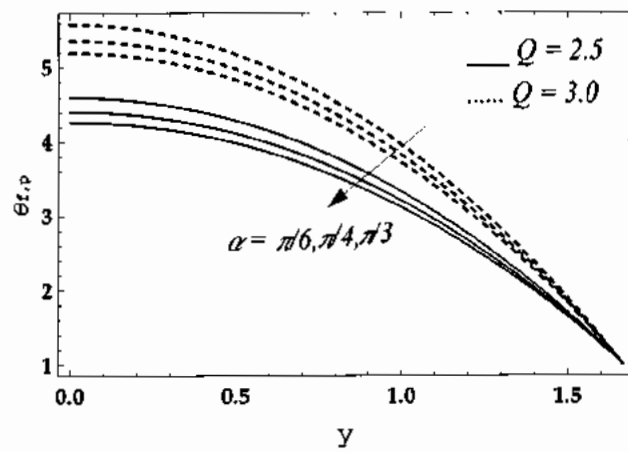


Fig. 5.5 Temperature field for different values of α and Q .

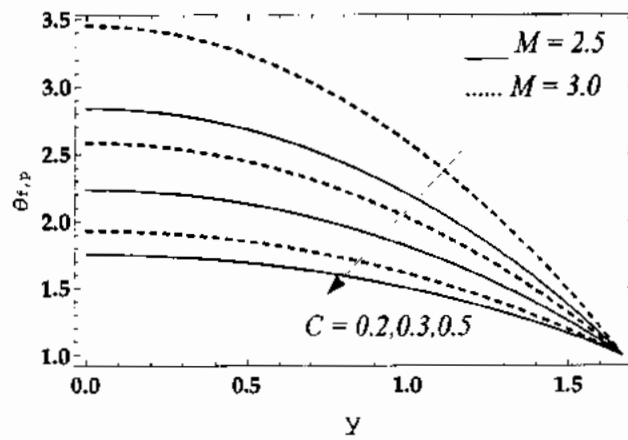


Fig. 5.6 Temperature field for different values of M and C .

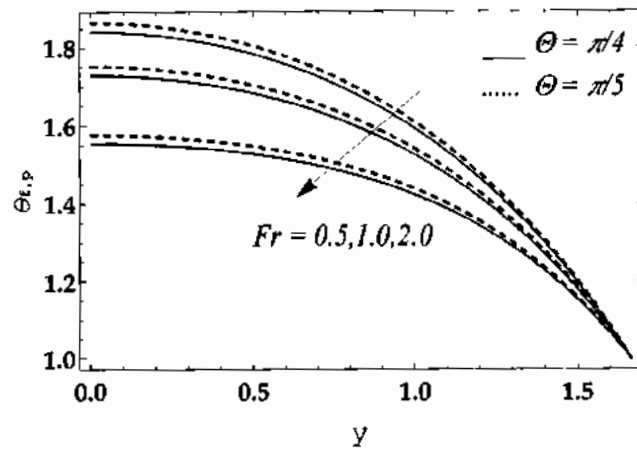


Fig. 5.7 Temperature field for different values of Θ and Fr .

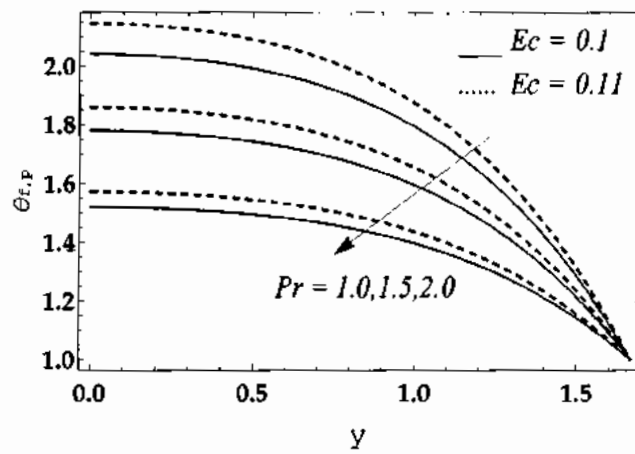


Fig. 5.8 Temperature field for different values of Ec and Pr .

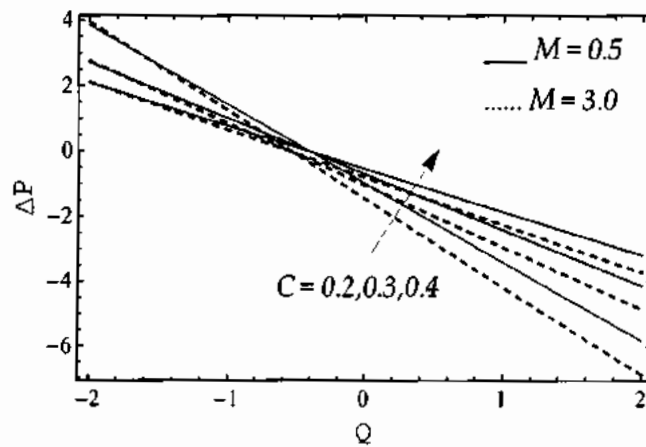


Fig. 5.9 Pressure field for different values of M and C .

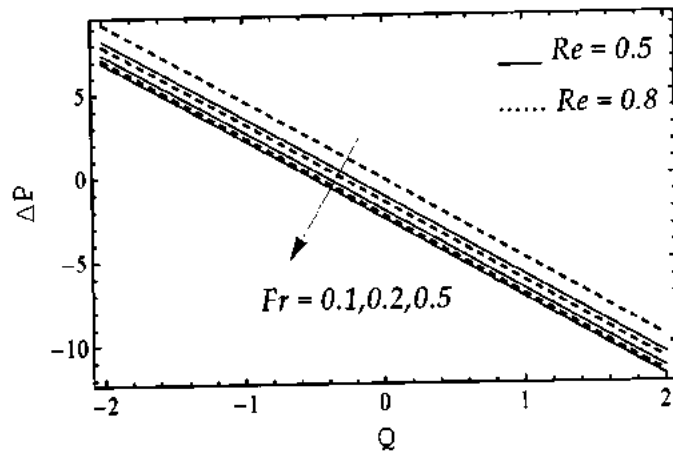


Fig. 5.10 Pressure field for different values of Fr and Re .

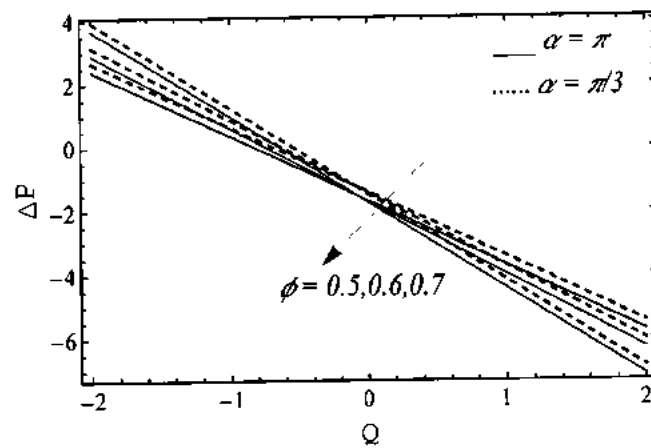


Fig. 5.11 Pressure field for different values of α and ϕ .

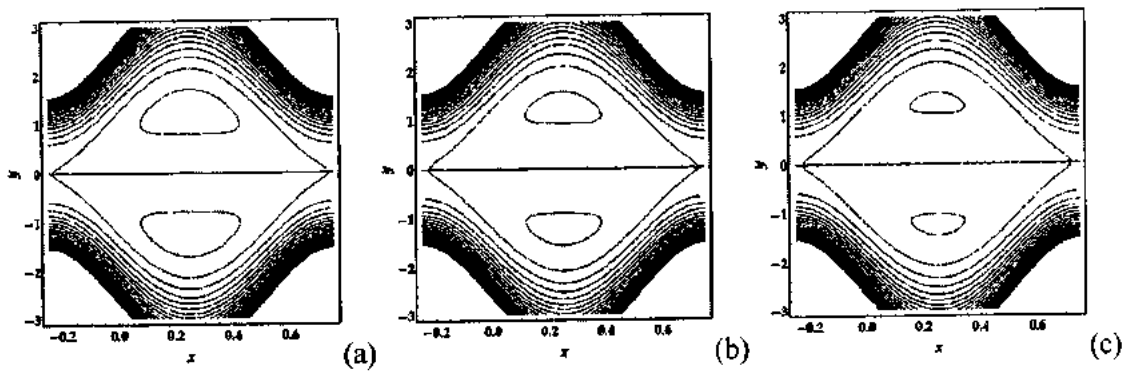


Fig. 5.12 Stream lines for different values of $\alpha = \frac{\pi}{3}, \frac{\pi}{6}, \frac{\pi}{9}$.

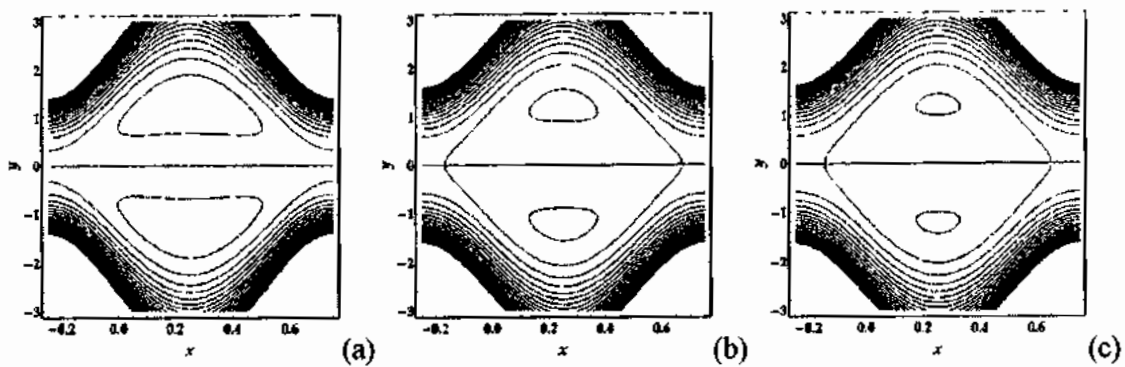


Fig. 5.13 Stream lines for different values of $C = 0.1, 0.3, 0.6$.

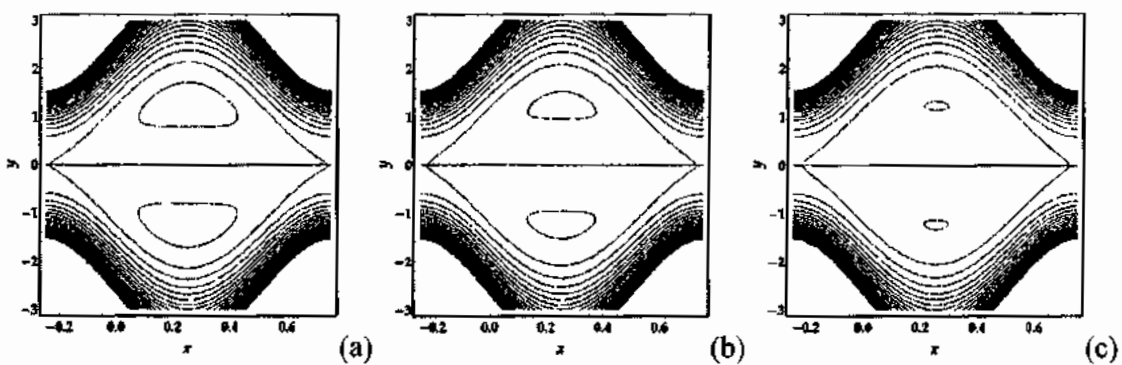


Fig. 5.14 Stream lines for different values of $Fr = 0.5, 1.0, 2.0$.

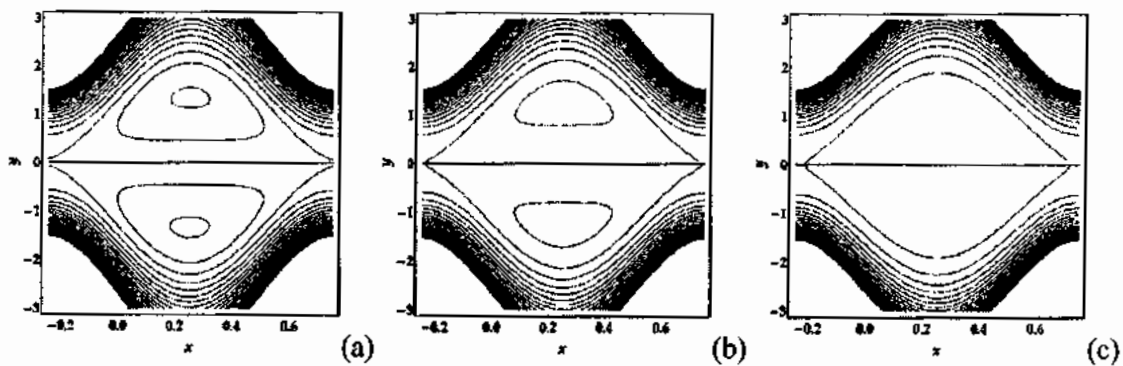


Fig. 5.15 Stream lines for different values of $M = 1, 2, 3$.

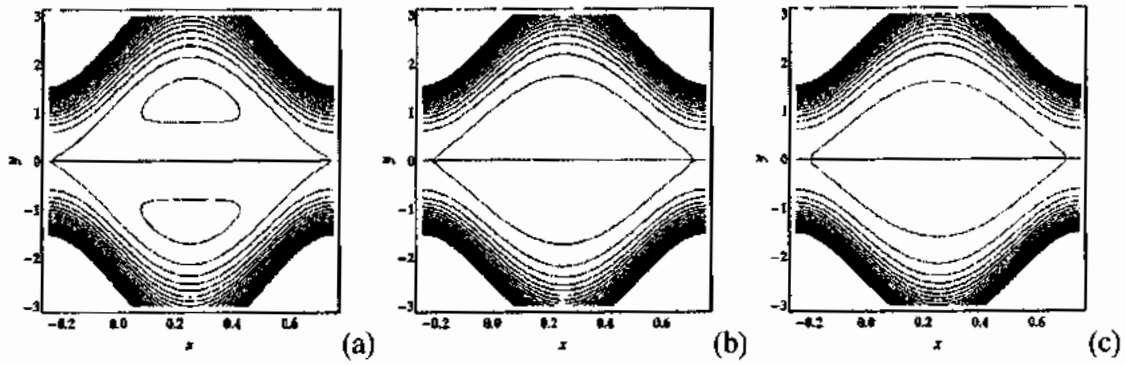


Fig. 5.16 Stream lines for different values of $\Theta = \frac{\pi}{3}, \frac{\pi}{6}, \frac{\pi}{9}$.

5.5 Conclusion

This chapter deals with the peristaltic movement of fluid and particle induced by inclined magnetic field with uniform channel. With the assumption of low Reynolds number and long wave length governing equations are solved for fluid and particle phase. The analytical result is obtained by solving the coupled linear differential equations.

- Velocity of the fluid reduces, the values are increased of C and M .
- The effect of Hartman number M and particle concentration C on the temperature is negative.
- The temperature profile enhances with greater values of Ec and Pr .
- With large values of Froude number Fr in all regions, pressure rise decreased.
- With increase of Froude number Fr bolus size decreases.

Chapter 6

Flow of particulate fluid in a channel with electric double layer effects along with heat and mass transfer

In the present chapter heat and mass transfer with the transverse magnetic field on peristaltic of two-phase flow (particle-fluid suspension) through a planar channel with peristaltic wave has been examined. The flow is observed under the influence of electric double layer and chemical reaction. The present flow problem is modelled using continuity, momentum, heat and diffusion equations, lubrication theory, to simplify the problem approximation in combination with creeping flow and long wavelength assumptions is used. Moreover, the electric effects are simplified using Debye linearization. Analytical solutions are found from the resulting coupled ordinary differential equations. The influence of various emerging parameters is discussed for velocity, temperature and concentration profile. Furthermore, the behavior of pressure rise and trapping mechanism using stream lines is sketched.

6.1 Geometry of the problem

Let the Cartesian coordinate system i.e. Y –axis is taken normal to the flow and X –axis is along the direction of the flow. Infinite plates parallel to X – axis bounds the fluid. A sinusoidal wave travel with the velocity c and amplitude b along the plate induces the flow displayed in Fig. (6.1).

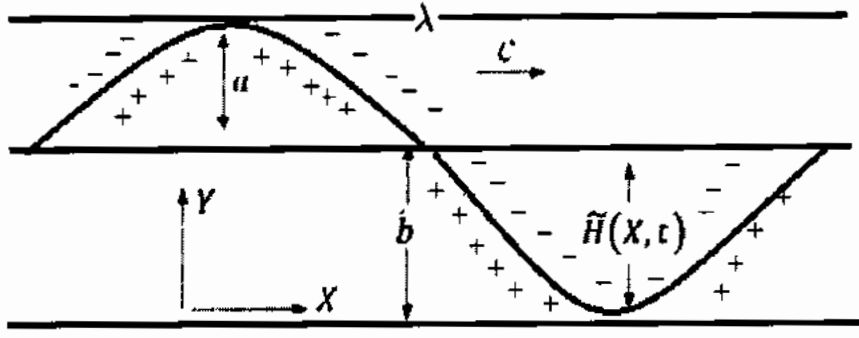


Fig. 6.1. Geometry of the flow problem.

A static electric charge is applied on the wall creating a double layer. Mathematically description of the wave along the wall is given in Eq. (4.1).

6.2 Mathematical formulation

The fluid is incompressible, electrically conducting, constant density with an applied electrokinetic body force through a longitudinal direction and a static magnetic field towards a transverse direction in Cartesian coordinate system (see Fig. 6.1).

The equation of continuity, momentum, energy and diffusion equation for fluid and particle phase are given as

$$\frac{\partial v_f}{\partial Y} + \frac{\partial u_f}{\partial X} = 0, \quad (6.1)$$

$$(1 - C)\rho_f \left(v_f \frac{\partial u_f}{\partial Z} + u_f \frac{\partial u_f}{\partial X} + \frac{\partial u_f}{\partial t} \right) = (1 - C) \left(\frac{\partial}{\partial X} S_{xx} + \frac{\partial}{\partial Y} S_{xy} \right) \quad (6.2)$$

$$+ \sigma B_0^2 u_f + \tilde{\rho}_e \bar{E} + (1 - C) \frac{\partial P}{\partial X} - (U_p - u_f) CS',$$

$$(1 - C)\rho_f \left(v_f \frac{\partial v_f}{\partial Y} + u_f \frac{\partial v_f}{\partial X} + \frac{\partial v_f}{\partial t} \right) \quad (6.3)$$

$$= (1 - C) \frac{\partial P}{\partial Y} - (V_p - v_f) CS' + (1 - C) \left(\frac{\partial}{\partial X} S_{yx} + \frac{\partial}{\partial Y} S_{yy} \right),$$

$$(1 - C)\rho_f c_p C \left(v_f \frac{\partial T_f}{\partial Y} + u_f \frac{\partial T_f}{\partial X} + \frac{\partial T_f}{\partial t} \right) = (1 - C) S_{xx} \left(\frac{\partial u_f}{\partial Y} \right) \quad (6.4)$$

$$\begin{aligned}
& +k_p(1-C)\left(\frac{\partial^2}{\partial X^2} + \frac{\partial^2}{\partial Y^2}\right)T_f - \rho_p c_p C(T_p - T_f) + CS'(U_f - U_p)^2, \\
(1-C)\left(\frac{\partial F_f}{\partial t} + U_f \frac{\partial F_f}{\partial X} + V_f \frac{\partial F_f}{\partial Y}\right) & = D_m(1-C)\left(\frac{\partial^2}{\partial X^2} + \frac{\partial^2}{\partial Y^2}\right)F_f \\
& + \rho_p c_p C(F_p - F_f) + \frac{D_m K_T}{T_m}(1-C)\left(\frac{\partial^2}{\partial X^2} + \frac{\partial^2}{\partial Y^2}\right)T_f - \bar{K}_c(F_f - F_0).
\end{aligned} \tag{6.5}$$

$$\frac{\partial V_p}{\partial Y} + \frac{\partial U_p}{\partial X} = 0, \tag{6.6}$$

$$C\rho_p\left(V_p \frac{\partial U_p}{\partial Y} + U_p \frac{\partial U_p}{\partial X} + \frac{\partial U_p}{\partial t}\right) = C \frac{\partial P}{\partial X} - CS'(U_f + U_p), \tag{6.7}$$

$$C\rho_p\left(V_p \frac{\partial V_p}{\partial Y} + U_p \frac{\partial V_p}{\partial X} + \frac{\partial V_p}{\partial t}\right) = C \frac{\partial P}{\partial Y} - CS'(V_p + V_f), \tag{6.8}$$

$$Cc_p\rho_p\left(V_p \frac{\partial T_p}{\partial Y} + U_p \frac{\partial T_p}{\partial X} + \frac{\partial T_p}{\partial t}\right) = -\rho_p c_p C(T_f - T_p), \tag{6.9}$$

$$\rho_p C\left(\frac{\partial F_p}{\partial t} + U_p \frac{\partial F_p}{\partial X} + V_p \frac{\partial F_p}{\partial Y}\right) = \rho_p c_p D_m(F_f - F_p). \tag{6.10}$$

Here, S is stress tensor of Jeffery fluid is represented in Eq. (1.2). The equations are transform in wave frame using Eq. (2.9) and Eq. (3.8).

Non-dimensional parameter are describe in Eq. (2.10), (3.9) and (4.10).

$$Sc = \frac{\mu_s}{\rho D_m}, Sr = \frac{\rho D_m K_T}{\mu_s T_m} \left(\frac{T_1 - T_0}{F_1 - F_0} \right), \Phi_{f,p} = \frac{F_{f,p} - F_0}{F_1 - F_0}, U_{HS} = \frac{-E_x \epsilon \zeta}{\mu_s c}. \tag{6.11}$$

are employed and take $\delta \rightarrow 0$ and $Re \rightarrow 0$ as wavelength in take as long and flow is creeping.

Eq. (6.1) – (6.10) reduces to

$$\frac{1}{\lambda_1 + 1} \frac{\partial^2 u_f}{\partial y^2} - M^2(u_f + 1) + m^2 U_{HS} \frac{\cosh my}{\cosh mh} = \frac{1}{1-C} \frac{dp}{dx'} \tag{6.12}$$

$$\frac{\partial^2 \theta_f}{\partial y^2} + PrEc \frac{1}{\lambda_1 + 1} \left(\frac{\partial u_f}{\partial y} \right)^2 = - \frac{PrEc}{M_1(1-C)} \left(\frac{dp}{dx} \right)^2, \quad (6.13)$$

$$\frac{1}{Sc} \frac{\partial^2 \Phi_f}{\partial y^2} - \gamma \Phi_f = -Sr \frac{\partial^2 \theta_f}{\partial y^2}. \quad (6.14)$$

$$\frac{dp}{dx} = N(u_f - u_p), \quad (6.15)$$

$$\theta_f = \theta_p, \quad (6.16)$$

$$\Phi_f = \Phi_p. \quad (6.17)$$

and their boundary conditions becomes

$$\theta'_f = 0, \quad \frac{\partial u_f}{\partial y} = \Phi'_f = 0, \text{ at } y = 0, \quad (6.18)$$

$$\theta_f = \Phi_f = 1, u_f = -1, \text{ at } y = h.$$

6.3 Solution of the problem

Exact solutions of velocities, temperature and concentration distribution presented as

$$u_f = - \frac{1}{C_{25}} [C_{22} \cosh 2\sqrt{1+\lambda_1} My + C_{23} + C_{24} \cosh my], \quad (6.19)$$

$$u_p = - \frac{1}{C_{25}} [C_{22} \cosh 2\sqrt{1+\lambda_1} My + C_{23} + C_{24} \cosh my] - \frac{1}{M_1} \frac{dp}{dx}, \quad (6.20)$$

$$\begin{aligned} \theta_{f,p} = & C_{29}y + C_{30}y^2 + C_{31} \cosh 2\sqrt{1+\lambda_1} My + C_{32} \cosh(\sqrt{1+\lambda_1}M - m)y \\ & + C_{33} \cosh 2my + C_{34} \cosh(\sqrt{1+\lambda_1}M + m)y, \end{aligned} \quad (6.21)$$

$$\begin{aligned}
\Phi_{f,p} = \frac{1}{C_{37}} [& C_{41} - C_{38} \cosh 2\sqrt{1+\lambda_1}My - C_{39} \cosh 2\sqrt{1+\lambda_1}My \cosh(my) \\
& + C_{40} \cosh 2my + C_{35} \cosh \sqrt{\gamma S_c}(h-y) + C_{36} \cosh \sqrt{S_c\gamma}y \\
& + C_{42} \sinh \sqrt{1+\lambda_1}My \sinh my + C_{35} \sinh \sqrt{\gamma S_c}(h-y) \\
& + C_{36} \sinh \sqrt{S_c\gamma}y]. \tag{6.22}
\end{aligned}$$

where

$$\begin{aligned}
C_{22} = \left(-mM^2 \frac{dp}{dx} + (1+\lambda_1)M^2 \frac{dp}{dx} + (-1+C)mM^2 U_{hs} \right) e^{h\sqrt{1+\lambda_1}m} \text{Cosh}(hmM) \text{Sech}(hmM) (1 \\
- \text{Tanh}(h\sqrt{1+\lambda_1}m))
\end{aligned}$$

$$\begin{aligned}
C_{23} = ((1+\lambda_1)M^2 - mM^2) \left((-1+C)M^2 - \frac{dp}{dx} \right) \text{Cosh}(hmM) e^{h\sqrt{1+\lambda_1}m} \text{Sech}(hmM) (1 - \\
\text{Tanh}(h\sqrt{1+\lambda_1}m)) \text{Cosh}(h\sqrt{1+\lambda_1}m),
\end{aligned}$$

$$\begin{aligned}
C_{24} = -\text{Sech}(hmM) (1 - \text{Tanh}(h\sqrt{1+\lambda_1}m)) e^{h\sqrt{1+\lambda_1}m} \text{Cosh}(h\sqrt{1+\lambda_1}m) (-1+C) (1 \\
+ \lambda_1) M^2 mM^2 U_{HS},
\end{aligned}$$

$$C_{25} = (-1+C)M^2((1+\lambda_1)M^2 - mM^2),$$

$$C_{26} = \text{Pr} * \frac{\text{Ec}}{n * (1-C)} * \left(\frac{dp}{dx} \right),$$

$$C_{27} = \frac{\text{Pr} * \text{Ec}}{1 + \lambda_1},$$

$$\begin{aligned}
C_{28} = C_{22}^2 C_{27} h M^4 + C_{24}^2 C_{27} h M^4 + 2C_{22}^2 C_{27} h \lambda_1 M^4 + 2C_{24}^2 C_{27} h \lambda_1 M^4 + C_{22}^2 C_{27} h \lambda_1^2 M^4 \\
+ C_{24}^2 C_{27} h \lambda_1^2 M^4 - 2C_{22}^2 C_{27} h M^2 mM^2 - 32C_{22}^2 C_{24} C_{27} h M^2 mM^2 \\
- 2C_{24}^2 C_{27} h M^2 mM^2 - 2C_{22}^2 C_{27} h \lambda_1 M^2 mM^2 - 32C_{22}^2 C_{24} C_{27} h \lambda_1 M^2 mM^2 \\
- 2C_{24}^2 C_{27} h \lambda_1 M^2 mM^2 + C_{22}^2 C_{27} h m M^4 + C_{24}^2 C_{27} h m M^4,
\end{aligned}$$

$$\begin{aligned}
C_{29} = & \frac{1}{8h(C_{25}(1 + \lambda_1)M^2 - C_{25}mM^2)^2} (C_{28} + 4(2 + C_{26}h^2)(C_{25}(1 + \lambda_1)M^2 - C_{25}mM^2)^2 \\
& + C_{27}(32C_{22}C_{24}(1 + \lambda_1)M^2mM^2 - (1 + 2h^2(1 \\
& + \lambda_1)M^2)(C_{22}(1 + \lambda_1)M^2 - C_{22}mM^2)^2 - (C_{24}(1 + \lambda_1)M^2 - C_{24}mM^2)^2(1 \\
& + 2h^2mM^2)) + C_{27}(C_{22}(1 + \lambda_1)M^2 - C_{22}mM^2)^2 \text{Cosh}(2h\sqrt{1 + \lambda_1}M) \\
& + C_{24}C_{27}(-8C_{22}\sqrt{1 + \lambda_1}MmM((1 + \lambda_1)M^2 + mM^2)\text{Cosh}(h(\sqrt{1 + \lambda_1}m - mM)) \\
& - 32C_{22}(1 + \lambda_1)M^2mM^2\text{Cosh}(h\sqrt{1 + \lambda_1}m)\text{Cosh}(hmM) \\
& + C_{24}(-(1 + \lambda_1)M^2 + mM^2)^2\text{Cosh}(2hmM) \\
& + 8C_{22}\sqrt{1 + \lambda_1}M^3mM\text{Cosh}(h(\sqrt{1 + \lambda_1}m + mM)) \\
& + 8C_{22}\lambda_1\sqrt{1 + \lambda_1}M^3mM\text{Cosh}(h(\sqrt{1 + \lambda_1}m + mM)) \\
& + 8C_{22}\sqrt{1 + \lambda_1}mmM^3\text{Cosh}(h(\sqrt{1 + \lambda_1}m + mM))),
\end{aligned}$$

$$C_{30} = \frac{-2C_{25}^2C_{26} + C_{22}^2C_{27}(1 + \lambda_1)M^2 + C_{24}^2C_{27}mM^2}{4C_{25}^2},$$

$$C_{31} = -\frac{C_{22}^2C_{27}}{8C_{25}^2},$$

$$C_{32} = -\frac{C_{24}^2C_{27}}{8C_{25}^2},$$

$$C_{33} = -\frac{C_{24}^2C_{27}}{8C_{25}^2},$$

$$C_{34} = -\frac{C_{22}C_{24}C_{27}MmM((1 + \lambda_1)^{3/2}M^2 - 2(1 + \lambda_1)MmM + \sqrt{1 + \lambda_1}mM^2)}{(C_{25}(1 + \lambda_1)M^2 - C_{25}mM^2)^2},$$

$$C_{35} = -2C_{25}^2C_{26} + C_{22}^2C_{27}(1 + \lambda_1)M^2 + C_{24}^2C_{27}mM,$$

$$\begin{aligned}
C_{36} = & -8C_{22}C_{24}C_{27}\lambda_1M^2mM^2Sc^3Sr\gamma^3\text{Cosh}(h\sqrt{1+\lambda_1}m)\text{Cosh}(hmM) + (4(1+\lambda_1)M^2 \\
& - Sc\gamma)((1+\lambda_1)^2M^4 + (mM^2 - Sc\gamma)^2 - 2(1+\lambda_1)M^2(mM^2 + Sc\gamma))((C_{35}Sr \\
& - 2C_{25}^2\gamma)(4mM^2 - Sc\gamma) + C_{24}^2C_{27}mM^2ScSr\gamma\text{Cosh}[(2hmM)]) - Sr(-C_{35}(4mM^2 \\
& - Sc\gamma)(-4(1+\lambda_1)^3M^6 + Sc\gamma(mM^2 - Sc\gamma)^2 + (1+\lambda_1)^2M^4(8mM^2 + 9Sc\gamma) \\
& - 2(1+\lambda_1)M^2(2mM^4 - 3mM^2Sc\gamma + 3Sc^2\gamma^2)) - C_{27}Sc\gamma(8C_{22}C_{24}(1 \\
& + \lambda_1)M^2mM^2(4(1+\lambda_1)M^2 - Sc\gamma)(4mM^2 - Sc\gamma) - C_{22}^2(1+\lambda_1)M^2(4mM^2 \\
& - Sc\gamma)((1+\lambda_1)^2M^4 + (mM^2 - Sc\gamma)^2 - 2(1+\lambda_1)M^2(mM^2 + Sc\gamma)) \\
& + C_{24}^2mM^2(-4(1+\lambda_1)^3M^6 + Sc\gamma(mM^2 - Sc\gamma)^2 + (1+\lambda_1)^2M^4(8mM^2 + 9Sc\gamma) \\
& - 2(1+\lambda_1)M^2(2mM^4 - 3mM^2Sc\gamma + 3Sc^2\gamma^2))))(\text{Cosh}(h\sqrt{Sc}\sqrt{\gamma}) \\
& + \text{Sinh}(h\sqrt{Sc}\sqrt{\gamma})) - C_{22}C_{27}MScSr\gamma(-C_{22}(1+\lambda_1)M(4mM^2 - Sc\gamma)((1+\lambda_1)^2M^4 \\
& + (mM^2 - Sc\gamma)^2 - 2(1+\lambda_1)M^2(mM^2 + Sc\gamma))\text{Cosh}(2h\sqrt{1+\lambda_1}M) \\
& - 4C_{24}mM(-2MmM(4(1+\lambda_1)^2M^2(4mM^2 - Sc\gamma) + Sc\gamma(-4(1+\lambda_1)mM^2 \\
& + Sc\gamma))\text{Cosh}(h\sqrt{1+\lambda_1}m)\text{Cosh}(hmM) + \sqrt{1+\lambda_1}(4(1+\lambda_1)m^2 - Sc\gamma)((1 \\
& + \lambda_1)M^2 + mM^2 - Sc\gamma)(4mM^2 - Sc\gamma)\text{Sinh}(h\sqrt{1+\lambda_1}m)\text{Sinh}[(hmM)]),
\end{aligned}$$

$$\begin{aligned}
C_{37} = & 2C_{25}^2(-1 + e^{2h\sqrt{Sc}\sqrt{\gamma}})\gamma(-4(1+\lambda_1)M^2 + Sc\gamma)(-4mM^2 + Sc\gamma)((1+\lambda_1)^2M^4 \\
& + (mM^2 - Sc\gamma)^2 - 2(1+\lambda_1)M^2(mM^2 + Sc\gamma)),
\end{aligned}$$

$$\begin{aligned}
C_{38} = & Sr * (C_{22}^2C_{27}(1+\lambda_1)M^2Sc\gamma(-4mM^2 + Sc\gamma)((1+\lambda_1)^2M^4 + (mM^2 - Sc\gamma)^2 - 2(1 \\
& + \lambda_1)M^2(mM^2 + Sc\gamma))),
\end{aligned}$$

$$C_{39} = (4(1+\lambda_1)M^2 - Sc\gamma)8C_{31}C_{33}C_{36}(1+\lambda_1)M^2mM^2Sc\gamma(4mM^2 - Sc\gamma)Sr,$$

$$\begin{aligned}
C_{40} = & (4(1+\lambda_1)M^2 - Sc\gamma)C_{24}^2C_{27}mM^2Sc\gamma((1+\lambda_1)^2M^4 + (mM^2 - Sc\gamma)^2 - 2(1+\lambda_1)M^2(mM^2 \\
& + Sc\gamma))Sr,
\end{aligned}$$

$$\begin{aligned}
C_{41} = & C_{35}(4(1+\lambda_1)M^2 - Sc\gamma)(4mM^2 - Sc\gamma)((1+\lambda_1)^2M^4 + (mM^2 - Sc\gamma)^2 - 2(1 \\
& + \lambda_1)M^2(mM^2 + Sc\gamma))Sr,
\end{aligned}$$

$$C_{42} = (Sr(1 + \lambda_1)M^2 - Sc\gamma)(4mM^2 - Sc\gamma)4C_{31}C_{33}C_{36}\sqrt{1 + \lambda_1}MmMSc\gamma((1 + \lambda_1)M^2 + mM^2 - Sc\gamma).$$

Some special case from the above solution can be obtain by

- The results of Newtonian viscous fluid can be found with $\lambda_1 = 0$.
- The above expressions for simple peristaltic flow over a planar channel of non-Newtonian fluid can be obtained by taking electrical field parameter (maximum electro-osmotic) $U_{HS} = 0$.
- The above expression can also be reduced for electro-kinetic peristaltic flow over a very thin Electric double layer (EDL) through electro-osmotic parameter $m \rightarrow \infty$.
- For $M = 0$ the above results reduces to the simple electro-kinetic peristaltic flow of non-Newtonian fluid.

Hence, the pressure gradient $\left(\frac{dp}{dx}\right)$ is calculated as

$$\frac{dp}{dx} = \frac{(1-C)\left(1+e^{2h\sqrt{1+\lambda_1}M}\right)hM^2\left((1+\lambda_1)M^2-m^2\right)m\sqrt{1+\lambda_1}MN}{m\left[CC_4\left(1+e^{2h\sqrt{1+\lambda_1}M}\right)h\sqrt{1+\lambda_1}M-\left(1+h\sqrt{1+\lambda_1}M+e^{2h\sqrt{1+\lambda_1}M}\left(-1+h\sqrt{1+\lambda_1}M\right)\right)\left((1+\lambda_1)M^2-m^2\right)N\right]} - \frac{C_4\left(1+e^{2h\sqrt{1+\lambda_1}M}\right)Qm\sqrt{1+\lambda_1}MN}{m\left[CC_4\left(1+e^{2h\sqrt{1+\lambda_1}M}\right)h\sqrt{1+\lambda_1}M-\left(1+h\sqrt{1+\lambda_1}M+e^{2h\sqrt{1+\lambda_1}M}\left(-1+h\sqrt{1+\lambda_1}M\right)\right)\left((1+\lambda_1)M^2-m^2\right)N\right]} \quad (6.23)$$

$$\frac{m\sqrt{1+\lambda_1}mN_1(-1+C)\left(-1+e^{2h\sqrt{1+\lambda_1}M}\right)\sqrt{1+\lambda_1}Mm^2U_{HS}+\sqrt{1+\lambda_1}MN_1C_3\left(1+e^{2h\sqrt{1+\lambda_1}M}\right)\sinh hm}{m\left[CC_4\left(1+e^{2h\sqrt{1+\lambda_1}M}\right)h\sqrt{1+\lambda_1}M-\left(1+h\sqrt{1+\lambda_1}M+e^{2h\sqrt{1+\lambda_1}M}\left(-1+h\sqrt{1+\lambda_1}M\right)\right)\left((1+\lambda_1)M^2-m^2\right)N\right]}.$$

The pressure rise is evaluated numerically using formula in Eq. (3.18)

6.4 Illustrations and discussion

In this section, the graphical results are presented for different emerging parameters in the governing flow problem. Graphical results are sketched in Fig. (6.2) - (6.16) for velocity distribution, temperature distribution, concentration distribution, pumping characteristics and streamlines. Numerical and analytical computations have been performed using a symbolic computational software *MATHEMATICA*.

Fig. (6.2) and (6.3) shows the variation of Hartman number M , electro-osmotic parameter m , particle volume fraction C and maximum electro-osmotic velocity U_{HS} for fluid velocity. From Fig. (6.2) that when magnetic field rises then a substantial decrement is noted in velocity distribution due to Lorence force. But it can be seen from this figure that electro-osmotic parameter m (which is inversely proportional to Debye length $\lambda_d \propto 1/m$), induce acceleration in the flow of a fluid markedly. It is observed from Fig. (6.3) that an enhancement in particle volume fraction C causes a considerable reduction in the velocity of the fluid as viscosity of the fluid increase. When U_{HS} increase it is clear from the figure that the flow behavior for single phase fluid is consistent but for $C \neq 0$ close to the center flow character is opposite when compare close to wall i.e. $y > 0.5$. Furthermore, the influence of electro-kinetic are associated with an electrostatic axial body force that attained an excellent hydrodynamic control as compared to Magnetohydrodynamics body force and such kinds of analysis are of significant importance to accurate manufacturing in micro pumps. In this figure, it is observed that an increment in electrical field parameter U_{HS} tends to rise the velocity profile significantly.

The behavior of temperature distribution $\theta_{f,p}$ shown in Fig. (6.4) - (6.6) for various involved parameters such as Hartman number M , Eckert number Ec , Prandtl number Pr , Electro-osmotic parameter m , particle volume fraction C and electrical field parameter U_{HS} . Fig. (6.4) reveals the variation of Eckert number on temperature profile. From Fig. (6.4) it is clear that increase

in Eckert number Ec greatly enhances the temperature distribution. Furthermore, the numerical values are appropriate for incompressible flows, however, with the large values of Eckert number are relevant to compressible and not appropriate for current study. Also in this figure, it can be seen that particle volume fraction C shows opposite trend for temperature distribution as particles are non-conducting. It depicts from Fig. (6.5) that an enhancement in Hartmann number M tends to enhance the temperature distribution greatly while the behavior for temperature distribution is reverse for the electro-osmotic parameter m . In Fig. (6.6) it is seen that an increment in Prandtl number Pr significantly enhances the temperature profile. The present results are deserved for those fluids which take high Prandtl number while reveal less important for those fluid which take a small Prandtl number. It depicts from Fig. (6.6) that electric field parameter U_{HS} markedly reduce the temperature profile.

Figs. (6.7) - (6.10) insights the variation of concentration distribution $\Phi_{f,p}$ against different values of Eckert number Ec , Schmidt number Sc , Chemical reaction parameter γ , Soret number Sr , particle volume fraction C , electric field parameter U_{HS} , electro-osmotic parameter m and Hartmann number M . It depicts from Fig. (6.7) that for large values of Eckert number Ec and Schmidt number Sc , the concentration distribution diminish. Since Schmidt number Sc describe the ratio between mass diffusivity and momentum diffusivity and is helpful to analyze the fluid flows in which there is concurrent mass and momentum diffusion process. Fig. (6.8) illustrates that an enhancement in Soret number Sr number tends to diminish the concentration distribution. The Soret effect also known as thermophoresis are applicable to liquid mixtures, which acts in a different and well-understood phenomena than gaseous mixtures. Furthermore, thermophoresis mechanism is applicable for thermo-migration in solids (i.e. multi-phase alloys). Fig. (6.8) also shows that with the increment in chemical reaction parameter γ concentration distribution tends to reduce. A chemical reaction has a significant role in concentration distribution and an increment in a chemical reaction are associated with the

interfacial mass transfer. For present study, it is considered $\gamma > 0$. Fig. (6.9) illustrates that with increase in particle volume fraction and electric field parameter significantly enhance the concentration distribution. In Fig. (6.10) Hartmann number rises then it provides a noticeable resistance to the concentration, however, electro-osmotic parameter m shows a favorable trend on concentration distribution.

The pumping mechanism is illustrated in Fig. (6.11) and (6.12) against particle volume fraction C , electro-osmotic parameter m , electric field parameter U_{HS} and Hartmann number M . Pressure rise Δp are estimated numerically using MATHEMATICA. Fig. (6.11) shows the variation of the particle volume fraction C and electric field parameter U_{HS} . It can be seen from this figure pumping rate increases due to the increment in electric field parameter U_{HS} in all the regions i.e. retrograde pumping region, free pumping region, and co-pumping region. However, the behavior in pumping rate is opposite due to the influence of particle volume fraction C . It depicts from Fig. (6.12) that an increment in Hartmann number M tends to enhance the pumping rate in a retrograde pumping region when $Q \in [-2, -1.1]$ and electro-osmotic parameter $m = 1$, while, the behavior become converse when $Q > -1.1$. It can also be seen here that when the electro-osmotic parameter $m = 6$ then the pumping rate rises only in the region when $Q \in [-2, -1.5]$ for all values of M whereas, it decreases for $Q > -1.5$. Peristaltic pumping is very helpful in a propagation of various kinds of fluids in a human body.

Trapping mechanism is viewed in form of streamlines. It is generally creation of internal circulating bolus enclosed by streamlines and it moves forward along with a peristaltic wave. Physically, this mechanism is very favorable for the creation of thrombus in blood and the propagation of food bolus i.e. in a gastrointestinal tract. For this purpose Fig. (6.13) to Fig. (6.16) shows streamlines for different physical emerging parameters such as particle volume fraction C , electro-osmotic parameter m , Hartmann number M and electric field parameter U_{HS} . Fig. (6.13) is sketched against different values of particle volume fraction. In this figure, it is

seen that an increment in particle volume fraction causes a significant increase in a number of a trapped bolus however the magnitude of the bolus varies very slowly. From Fig. (6.14), it illustrates that large values of Hartmann number M , trapping bolus significantly loses his magnitude also the number of boluses reduces. It depicts from Fig. (6.15) that electro-osmotic parameter m does not cause any major effect on contour lines. An increment in electro-osmotic parameter causes a slight effect on the magnitude of the bolus. Moreover, we can see in Fig. (6.16), that electric field parameter U_{HS} shows a major influence on contour lines as compared to electro-osmotic parameter m . The number of trapping bolus decreases significantly with the increment in electric field parameter U_{HS} .

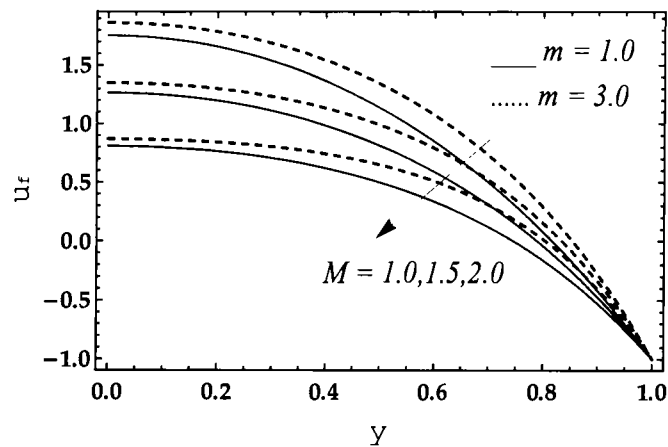


Fig. 6.2. Velocity distribution for various values of M and m .

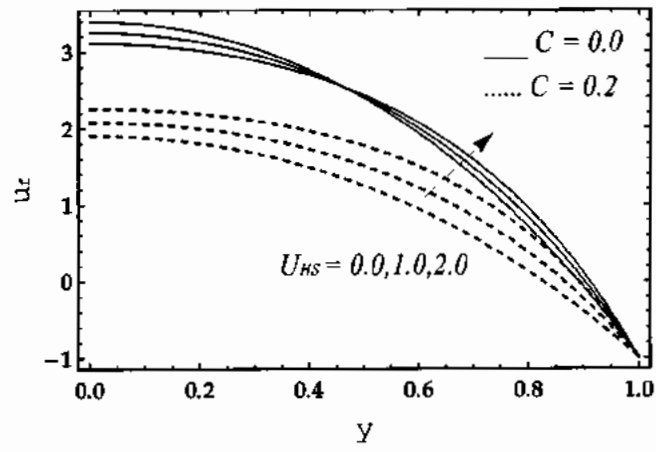


Fig. 6.3. Velocity distribution for various values of U_{HS} and C .

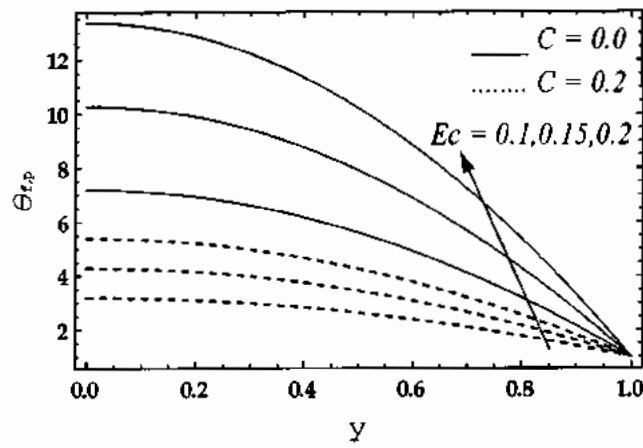


Fig. 6.4. Temperature distribution for various values of C and Ec .

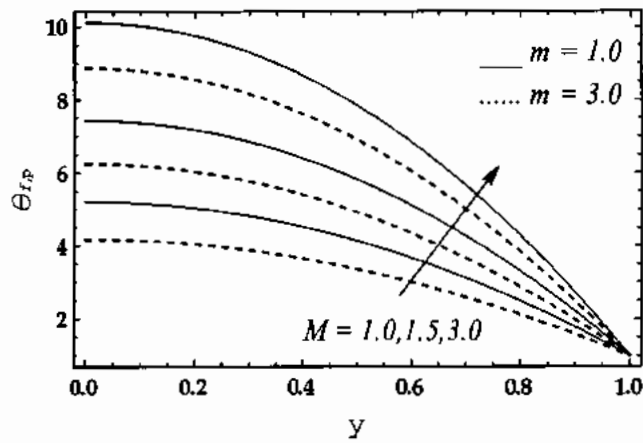


Fig. 6.5. Temperature distribution for various values of M and m .

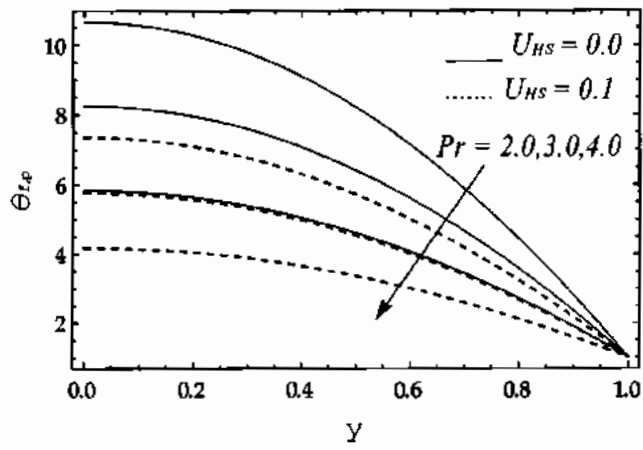


Fig. 6.6. Temperature distribution for various values of U_{HS} and Pr .

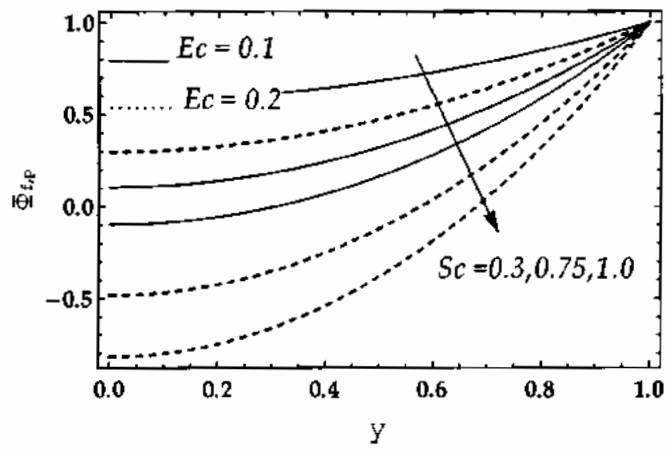


Fig. 6.7. Concentration distribution for various values of Sc and Ec .

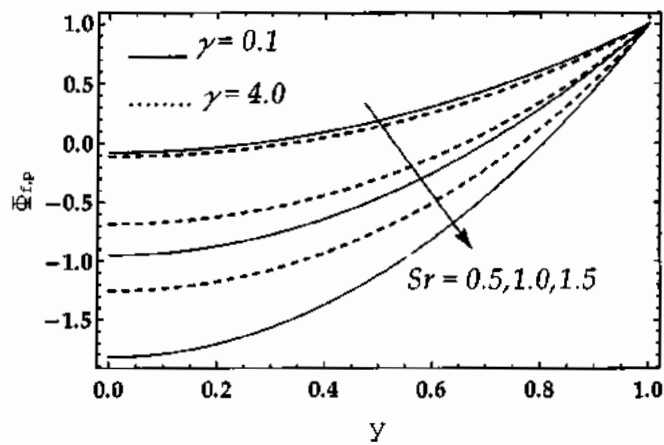


Fig. 6.8. Concentration distribution for various values of Sr and γ .

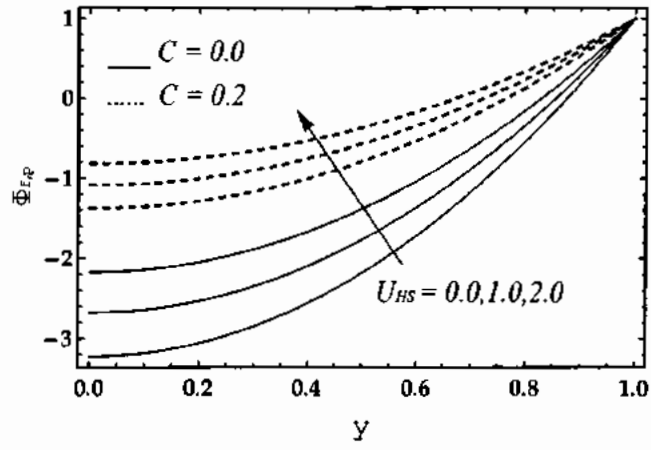


Fig. 6.9. Concentration distribution for various values of U_{HS} and C .

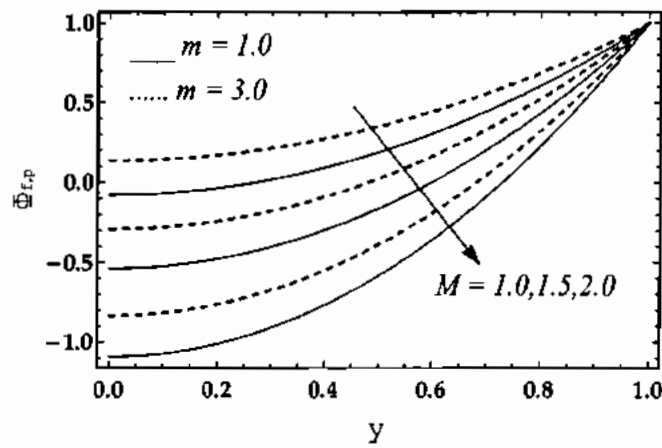


Fig. 6.10. Concentration distribution for various values of m and M .

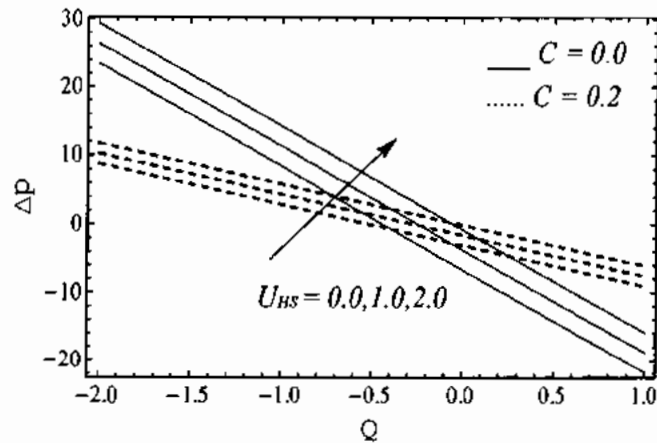


Fig. 6.11. Pressure rise vs. volumetric flow rate for various values of U_{HS} and C .

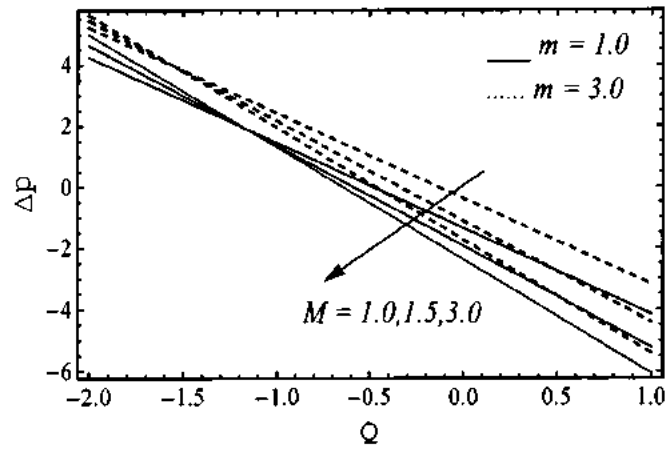


Fig. 6.12. Pressure rise vs. volumetric flow rate for various values of M and m .

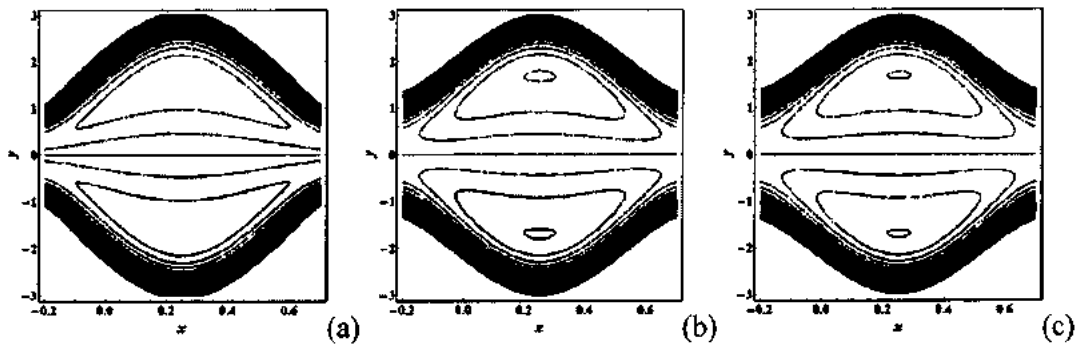


Fig. 6.13. Contour lines for multiple values of C . (a) 0, (b) 0.2, (c) 0.4.

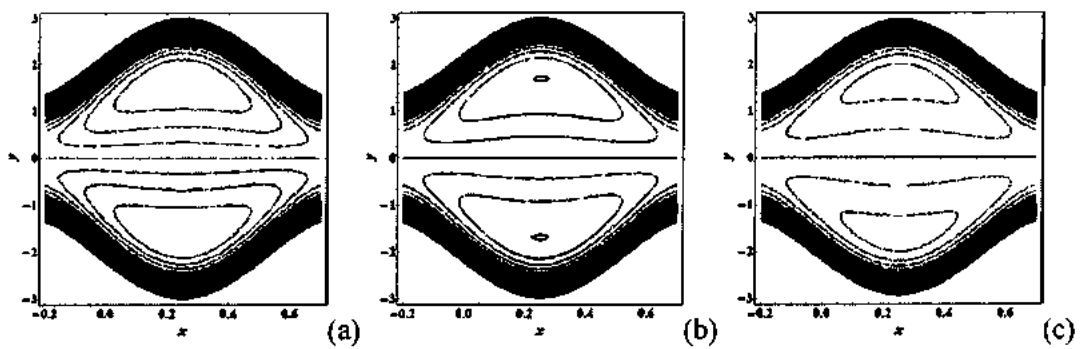


Fig. 6.14. Contour lines for multiple values of M . (a) 0.5, (b) 1, (c) 1.5.

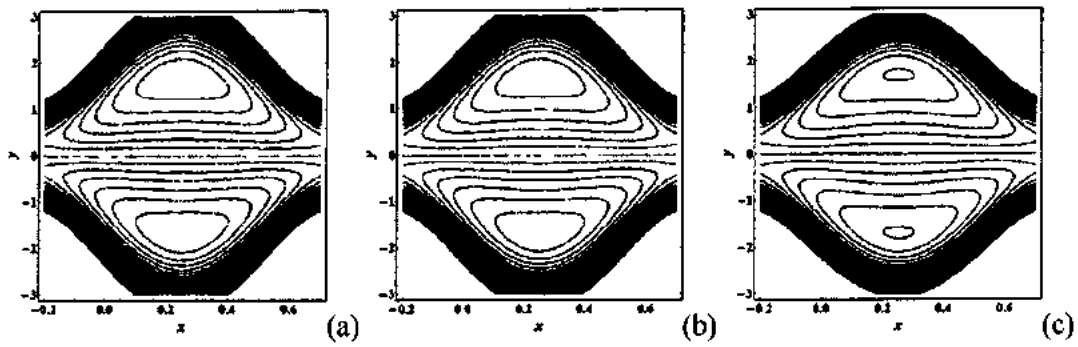


Fig. 6.15. Contour lines for multiple values of m . (a) 0, (b) 1, (c) 2.

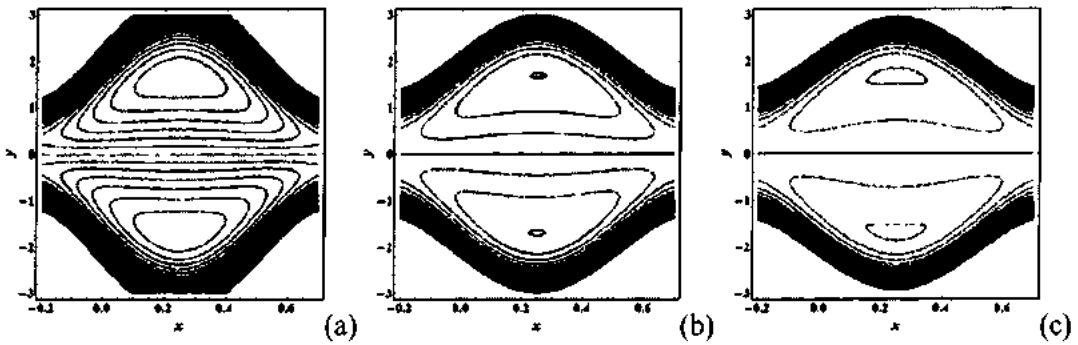


Fig. 6.16. Contour lines for multiple values of U_{HS} . (a) 0, (b) 1, (c) 2.

6.5 Conclusion

In this chapter, the peristaltic movement of heat and mass transfer with a transverse magnetic field induced motion of particle and fluid suspension (two-phase flow) through a planar channel has been investigated. Simultaneous effects of a static electric field and chemical are also taken into present study. To model the present model, Debye linearization and lubrication theory have been used. The effect of different parameters is taken into account with the help of graphs and streamlines. Following are some main finding of the study.

- Electric field and electro-osmotic parameter enhance the velocity distribution markedly.

- Temperature profile reduces significantly due to the increment in Electric field and electro-osmotic parameter.
- Prandtl number, Eckert number, and Hartmann number tend to increase the temperature profile, however, particle volume fraction depicts converse behaviour.
- Concentration profile decreases due to the increment in Schmidt number and Chemical reaction parameter.
- The Soret number and Hartmann number also shows a significant resistance in concentration distribution.
- Particle volume fraction and electric field parameter are favourable for a concentration distribution.
- Pumping rate increases in all the regions due to the influence of electric field and electro-osmotic parameter.
- Electric field parameter shows major influence on trapping and causes a reduction in trapping bolus.
- The present study can also be reduced to Newtonian fluid model by taking $\lambda_1 = 0$.

Chapter 7

Flow of particulate fluid in a rotating channel with wall properties and magnetic field

This chapter devoted to discuss the peristaltic flow of two phase fluids in a rotating channel with wall properties in the occurrence of magnetic field. Law of conservation of mass and momentum is used to formulate the problem. All the governing equations have been solved under the condition of low Reynolds number and long wavelength. The exact solution of coupled differential equations is obtained. The graphical aspects of fluid phase, particulate phase velocity and flow rates have been analyzed. The effects of pertinent parameters have been discussed.

7.1 Geometry of the problem

Consider a channel rotating about Z – axis and the plates are taken parallel to X – axis extended infinitely in Y – axis. A symmetric sinusoidal wave travels with the speed c in X direction described analytically in Eq. (4.1).

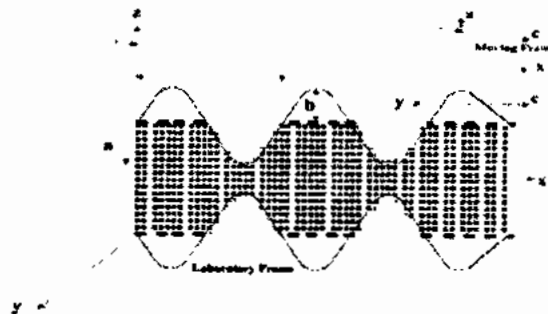


Fig. 7.1. Geometry of the problem.

7.2 Mathematical formulation

To define the velocity of flowing fluid

$$V = (U(X, Z, t), V(X, Z, t), W(X, Z, t)). \quad (7.1)$$

The velocities U , V and W having dimensions X and Z . Here, laminar incompressible Newtonian base fluid with small particles are assumed. A magnetic field is applied perpendicular to flow. Law of conservation of mass and momentum in component form is described in Eq. (7.2) - (7.9) for both fluid and particle phase.

$$\frac{\partial U_f}{\partial X} + \frac{\partial W_f}{\partial Z} = 0, \quad (7.2)$$

$$(1-C)\rho_f \left(\frac{\partial U_f}{\partial t} + U_f \frac{\partial U_f}{\partial X} + W_f \frac{\partial U_f}{\partial Z} \right) - 2\Omega V_f = -(1-C) \frac{\partial P}{\partial X} + (1-C)\mu_s \left(\frac{\partial^2 U_f}{\partial X^2} + \frac{\partial^2 U_f}{\partial Z^2} \right) + CS'(U_p - U_f) - \sigma B_0^2 U_f. \quad (7.3)$$

$$(1-C)\rho_f \left(\frac{\partial V_f}{\partial t} + U_f \frac{\partial V_f}{\partial X} + W_f \frac{\partial V_f}{\partial Z} \right) + 2\Omega U_f = -(1-C) \frac{\partial P}{\partial Y} + (1-C)\mu_s \left(\frac{\partial^2 V_f}{\partial X^2} + \frac{\partial^2 V_f}{\partial Z^2} \right) + CS'(V_p - V_f) \quad (7.4)$$

$$(1-C)\rho_f \left(\frac{\partial W_f}{\partial t} + U_f \frac{\partial W_f}{\partial X} + W_f \frac{\partial W_f}{\partial Z} \right) = -(1-C) \frac{\partial P}{\partial Z} + (1-C)\mu_s \left(\frac{\partial^2 W_f}{\partial X^2} + \frac{\partial^2 W_f}{\partial Z^2} \right) + CS'(W_p - W_f), \quad (7.5)$$

$$\frac{\partial U_p}{\partial X} + \frac{\partial W_p}{\partial Z} = 0, \quad (7.6)$$

$$C\rho_p \left(\frac{\partial U_p}{\partial t} + U_p \frac{\partial U_p}{\partial X} + W_p \frac{\partial U_p}{\partial Z} \right) = C \frac{\partial P}{\partial X} + CS'(U_f - U_p), \quad (7.7)$$

$$C\rho_p \left(\frac{\partial V_p}{\partial t} + U_p \frac{\partial V_p}{\partial X} + W_p \frac{\partial V_p}{\partial Z} \right) = C \frac{\partial P}{\partial Y} + CS'(V_f - V_p), \quad (7.8)$$

$$C\rho_p \left(\frac{\partial W_p}{\partial t} + U_p \frac{\partial W_p}{\partial X} + W_p \frac{\partial W_p}{\partial Z} \right) = C \frac{\partial P}{\partial Z} + CS'(W_f - W_p), \quad (7.9)$$

The equations are transform in wave frame using Eq. (2.9) and Eq. (3.8).

Using non-dimensional parameters defined in Eq. (2.10), (3.9) and (4.10) and simplifying using long wavelength and low Reynolds number, the governing equations become

$$\frac{dp}{dx} = 2\gamma^* v_f + \frac{\partial^2 u_f}{\partial z^2} - M^2(u_f + 1) + CM_1(u_p - u_f), \quad (7.10)$$

$$\frac{\partial^2 v_f}{\partial z^2} = 2\gamma^*(u_f + 1), \quad (7.11)$$

Where, $\gamma^* = \frac{R\Omega a}{c}$ is the Taylors number and for particulate phase

$$\frac{dp}{dx} = (1-C)M_1(u_f - u_p), \quad (7.11)$$

At $z = h(x, t) = 1 + \eta(x, t)$

Where $\eta(x, t) = \phi \cos 2\pi(x - t)$, $\phi = \frac{b}{a}$ (amplitude ratio) and $0 \leq \phi \leq 1$.

Represent the flexible wall with the governing equation described as:

$$\tilde{L}(\eta) = p - p_0 \quad (7.12)$$

The pressure on the external surface of the wall due to tension in the muscle is p_0 , which is taken as zero here. $z = 1 + \eta$ is the continuity of stress with x-momentum equation is used:

\tilde{L} is used an operator for the motion of stretched membrane of viscosity damping forces which is given below

$$\tilde{L} = \tilde{K} + \tilde{m} \frac{\partial^2}{\partial t^2} + \tilde{D} \frac{\partial}{\partial t} + \tilde{B} \frac{\partial^4}{\partial x^4} - \tilde{T} \frac{\partial^2}{\partial x^2}, \quad (7.13)$$

In the view of above equation, \tilde{K} , \tilde{m} , \tilde{D} , \tilde{B} and \tilde{T} is the spring stiffness, mass per unit area, the

coefficient of the viscous damping membrane, the flexural rigidity of the plate, the elastic tension is the membrane.

$$\frac{\partial p}{\partial x} = E_1 \frac{\partial^2 \eta}{\partial t^2 \partial x} + E_2 \frac{\partial^2 \eta}{\partial t \partial x} + E_3 \frac{\partial^5 \eta}{\partial x^5} - E_4 \frac{\partial^3 \eta}{\partial x^3} + E_5 \frac{\partial \eta}{\partial x} \quad (7.14)$$

$$E_1 \frac{\partial^2 \eta}{\partial t^2 \partial x} + E_2 \frac{\partial^2 \eta}{\partial t \partial x} + E_3 \frac{\partial^5 \eta}{\partial x^5} - E_4 \frac{\partial^3 \eta}{\partial x^3} + E_5 \frac{\partial \eta}{\partial x} = 2\gamma v_f + \frac{\partial^2 u_f}{\partial z^2} - M^2(u_f + 1) + CM_1(u_p - u_f) \quad (7.15)$$

$$E_1 \frac{\partial^2 \eta}{\partial t^2 \partial x} + E_2 \frac{\partial^2 \eta}{\partial t \partial x} + E_3 \frac{\partial^5 \eta}{\partial x^5} - E_4 \frac{\partial^3 \eta}{\partial x^3} + E_5 \frac{\partial \eta}{\partial x} = (1 - C)M_1(u_f - u_p) \quad (7.16)$$

At $z = 1 + \eta$, in which $E_1 = \frac{ma^3c}{\lambda^3\mu}$, $E_2 = \frac{Da^3}{\lambda^2\mu}$, $E_3 = \frac{Ba^3}{c\lambda^5\mu}$, $E_4 = \frac{Ta^3}{c\lambda^3\mu}$ and $E_5 = \frac{Ka^3}{\lambda\mu}$ are the non-

dimensional elasticity parameters.

Along with non-dimensional boundary conditions are describe

$$\frac{du_f}{dz}(0) = 0, \quad v_f(0) = 0, \quad (7.17)$$

$$u_f(h) = -1, \quad v_f(h) = 0. \quad (7.18)$$

7.3 Solution of the problem

The exact solution is represented as

$$u_f = \frac{(-8\gamma^*C_{45} + 4\gamma^*((-M^2 + C_{45})C_{43} + 4\gamma^*C_{44})\text{Cosh}(C_{47}z) + 4\gamma^*((M^2 + C_{45})C_{43} - 4\gamma^*C_{44})\text{Cosh}(C_{46}z))}{8\gamma^*T} \quad (7.19)$$

$$v_f = \frac{\left(-8\gamma^*C_{45} \left(\frac{dp}{dx} \right) - (-1 + C) \left(\begin{array}{l} 8\gamma^{*2} (4\gamma^*C_{45} - (M^2 + C_{45})C_{43}) \text{Cosh}(C_{47}z) C_{43} \\ -8\gamma^{*2} (4\gamma^*C_{45} + (-M^2 + C_{45})C_{43}) \text{Cosh}(C_{46}z) \end{array} \right) \right)}{(16(-1 + C)\gamma^{*2}C_{45})} \quad (7.20)$$

F_1 is the primary velocity and F_2 is the secondary velocity are defined, respectively,

$$F_1 = \frac{Q_f}{1 - C} = \int_0^h u_f dz \quad (7.21)$$

$$F_2 = \frac{Q_p}{C} = \int_0^h v_f dz \quad (7.22)$$

Where

$$C_{43} = \frac{-\left(\frac{\partial p}{\partial x} (\text{Cosh}(hC_{47}) - \text{Cosh}(hC_{46})) \text{Sech}[hC_{47}] \text{Sec}(hC_{46})\right)}{(T(-1+C))},$$

$$C_{44} = \frac{\frac{\partial p}{\partial x} (-M^2 \text{Cosh}(hC_{47}) + T \text{Cosh}(hC_{47}) + M^2 \text{Cosh}(hC_{46}) + T \text{Cosh}(hC_{46})) \text{Sech}(hC_{47}) \text{Sech}(hC_{46})}{4(\gamma^* T(-1+C))},$$

$$C_{45} = \sqrt{M^4 - 16\gamma^{*2}}$$

$$C_{46} = \frac{\sqrt{C_{45} + M^2}}{\sqrt{2}}$$

$$C_{47} = \frac{\sqrt{M^2 - C_{45}}}{\sqrt{2}}$$

7.4 Illustrations and discussion

In the above analysis, the simplified governing equations for peristaltic transportation of rotating particulate fluid having compliant walls has been solved in the existence of applied magnetic field. The exact solutions have been achieved for fluid and particulate phases velocity components. Also, the expressions for flow rates are measured for both the velocity profiles. In this section, it is discussed the graphical results which have been observed for different features of the problem under the prominent effects of pertinent parameters. Fig. (7.2) - (7.4) have been plotted to see the effects of particle volume fraction C , magnetic field M and rotation parameter γ^* on fluid phase velocity U_f . Fig. (7.5) - (7.7) describe the influence of all above mentioned parameters on particulate phase velocity U_p . Fig. (7.8) - (7.10) show the flow rate F_1 for the fluid phase and Fig. (7.11) - (7.13) are drawn for the flow rate F_2 for the particulate phase.

It has been observed from the Fig. (7.2) that fluid velocity decreases along axial direction x under the variation of C . It is also noted that the profile of velocity gets maximum altitude at the middle of channel. It illustrates from Fig. (7.3) that magnetic field causes slowing down of the flow due to Lorentz force. From Fig. (7.4), one can see that velocity is decreasing with the rising effects of rotation parameter γ^* which is evident that velocity reduces in the presence of rotation. From Fig. (7.5) to Fig. (7.7), it is seen that all the above discussed features are very similar for the particle phase velocity as that of seen in fluid phase velocity. The only difference which can be clearly verified from these figures is that the particulate phase velocity is relatively large as compared to fluid phase velocity for the same values of the parameters.

From Fig. (7.8), it can be easily reflected that fluid flow rate is decreasing in left half ($x = [0,0.5]$) of the axial length and increases in the right half ($x = (0.5,1]$) with the variation of C . It is depicted from Fig. (7.9) that for magnetic field, the results are quite opposite to that of C in both sides. However, the variation in left part is more prominent as compared to the other part. Almost same behavior is observed for rotation parameter as that of MHD parameter but here the variation is wider across the two halves of the axial coordinate x (see Fig. 7.10). It is also seen that the flow rate profile changes its concavity at the center i.e., $x = 0.5$. It can be seen from Fig. (7.11) that particulate flow rate increased in left part and decreased in right part under the increasing values of C . Fig. (7.12) denotes that the flow rate in left side is decreasing with the rise of magnetic field and decreases in the right side. It can be discussed from Fig. (7.13) that flow rate experiences opposite results with the variation of rotation parameter than that of measured in the case of magnetic field. It is also observed from Fig. (7.8) - (7.13) that fluid flow rate gets maximum value in the interval ($x = (0.5,1]$) and minimum in the interval ($x = [0,0.5]$) while particulate fluid flow rate reveals totally opposite situation.

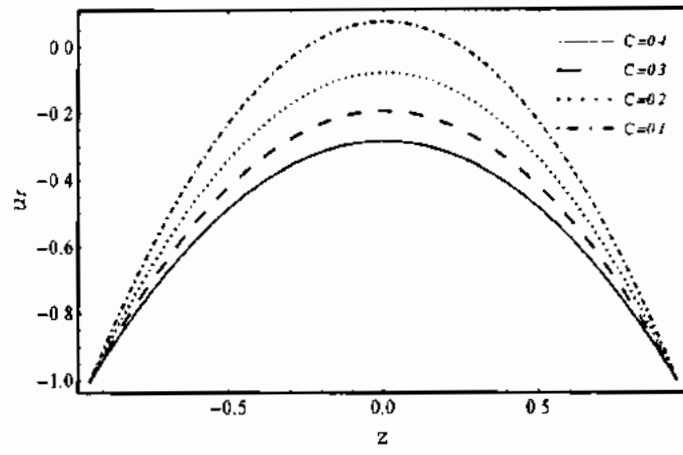


Fig. 7.2. Fluid velocity for various values of C .

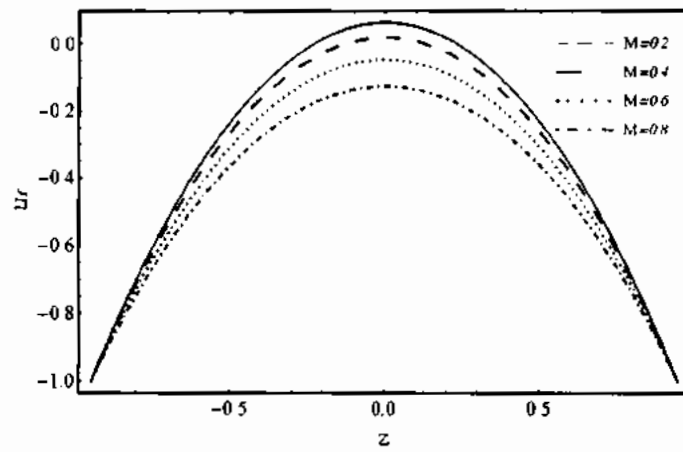


Fig. 7.3 Fluid velocity for various values of M .

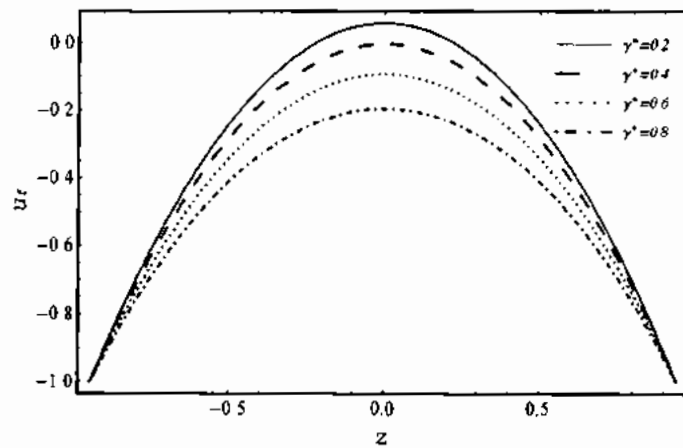


Fig. 7.4. Fluid velocity for various values of γ^* .

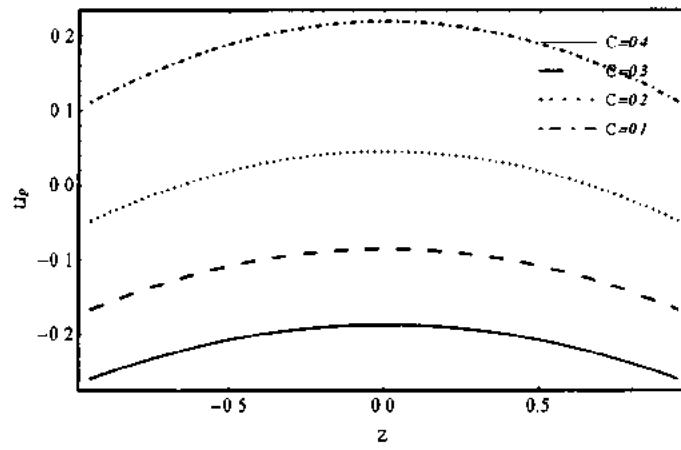


Fig. 7.5. Particulate velocity for various values of C .

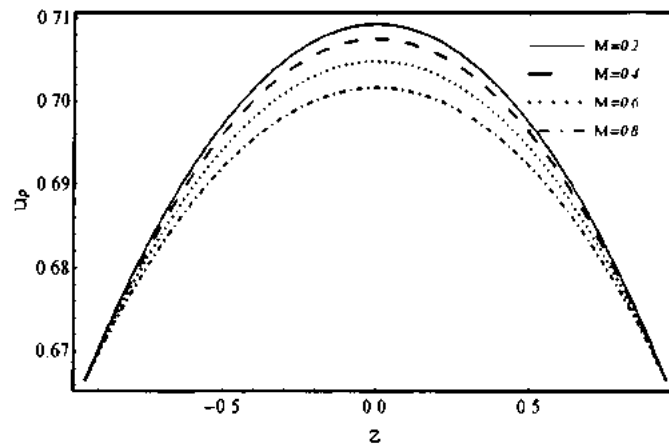


Fig. 7.6. Particulate velocity for various values of M .

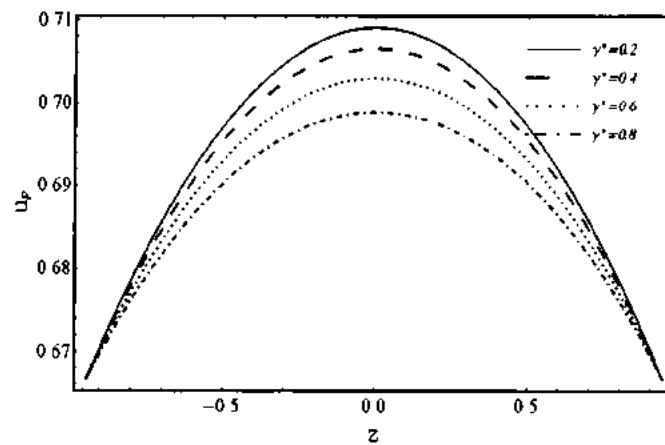


Fig. 7.7. Particulate velocity for various values of γ^* .

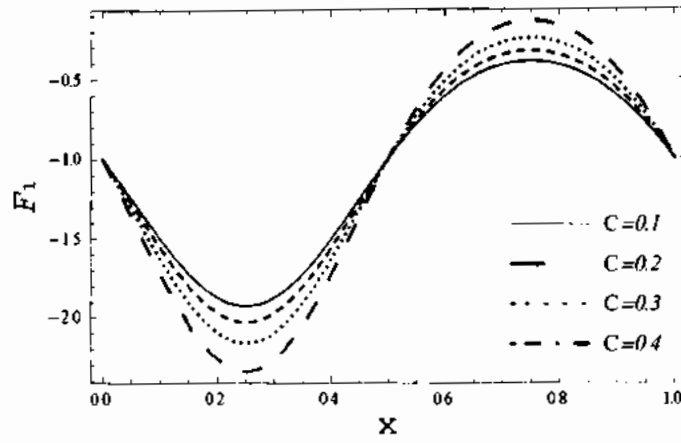


Fig. 7.8. Time-mean flow rate F_1 for various values of C .

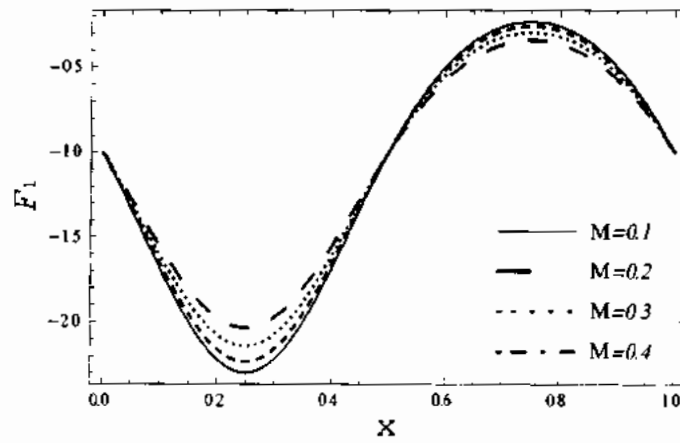


Fig. 7.9. Time-mean flow rate F_1 for various values of M .

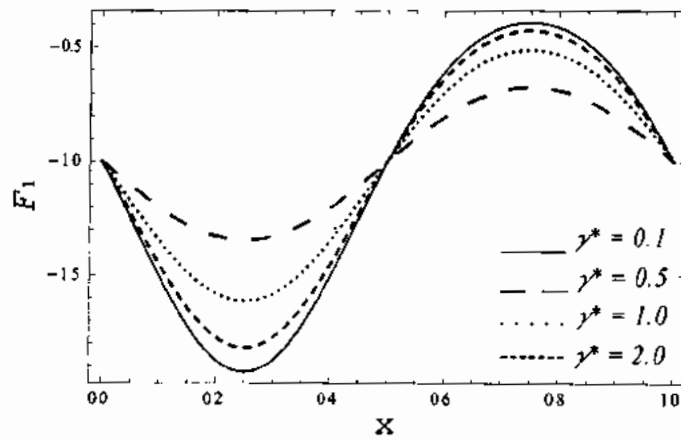


Fig. 7.10. Time-mean flow rate F_1 for various values of γ^* .

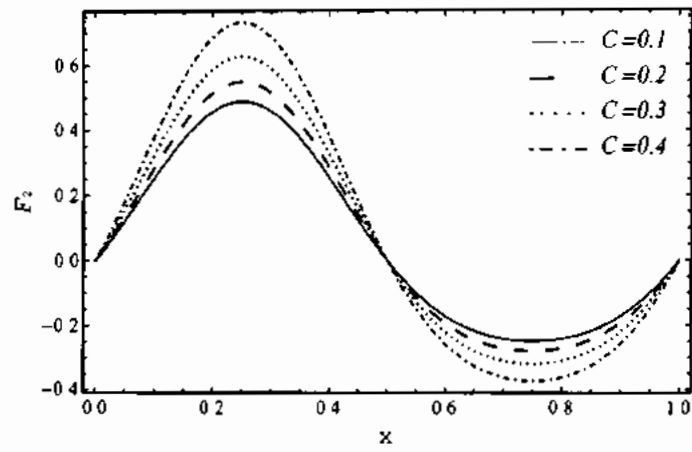


Fig. 7.11 Time-mean flow rate F_2 for various values of C .

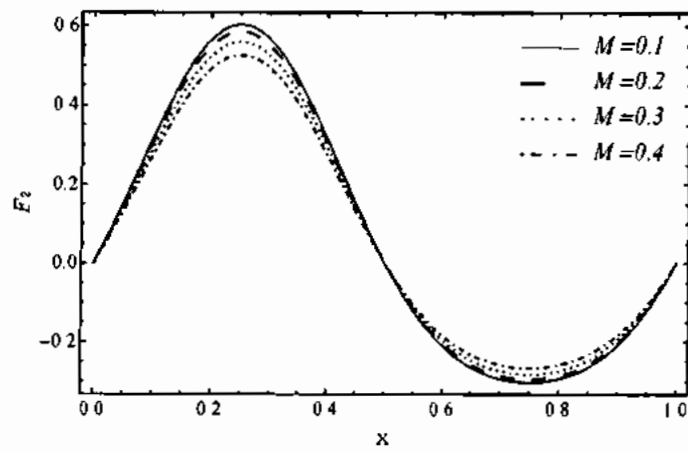


Fig. 7.12. Time-mean flow rate F_2 for various values of M .

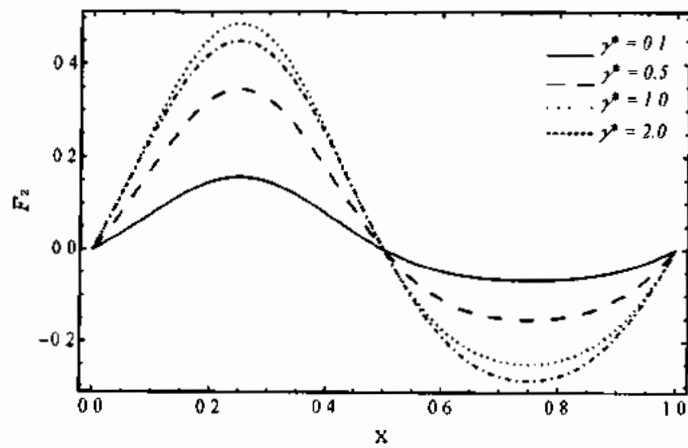


Fig. 7.13. Time-mean flow rate F_2 for various values of γ^* .

7.5 Concluding remarks

In this chapter peristaltic flow of two-phase fluid with particle volume fraction and magnetic field in the presence of compliant wall over a rotating disk is investigated. Exact solution obtained by the formulation of the differential equations. The main theme of the existing problem is summarized as follows.

- The different parameters applied, like non-uniform parameters and phase difference control the fluid transport phenomena.
- The axial velocity increases with different values of particle volume fraction.
- Velocity of magnetic field and rotation parameter are decreased.
- Time mean velocity increase with particle volume fraction in first half of channel whose opposite result for $x > 0.5$ is observed.
- A decrement is observed in F_1 when increasing values of Hartman number and rotation parameter.
- Rotation parameter positively secondary mean velocity.

Chapter 8

Flow of particulate fluid in a curved configuration with heat and mass transfer

This chapter addresses the influence of particulate-fluid suspension on asymmetric peristaltic motion through a curved configuration with mass and heat transfer. A strong motivation for current study are its applications, to examine the two-phase peristaltic motion between small muscles for different biological fluids can resemble the current geometry. The mathematical formulation of problem uses continuity, momentum, energy and mass transfer equations. Exact solutions are presented for velocity, temperature and concentration distributions. All the parameters such as Prandtl number, suspension parameter, particle volume fraction, curvature parameter, volumetric flow rate, Schmidt number, phase difference, Eckert number, and Soret number discussed graphically for peristaltic pumping, velocity, temperature and concentration distributions. The streamlines are also plotted with the aid of contour plots.

8.1 Geometry of the problem

Consider a curved channel centered at O . The center of channel have radius R and r is the distance from center at channel to walls, X is taken along the center line of channel. A sinusoidal wave move on both the walls described in equations. The geometry of walls are described mathematically as

$$\text{Upper wall:} \quad H_1(X,t) = a_1 \cos[2\pi X \lambda^{-1} - 2\pi \lambda^{-1} ct] + d_1, \quad (8.1)$$

$$\text{Lower wall:} \quad H_2(X,t) = b_1 \cos[2\pi X \lambda^{-1} + \Theta - 2\pi \lambda^{-1} ct] - d_2, \quad (8.2)$$

In above equation, the phase difference Θ' having range $0 \leq \Theta' \leq \pi$ whereas $\Theta' = \pi$ associated with a waves are in phase and $\Theta' = 0$ related to symmetric channel having waves out of phase. The other constants satisfies the following condition

$$a_1^2 + b_1^2 + 2a_1b_1 \cos \Theta' \leq (d_1 + d_2)^2. \quad (8.3)$$

Here, a_1 and b_1 is the amplitudes of the wave d_1 and d_2 are fixed distance of upper and lower wall from center of channel respectively.

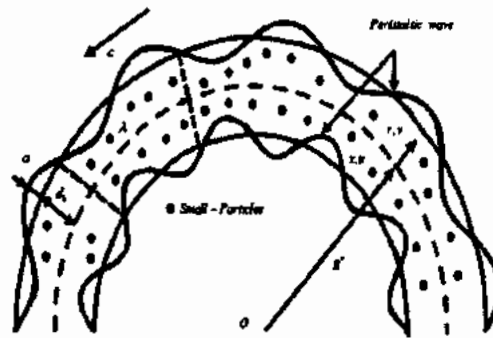


Fig. (8.1) Geometry of the problem

8.2 Mathematical formulation

Let us consider an asymmetric peristaltic transport of viscous fluid with incompressible, constant density and irrotational properties having small particles propagating with constant celerity. Equations for continuity, momentum, heat and mass transfer for Newtonian base fluid and particles are describe in Eq. (8.4) - (8.13).

$$\frac{\partial \left[(R + R') V_f \right]}{\partial R} + R' \frac{\partial U_f}{\partial X} = 0, \quad (8.4)$$

$$(1-C)\rho_f \left(\frac{\partial V_f}{\partial t} + V_f \frac{\partial V_f}{\partial R} + \frac{U_f R^*}{R+R^*} \frac{\partial V_f}{\partial X} + \frac{U_f^2}{R+R^*} \right) = -(1-C) \frac{\partial P}{\partial R} + \frac{2\mu_s(1-C)}{(R+R^*)^2} \frac{\partial}{\partial R} \left[\frac{\partial V_f}{\partial R} (R^*+R) \right] + \frac{\mu_s(R^*-R^*C)}{(R^*+R)} \frac{\partial}{\partial X} \left(\frac{\partial U_f}{\partial R} + \frac{R^*}{R^*+R} \frac{\partial V_f}{\partial X} - \frac{U_f}{R^*+R} \right) - (1-C) \left(\frac{2\mu_s}{R+R^*} \right) \left(\frac{R^*}{R^*+R} \frac{\partial U_f}{\partial X} + \frac{V_f}{R^*+R} \right) + CS'(V_p - V_f), \quad (8.5)$$

$$(1-C)\rho_f \left(\frac{\partial U_f}{\partial t} + V_f \frac{\partial U_f}{\partial R} + \frac{R^*}{R^*+R} U_f \frac{\partial U_f}{\partial X} + \frac{U_f V_f}{R+R^*} \right) = -\frac{R^*(1-C)}{R+R^*} \frac{\partial P}{\partial X} + \frac{\mu_s(1-C)}{(R+R^*)^2} \frac{\partial}{\partial R} \left[\frac{\partial U_f}{\partial R} (R^*+R)^2 \right] + (1-C) \frac{\mu_s}{(R+R^*)^2} \frac{\partial}{\partial R} \left[\left(\frac{R^*}{R^*+R} \frac{\partial V_f}{\partial X} - \frac{U_f}{R+R^*} \right) (R^*+R)^2 \right] + (1-C) \left(\frac{2\mu_s R^*}{R^*+R} \right) \frac{\partial}{\partial X} \left[\left(\frac{\partial U_f}{\partial X} \frac{R^*}{R^*+R} + \frac{V_f}{R^*+R} \right) \right] + CS'(U_p - U_f), \quad (8.6)$$

$$(1-C)\rho_f c_p \left(\frac{\partial T_f}{\partial t} + V_f \frac{\partial T_f}{\partial R} + \frac{U_f R^*}{R+R^*} \frac{\partial T_f}{\partial X} \right) = k_p (1-C) \left(\frac{\partial^2 T_f}{\partial R^2} + \frac{1}{R^*+R} \frac{\partial T_f}{\partial R} + \left(\frac{R^*}{R^*+R} \right)^2 \frac{\partial^2 T_f}{\partial X^2} \right) + \rho_f c_p C (T_p - T_f) + CS'(U_f - U_p)^2, \quad (8.7)$$

$$(1-C) \left(\frac{\partial F_f}{\partial t} + V_f \frac{\partial F_f}{\partial R} + \frac{U_f R^*}{R+R^*} \frac{\partial F_f}{\partial X} \right) = D_m (1-C) \left(\frac{\partial^2 F_f}{\partial R^2} + \frac{1}{R^*+R} \frac{\partial F_f}{\partial R} + \frac{\partial^2 F_f}{\partial X^2} \left(\frac{R^*}{R^*+R} \right)^2 \right) + \frac{D_m}{T_m} (k_T - k_T C) \left(\frac{\partial^2 T_f}{\partial R^2} + \frac{1}{R+R^*} \frac{\partial T_f}{\partial R} + \left(\frac{R^*}{R+R^*} \right)^2 \frac{\partial^2 T_f}{\partial X^2} \right) + \rho_f c_p CS'(F_p - F_f), \quad (8.8)$$

$$\frac{\partial \left[(R^* V_p + R V_p) \right]}{\partial R} + \frac{\partial U_p}{\partial X} R^* = 0, \quad (8.9)$$

$$\rho_p \left(C \frac{\partial V_p}{\partial t} + C \frac{\partial V_p}{\partial R} V_p + C \frac{U_p R^*}{R^*+R} \frac{\partial V_p}{\partial X} + C \frac{U_p^2}{R+R^*} \right) = -C \frac{\partial P}{\partial R} - S'C (V_p - V_f), \quad (8.10)$$

$$\rho_p \left(C \frac{\partial U_p}{\partial t} + V_p C \frac{\partial U_p}{\partial R} + \frac{R^* C}{R^*+R} U_p \frac{\partial U_p}{\partial X} + \frac{U_p C U_p}{R^*+R} \right) = -\frac{R^* C}{R^*+R} \frac{\partial P}{\partial X} + S'C (U_f - U_p), \quad (8.11)$$

$$\rho_f c_p C \left(\frac{\partial T_p}{\partial t} + V_p \frac{\partial T_p}{\partial R} + \frac{U_p R^*}{R+R^*} \frac{\partial T_p}{\partial X} + \frac{U_p V_p}{R+R^*} \right) = \rho_f c_p C (T_p - T_f), \quad (8.12)$$

$$\rho_p C \left(\frac{\partial F_p}{\partial t} + V_p \frac{\partial F_p}{\partial R} + \frac{R^*}{R+R^*} U_p \frac{\partial F_p}{\partial X} + \frac{U_p V_p}{R+R^*} \right) = \rho_p c_p C (F_f - F_p). \quad (8.13)$$

The equations are transform in wave frame using Eq. (2.9) and Eq. (3.8).

Non-dimensional parameter are in Eq. (2.10), (3.9), (4.10), (6.12) and

$$k = \frac{R^*}{d}, h_1^* = \frac{\bar{h}_1}{d_1}, NA = SrSc, h_2^* = \frac{\bar{h}_2}{d_1}, d^* = \frac{\bar{d}_2}{d_1}, a^* = \frac{\bar{a}_1}{d_1}, b^* = \frac{\bar{b}_1}{d_1}. \quad (8.14)$$

Along with assumption that wave length as long and flow creeping all the interial term tends to zero. The governing equations (8.4) – (8.13) becomes

$$\frac{dp}{dx} = \left(\frac{k+r}{k} \right) \left(\frac{1}{k+r} \frac{\partial}{\partial r} \left(\frac{\partial u_f}{\partial r} (k+r)^2 \right) + \frac{\partial}{\partial r} \left(-\frac{u_f}{r+k} (k+r)^2 \right) \right) + M_1 C (u_p - u_f), \quad (8.15)$$

$$\frac{\partial^2 \theta_f}{\partial r^2} + \frac{1}{(k+r)} \frac{\partial \theta_f}{\partial r} = -Pr M_1 (\theta_p - \theta_f) - \left(\sqrt{Pr Ec M_1 C} u_p - \sqrt{Pr Ec M_1 C} u_f \right)^2, \quad (8.16)$$

$$\frac{\partial^2 \phi_f}{\partial r^2} + \frac{1}{(k+r)} \frac{\partial \phi_f}{\partial r} + NA \left(\frac{\partial^2 \theta_f}{\partial r^2} + \frac{1}{(r+k)} \frac{\partial \theta_f}{\partial r} \right) = -C M_1 (\phi_p - \phi_f), \quad (8.17)$$

$$\frac{dp}{dx} = (1-C) M_1 (u_f - u_p). \quad (8.18)$$

Along with boundary conditions

$$\left. \begin{aligned} u_f(h_1) &= -1 \\ u_f(h_2) &= -1 \\ \theta_f(h_1) &= 1, \theta_f(h_2) = 0, \\ \phi_f(h_1) &= 1, \phi_f(h_2) = 0. \end{aligned} \right\} \quad (8.19)$$

Where

$$\left. \begin{aligned} h_1(x) &= 1 + a \cos(x), \\ h_2(x) &= -b - d \cos(x + \Theta^*) \end{aligned} \right\} \quad (8.20)$$

8.3 Solution of the problem

Exact solution of fluid and particle phase are obtained as

$$u_f = \frac{C_{48} + C_{49}r + C_{50}r^2 + C_{51}r^3 + C_{52} \log(r+k) + C_{53}r \log(r+k) + C_{54}r^2 \log(r+k)}{r+k}, \quad (8.21)$$

$$u_p = \frac{C_{48} + C_{49}r + C_{50}r^2 + C_{51}r^3 + C_{52} \log(r+k) + C_{53}r \log(r+k) + C_{54}r^2 \log(r+k)}{r+k} - \frac{1}{(1-C)M_1} \frac{dp}{dx}, \quad (8.22)$$

$$\theta_{f,p} = C_{55} + C_{56} \log(r+k) + C_{57}r + C_{58}r^2, \quad (8.23)$$

$$\phi_{f,p} = C_{59} + C_{60} \log(r+k) + C_{61}r + C_{62}r^2, \quad (8.24)$$

Where

$$C_{48} = \frac{2k(h_1 - h_2) \left[6 + C \left(-6 + \frac{dp}{dx} \{ 3k(h_1 + h_2) + 2(h_1^2 + h_1h_2 + h_2^2) \} \right) \right]}{6(-1+C)(h_1 - h_2)(2k + h_1 + h_2)} + \frac{\frac{dp}{dx} 3(-1+C)k \left[(k + h_1)^2 h_2 \log(h_1 + k)(h_2 + 2k) - (2kh_1 + h_1^2)(h_2 + k)^2 \log(h_1 + k) \right]}{6(-1+C)(h_1 - h_2)(2k + h_1 + h_2)},$$

$$C_{49} = \frac{(-h_2 + h_1) \left[3 + C \left\{ -3 + \frac{dp}{dx} (-3k^2 + h_1^2 + h_1h_2 + h_2^2) \right\} \right]}{3(-1+C)(h_1 - h_2)(2k + h_1 + h_2)} + \frac{3(1-C)k^2 \frac{dp}{dx} \left[(k + h_1)^2 \log(h_1 + k) - (h_2 + k)^2 \log(h_2 + k) \right]}{3(-1+C)(-h_2 + h_1)(2k + h_1 + h_2)},$$

$$C_{50} = \frac{\frac{dp}{dx} -2C(h_1 - h_2)(2k + h_1 + h_2) + 3(1-C) \left[k(k + h_1)^2 \log(h_1 + k) - (h_2 + k)^2 k \log(h_2 + k) \right]}{6(-1+C)(h_1 - h_2)(2k + h_1 + h_2)},$$

$$C_{51} = \frac{C}{3(1-C)},$$

$$C_{52} = k^2 \frac{dp}{dx},$$

$$C_{53} = \frac{\frac{dp}{dx} k^3 \left((-1+C)(h_1 - h_2)(h_1 + h_2) + 2k \left((-1+C)h_1 + h_2 - Ch_2 \right) \right)}{2(-1+C)(h_1 - h_2)(2k + h_1 + h_2)},$$

$$C_{54} = \frac{k}{2} \frac{dp}{dx},$$

$$C_{55} = \frac{\left(4 + CEcM_1 \left(\frac{dp}{dx} \right)^2 \text{Pr} h_2 (2k + h_2) \right) \log k + h_1 - CEcM_1 \left(\frac{dp}{dx} \right)^2 (2 \text{Pr} h_1 k + \text{Pr} h_1 h_1) \log(k + h_2)}{4(\log k + h_1 - \log(k + h_2))},$$

$$C_{56} = \frac{-4 + CEcM_1 \left(\frac{dp}{dx} \right)^2 \text{Pr} (h_1 - h_2) (2k + h_1 + h_2)}{4 (\log(k + h_1) - \log(k + h_2))}$$

$$C_{57} = -\frac{1}{2} CEcM_1 k \left(\frac{dp}{dx} \right)^2 \text{Pr},$$

$$C_{58} = -\frac{1}{2} CEcM_1 \left(\frac{dp}{dx} \right)^2 \text{Pr},$$

$$C_{59} = \frac{-\left(-4 + CEcM_1 NA \left(\frac{dp}{dx} \right)^2 \text{Pr} h_2 (2k + h_2) \right) \log(k + h_1) - CEcM_1 \left(\frac{dp}{dx} \right)^2 NA \text{Pr} h_1 (2k + h_1) \log(k + h_2)}{4 (\log(k + h_1) - \log(k + h_2))}$$

$$C_{60} = \frac{-4 + CEcM_1 NA \left(\frac{dp}{dx} \right)^2 \text{Pr} (h_1 - h_2) (2k + h_1 + h_2)}{4 (\log(k + h_1) - \log(k + h_2))}$$

$$C_{61} = -\frac{NA}{2} CEcM_1 k \left(\frac{dp}{dx} \right)^2 \text{Pr},$$

$$C_{62} = -\frac{NA}{2} CEcM_1 \left(\frac{dp}{dx} \right)^2 \text{Pr},$$

The rate of volume flow is given by

$$Q = \int_{h_1}^{h_2} u_f (1 - C) dr + \int_{h_1}^{h_2} u_p C dr, \quad (8.25)$$

Pressure gradient is represented as,

$$\begin{aligned} \frac{dp}{dx} = & \frac{36(-1+C)M_1(h_1-h_2) \left(-(h_2+Q-h_1)(h_1+2k+h_2) + 2(h_1+k)(h_2+k) \log\left(\frac{k+h_1}{k+h_2}\right) \right)}{(h_1-h_2)^2(2k+h_1+h_2) \left(36+M_1 \left\{ -6(-3+C)k^2 + 3(3+C)k(h_1+h_2) + 4C(h_1^2+h_1h_2+h_2^2) \right\} \right)} + \\ & \frac{36(-1+C)M_1(h_1-h_2) \left(-(Q+h_2-h_1)(h_1+h_2+2k) + 2(h_1+k)(h_2+k) \log\left(\frac{k+h_1}{k+h_2}\right) \right)}{12M_1(h_1+k)^2 \left(2C(h_2-h_1)(h_2+k)^2 + (h_2+k)^2 3(-1+C)k \log\left(\frac{k+h_1}{k+h_2}\right) \log\left(\frac{k+h_1}{k+h_2}\right) \right)} \end{aligned} \quad (8.26)$$

The pressure rise is evaluated numerically using formula in Eq. (3.18)

8.4 Illustrations and discussion

The aim of this section is to see the variation of different parameters on peristaltic pumping (Δp), streamlines, velocity ($u_{f,p}$), pressure gradient (dp/dx), temperature ($\theta_{f,p}$) and concentration distributions ($\phi_{f,p}$). Numerical computation is used by *shooting algorithm* in *MATHEMATICA* software. Particularly, we explored the variation of physical quantities i.e. particle volume fraction C , suspension parameter M_1 , curvature parameter k , volumetric flow rate Q , phase difference Θ' , Prandtl number Pr , Eckert number Ec , Schmidt number Sc and Soret number Sr , respectively.

Fig. (8.2) and (8.3) depict the variation of particle volume fraction C on velocity profiles. It reveals from both figures that due to increment in the value of C , the variation in velocity is very small, however, velocity of fluid acts oppositely close the curvy walls. In the presence of solid particles, the drag force rises and there is retardation in the flow. Fig. (8.4) and (8.5) indicates that large values of curvature parameter k tends to resist the flow markedly whereas, it is opposite close to the wall $r > 0.1$, it fails to produce a significant resistance and as a result, the velocity of the fluid rises. Fig. (8.6) and (8.7) is drawn to visualize the pumping features. In Fig. (8.6) it is observed that the magnitude of pumping rate is very high in peristaltic pumping region as well as in retrograde pumping and increases for higher values of particle volume fraction C . However, its attitude becomes reverse at $Q = 0.6$ and reveals opposite influence in the co-pumping region. It is clear from Fig. (8.7) that suspension parameter M_1 significantly enhances the pressure rise in retrograde and peristaltic pumping regions while its behavior becomes converse at $Q = 0.5$ and depicts opposite behavior in the co-pumping region.

Fig. (8.8) - (8.10) represents the temperature distributions consists of the present results. From Fig. (8.8) and (8.9), it is concluded that particle volume fraction C and curvature

parameter k markedly enhance the temperature profile. Fig. (8.10) shows the variation of Prandtl number Pr and Eckert number Ec on temperature distribution. In this figure, we can see that both the parameters enhances the temperature. Inspection of Fig. (8.10) also reveals that when Prandtl number is high, then thermal diffusivity is more prominent on momentum diffusivity.

Fig. (8.11) - (8.14) are plotted for concentration distributions to see the physical effects of involved parameters. It can be viewed from Fig. (8.11) that concentration distribution significantly diminishes due to a greater influence of particle volume fraction. However, for large values of curvature parameter, concentration distribution markedly rises (see Fig. (8.12)). From Fig. (8.13) it can be seen that higher values of Eckert number and Prandtl number produces a marked reduction in a concentration distribution. Fig. (8.14) is plotted for $NA(=ScSr)$ (product of Schmidt number and Soret number) . Schmidt number $Sc\left(=\frac{\mu_s}{\rho D_m}\right)$ is the ratio b/w momentum and mass diffusivity and it is beneficial to determine the convection process of mass & momentum diffusion. This figure reveals that an increment in NA tends to resists the concentration distribution. It happens because mass diffusivity becomes more dominated over momentum diffusivity and due to higher soret number, the particles move to cold region from hot region and as a result, the concentration distribution diminish.

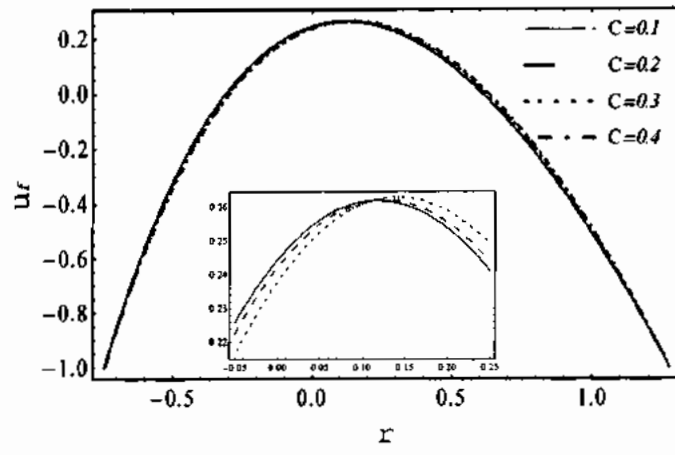


Fig 8.2. Fluid velocity for multiple values of C .

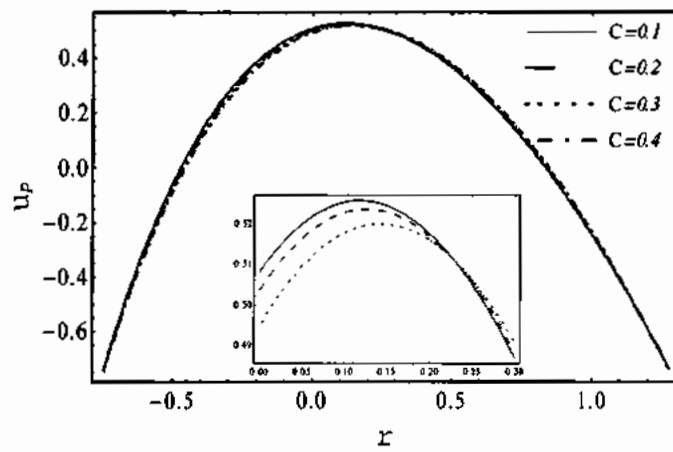


Fig 8.3. Particulate velocity for multiple values of C .

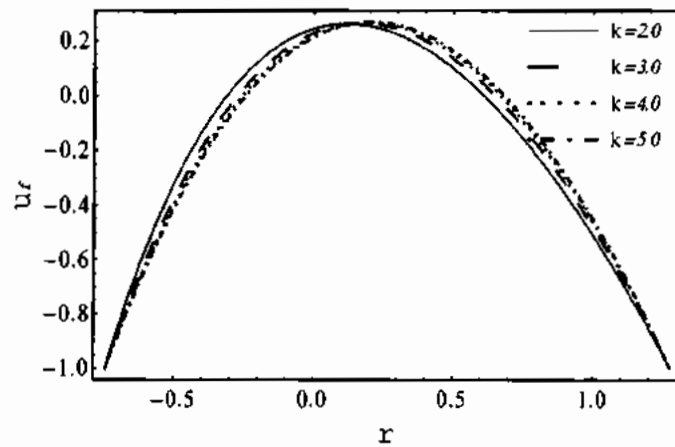


Fig 8.4. Fluid velocity for multiple values of k .

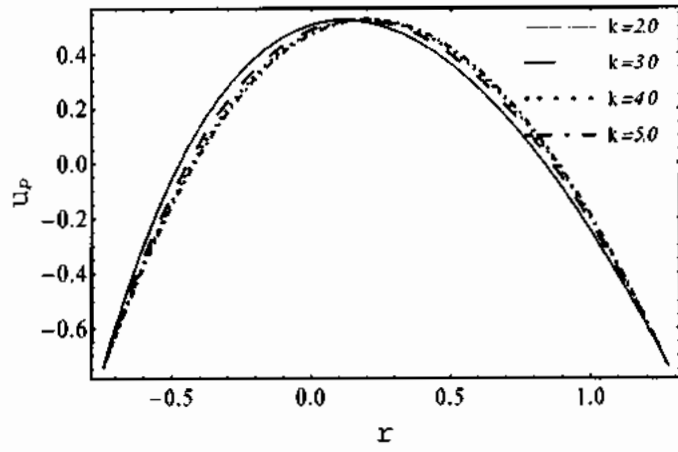


Fig 8.5. Particulate velocity for various values of k .

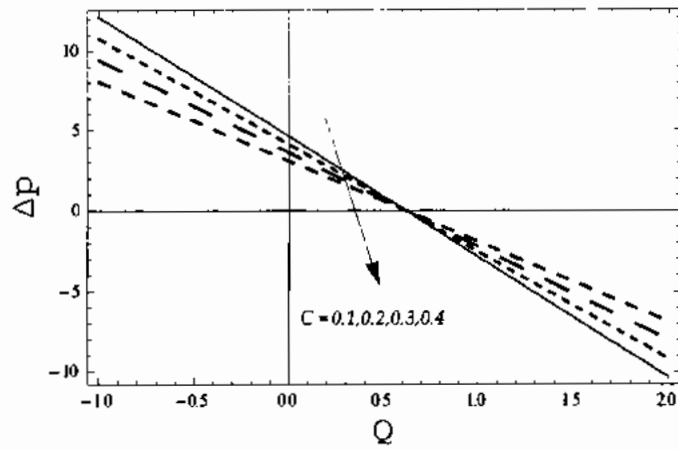


Fig. 8.6. Pressure rise vs. volume flow rate for various values of C .

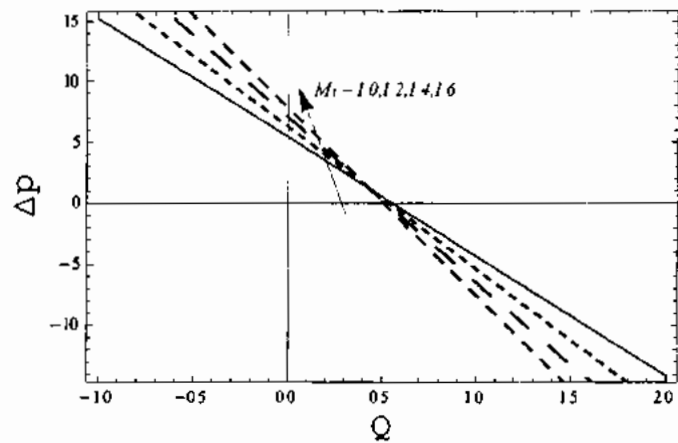


Fig. 8.7. Pressure rise vs. volume flow rate for various values of M_1 .

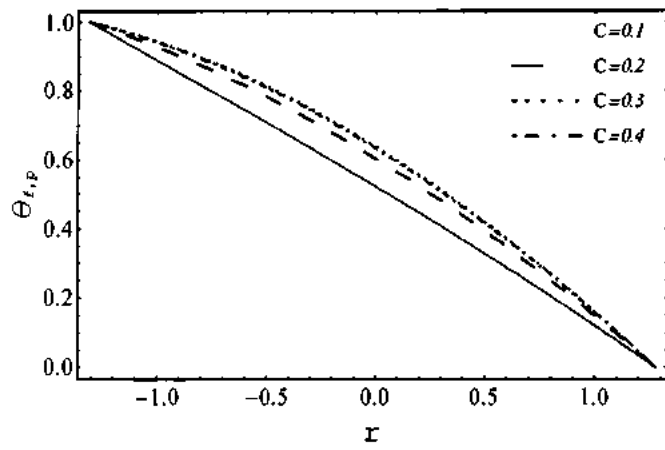


Fig 8.8. Temperature profile for various values of C .

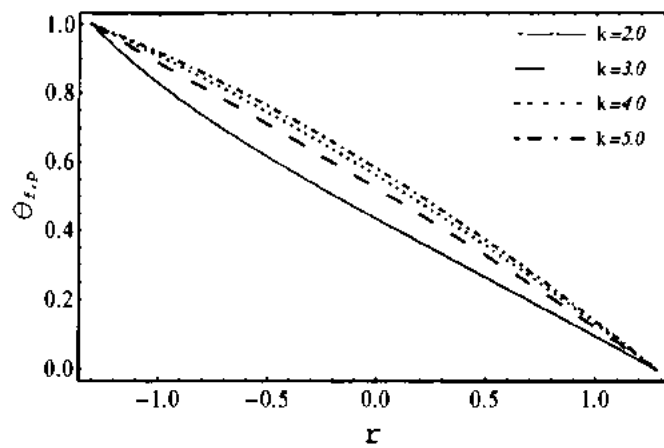


Fig 8.9. Temperature profile for multiple values of k .

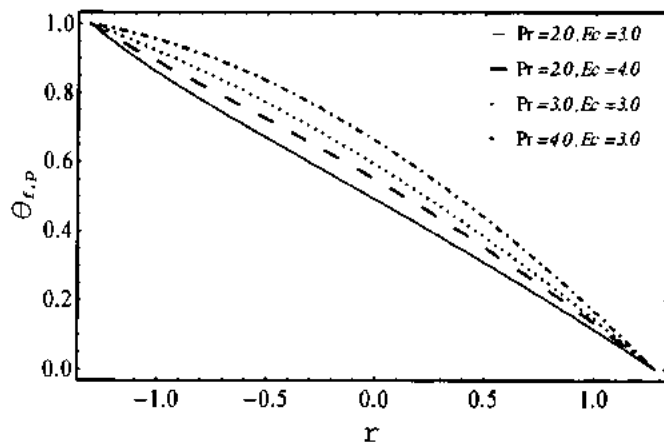


Fig 8.10. Temperature profile for multiple values of Pr and Ec .

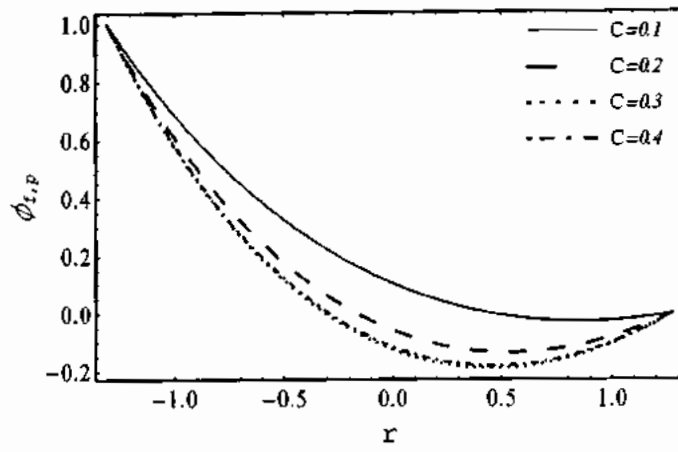


Fig 8.11. Temperature profile for multiple values of C .

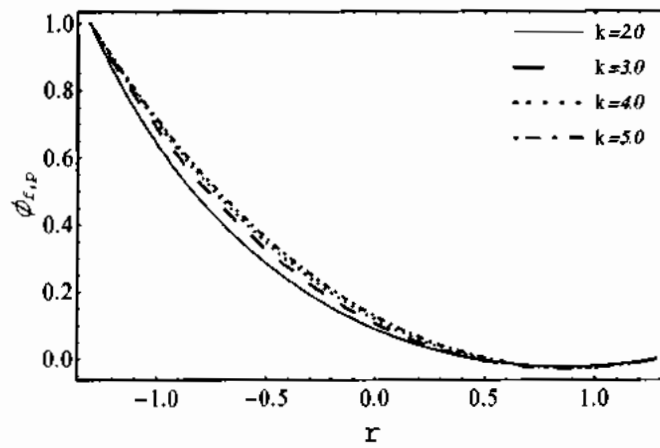


Fig 8.12. Temperature profile for multiple values of k .

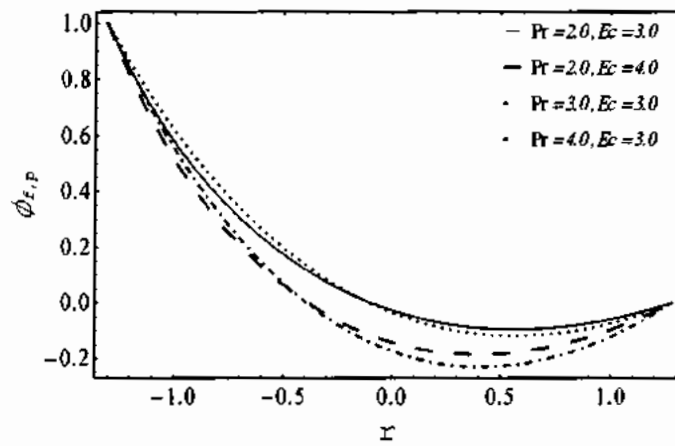


Fig 8.13. Concentration profile for multiple values of Pr and Ec .

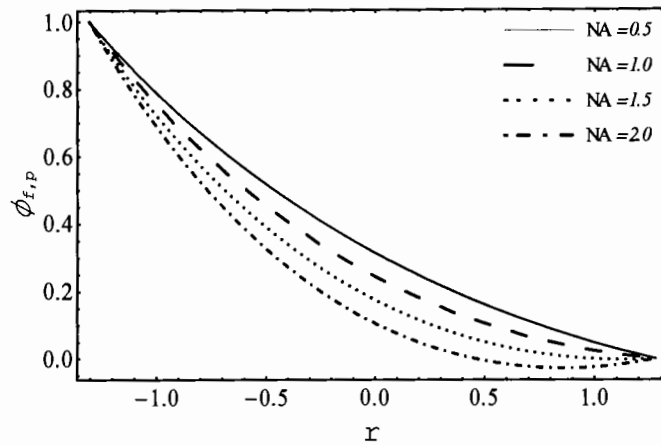


Fig 8.14. Concentration profile for multiple values of NA .

8.5 Conclusion

The viscous particle-fluid (“two-phase”) model has been used to investigate the simultaneous impact of mass and heat transfer on peristaltic transport through an asymmetric curve channel. The exact solution expressions of velocity, concentration, pressure gradient and temperature are obtained, whereas numerical integration has been carried to explore the pumping features. Graphical illustrations are presented against multiple values of involved sundry parameters. The important findings are described below

- There is a critical value of r around which the velocity distribution acts opposite.
- Pressure gradient enhances due to the increase in volume flow rate and phase difference.
- Pressure gradient tends to diminish significantly for large values of C .
- Pressure change in peristaltic pumping and retrograde pumping region decreases for higher values of C and opposite for suspension parameter M_1 .
- Prandtl number, particle volume fraction, and the Eckert number have an increasing impact on temperature profile.

- Curvature parameter fails to provide a significant resistance temperature distribution, while its attitude is converse for concentration profile.
- Concentration profile acts in similar form against C and NA (product of $SrSc$).

Chapter 9

Flow of bubbly fluid in water with magnetic field

This chapter established the theoretical and analytical analysis of a unidirectional laminar bubbly two-phase flow in a symmetric channel with flexible wall. The two-phase model uses water as base fluid with hydrogen bubble suspended in it. Rayleigh-Plesset equation in term of volume fraction is used to model void produce due to presence of hydrogen. The flow is driven by symmetric peristaltic movement of the wall. A uniform magnetic field in the transverse direction of peristaltic motion is applied. Homotopy perturbation Method is utilized to formulate the series solution, after simplifying the differential governing equations under the influence of low Reynolds number and long wave length. The volume of the void and radius of the bubble is analyzed graphically.

9.1 Geometry of the problem

The geometry of the problem is displayed in figure (9.1). The mathematical formulation of the traveling sinusoidal wave is given as

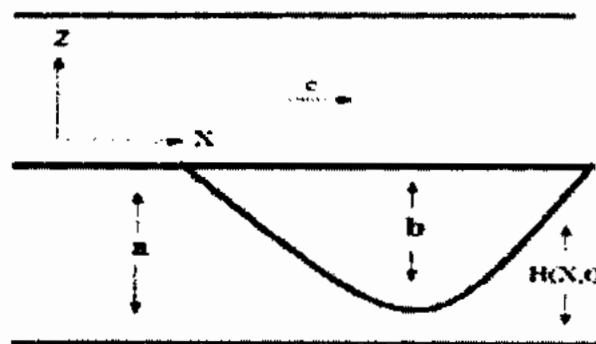


Fig 9.1. Geometry of the problem

$$Z = H(X, t) = \begin{cases} a(1 - \eta_1(X, t)), & \text{if } t < X < t + 1, \\ a(1 - \phi), & \text{otherwise} \end{cases} \quad (9.1)$$

Where $\eta_1(x, t) = \phi \sin\left(\frac{2\pi}{\lambda}(X - ct)\right)$, $\phi = \frac{b}{a}$ (amplitude ratio) and $0 \leq \phi \leq 1$.

9.2 Mathematical formulation

In the present model, we take U and W as velocity components of the fluid ρ_L and ρ_{G_0} is the density of the liquid and gas. Bubble population per unit liquid volume is η_1 and R is the upstream bubble radius. Volume of the void is represented by ν , where S^* is the surface tension. The equation of continuity and momentum transfer for fluid phase and Rayleigh-Plesset equation in term of bubble radius, with assumption that velocity follow inverse square law with respect to radius of bubble [62].

$$\frac{\partial U}{\partial X} + \frac{\partial W}{\partial Z} = \frac{\eta}{(1 - \eta\nu)} \left(\frac{\partial \nu}{\partial t} + U \frac{\partial \nu}{\partial X} + W \frac{\partial \nu}{\partial Z} \right), \quad (9.2)$$

$$\rho_L \left(\frac{\partial U}{\partial t} + U \frac{\partial U}{\partial X} + W \frac{\partial U}{\partial Z} \right) = -(1 - \eta\nu) \frac{\partial P}{\partial X} + \mu_s \left(\frac{\partial^2 U}{\partial X^2} + \frac{\partial^2 W}{\partial Z^2} \right) + \frac{\eta}{3(1 - \eta\nu)} \left(\frac{\partial \nu}{\partial t} + U \frac{\partial \nu}{\partial X} + W \frac{\partial \nu}{\partial Z} \right) - \sigma B_0^2 U, \quad (9.3)$$

$$\rho_L \left(\frac{\partial W}{\partial t} + U \frac{\partial W}{\partial X} + W \frac{\partial W}{\partial Z} \right) = -(1 - \eta\nu) \frac{\partial P}{\partial Z} + \mu_s \left(\frac{\partial^2 U}{\partial X^2} + \frac{\partial^2 W}{\partial Z^2} \right) + \frac{\eta}{3(1 - \eta\nu)} \left(\frac{\partial \nu}{\partial t} + U \frac{\partial \nu}{\partial X} + W \frac{\partial \nu}{\partial Z} \right), \quad (9.4)$$

$$\begin{aligned} R \left(\frac{\partial^2 R}{\partial t^2} + U \frac{\partial^2 R}{\partial X \partial t} + \frac{\partial U \partial R}{\partial t \partial X} + \frac{\partial W \partial R}{\partial t \partial Z} + W \frac{\partial^2 R}{\partial t \partial Z} + U \frac{\partial^2 R}{\partial t \partial X} + U \frac{\partial^2 R}{\partial X^2} + U \frac{\partial U \partial R}{\partial X \partial X} + U W \frac{\partial^2 R}{\partial Z \partial X} \right. \\ \left. + U \frac{\partial W \partial R}{\partial Z \partial X} + W U \frac{\partial^2 R}{\partial Z \partial X} + W \frac{\partial^2 R}{\partial t \partial Z} + W \frac{\partial U \partial R}{\partial Z \partial X} + W^2 \frac{\partial^2 R}{\partial Z^2} + W \frac{\partial W \partial R}{\partial Z \partial Z} \right) + \\ \frac{3}{2} \left(\frac{\partial R}{\partial t} + U \frac{\partial R}{\partial X} + W \frac{\partial R}{\partial Z} \right)^2 = \frac{P_v - P}{\rho_L} + \frac{\rho_{G_0}}{\rho_L} \left(\frac{R_0}{R} \right)^{3k} - \frac{2S^*}{\rho_L R} - \frac{4\nu_L}{R} \left(\frac{\partial R}{\partial t} + U \frac{\partial R}{\partial X} + W \frac{\partial R}{\partial Z} \right). \end{aligned} \quad (9.5)$$

Equation (9.2) is represented continuity equation and momentum equations are represented by Eq. (9.3) and Eq. (9.4). Variation radius bubble is represented in Eq. (9.5).

The equations are transform in wave frame using Eq. (2.9) and Eq. (3.8).

$$W_0 = \frac{R_e}{W_e}, \tau' = \frac{\tau}{R_e}. \quad (9.6)$$

Where Weber number W_0 and cavitation number τ' .

Using non-dimensional parameters defined in Eq. (2.10), (3.9), (4.10), (6.12), (9.6) and employing $\delta \rightarrow 0$ and $Re \rightarrow 0$ the (9.2) – (9.5) becomes

$$\frac{\partial p}{\partial x} = \frac{1}{3(1-\eta\nu)} \frac{\partial^2 w_f}{\partial z^2} + \frac{\eta}{3(1-\eta\nu)^2} w_f \frac{\partial \nu}{\partial z} - M^2 w_f, \quad (9.7)$$

$$\frac{\partial p}{\partial z} = 0, \quad (9.8)$$

$$4 \frac{w_f}{r} \frac{\partial r}{\partial z} + \frac{2}{W_0 r} + \frac{\tau'}{2r^{3k}} = 0, \quad (9.9)$$

$$\frac{\partial \nu}{\partial z} + \frac{6 \cdot (36\pi)^{1/3}}{W_0} \nu^{1/3} + \frac{3}{2} \tau' \left(\frac{4\pi}{3} \right)^{k'} \nu^{1-k'} = 0, \quad (9.10)$$

Flow equation of flexible wall is represented as

$$\tilde{L}(\eta) = p - p_0 \quad (9.11)$$

\tilde{L} is an operator for stretched membrane which is taken as

$$\tilde{L} = \tilde{K} \frac{\partial}{\partial x} + \tilde{m} \frac{\partial^2}{\partial t^2} + \tilde{D} \frac{\partial}{\partial t} + \tilde{B} \frac{\partial^4}{\partial x^4} - \tilde{T} \frac{\partial^2}{\partial x^2}, \quad (9.12)$$

In the view of above equation, \tilde{K} , \tilde{m} , \tilde{D} , \tilde{B} and \tilde{T} are the spring stiffness, mass per unit area, the flexural rigidity of the plate, the coefficient of the viscous damping membrane and the elastic tension is the membrane. The pressure from outside the wall owing to tension in muscle is p_0 , which is taken as zero here. The relation is used in stress with x-momentum equation of liquid matrix.

Along with non-dimensional boundary conditions

$$w(h) = -1, \quad w'(0) = 0, \quad r(0) = 0, \quad \nu(0) = 0. \quad (9.13)$$

Equation (9.10) represents equation for volume of void fraction in term of bubble radius can

be defined as $\nu = \frac{4}{3} \pi r^3$, If bubble is assumed to be spherical.

9.3 Solution of the problem

Solution of the velocity and volume fraction of the bubble is

$$\begin{aligned}
 w_f = & \frac{1}{80W_0^2} 9^{-1-k} (-6402^{1/3} 3^{\frac{19}{3}+2k} \frac{\partial^2 p}{\partial x^2} \pi^{2/3} (h^4 - y^4) \eta^3 + 202^{2/3} 3^{\frac{8}{3}+k} W_0 \eta (43^k h^3 \frac{\partial p}{\partial x} \pi^{1/3} - \\
 & 23^{1+k} h^2 \pi^{1/3} (-2 + \frac{\partial p}{\partial x} y^2) + h^4 \frac{\partial p}{\partial x} (53^k \pi^{1/3} - 272^{3+2k} \frac{\partial p}{\partial x} \pi^{\frac{1}{3}+k} \eta^2 \tau') + y^2 (3^k \pi^{1/3} (-12 + \\
 & \frac{\partial p}{\partial x} (-4 + y)y) + 272^{3+2k} \frac{\partial^2 p}{\partial x^2} \pi^{\frac{1}{3}+k} y^2 \eta^2 \tau')) + W_0^2 (-619^k h^6 M^4 \frac{\partial p}{\partial x} + 9^k M^4 y^4 (-30 + \frac{\partial p}{\partial x} y^2) + \\
 & 103^{1+2k} M^2 y^2 (18 \frac{\partial^2 p}{\partial x^2} y^2 \eta^3 - 12(1 + \eta) + \frac{\partial p}{\partial x} y^2 (3 + 2\eta)) + 53^{2+k} 4^{1+k} h^3 \frac{\partial p}{\partial x} \pi^k \eta \tau' + \\
 & 15h^4 (59^k M^4 (-2 + \frac{\partial p}{\partial x} y^2) + 109^k M^2 \frac{\partial p}{\partial x} (3 + 2\eta + 18 \frac{\partial p}{\partial x} \eta^3) + 3 \frac{\partial p}{\partial x} \eta \tau' (5(12\pi)^k - \\
 & 274^{1+2k} \frac{\partial p}{\partial x} \pi^{2k} \eta^2 \tau')) + 45(-43^k (43^k + 3(4\pi)^k y^2 \eta \tau') + \frac{\partial p}{\partial x} y^2 (83^{1+2k} + 83^{1+2k} \eta + \\
 & 89^k \eta^2 - 4^{1+k} (3\pi)^k y \eta \tau' + (12\pi)^k y^2 \eta \tau') + 36 \frac{\partial^2 p}{\partial x^2} y^2 \eta^3 (49^k + 49^k \eta + 3(4\pi)^{2k} y^2 \tau'^2)) - \\
 & 53^{1+k} h^2 (3^k M^4 y^2 (-12 + \frac{\partial p}{\partial x} y^2) + 43^{1+k} M^2 (18 \frac{\partial^2 p}{\partial x^2} y^2 \eta^3 - 2(1 + \eta) + \frac{\partial p}{\partial x} y^2 (3 + 2\eta)) + \\
 & 6(83^{2+k} \frac{\partial^2 p}{\partial x^2} \eta^3 (1 + \eta) - 32^{1+2k} \pi^k \eta \tau' + \frac{\partial p}{\partial x} (43^{1+k} + 43^k \eta^2 + 3\eta(43^k + (4\pi)^k y^2 \tau'))))
 \end{aligned} \tag{9.14}$$

$$\begin{aligned}
 v = & 1 - \frac{12 \times 6^{2/3} \pi^{1/3} z}{W_0} - \frac{12 \times 6^{2/3} \pi^{1/3} z}{(-2+k)W_0} + \frac{6 \times 6^{2/3} k \pi^{1/3} z}{(-2+k)W_0} - 2^{2k} 3^{1-k} \pi^k z \tau' - \frac{2^{2k} 3^{1-k} \pi^k z \tau'}{-2+k} + \\
 & \frac{2^{-1+2k} 3^{1-k} k \pi^k z \tau'}{-2+k} + \frac{108(3\pi)^{1/3} z (-\frac{z(4 \times 6^{2/3} \pi^{1/3} + (\frac{4\pi}{3})^k W_0 \tau')}{W_0})^{2/3}}{5(-2+k)W_0} - \\
 & \frac{54k^*(3\pi)^{1/3} z (-\frac{z(4 \times 6^{2/3} \pi^{1/3} + (\frac{4\pi}{3})^k W_0 \tau')}{W_0})^{2/3}}{5(-2+k)W_0} - \frac{\frac{2}{23} + 3k^* \frac{8}{33} - 2k^* k^* z^2 \tau' (-\frac{z(4 \times 6^{2/3} \pi^{1/3} + (\frac{4\pi}{3})^k W_0 \tau')}{W_0})^{-k^*}}{(-2+k)W_0} - \\
 & \frac{2^{-2+5k^*} 3^{2-3k^*} k^* z^2 \tau'^2 (-\frac{z(4 \times 6^{2/3} \pi^{1/3} + (\frac{4\pi}{3})^k W_0 \tau')}{W_0})^{-k^*}}{-2+k^*}
 \end{aligned} \tag{9.15}$$

9.4 Illustrations and discussion

To examine the impacts of several parameters Hartmann number M , Weber number W_0 , Cavitation number τ' , behaviour index k^* Bubble population per unit liquid volume η , is plotted for Bubble radius R , Volume of the void v and velocity of fluid w from Fig. (9.2) - (9.12).

The impact of transvers magnetic field parameter M on the fluid velocity, which is decreasing due to Lorenz opposing forces as shown in Fig. (9.2). Notice that if we rising the value of Weber number the behaviour of flow is increasing for the fixed values of the other parameters presented in Fig. (9.3). The effect of cavitation number shows different behavior. Fig. (9.4) illustrate that when increase the value of σ then it is noticed that the flow is reducing. The flow behavior index k^* as indicates in Fig (9.5) and (9.6). If we take the value of index $k^* > 1$ in Fig. (9.4) and $k^* < 1$ in Fig (9.5) the flow behaviour decreased.

The void fraction distribution behavior in the flow. The flow evaporates due to the quasi-statically unstable, mean the void fraction bubbles rapidly approaches to unity. Fig. (9.7) indicates that the increase in value of W_0 give the result to decrease the void fraction. With rising the values of cavitation number and index k^* the flow for the void fraction is also increase in Fig. (9.8) and (9.9). Radius of the bubble is investigated in Fig. (9.10) for the different vales of Weber number. It is observed that the flow behavior is reduced when we increase the values of W_0 . Instead of this if we examine the flow behavior for the radius of the bubble with different parameters such as cavitation number and index k^* the graph is increasing as shown in Fig. (9.11) and (9.12)

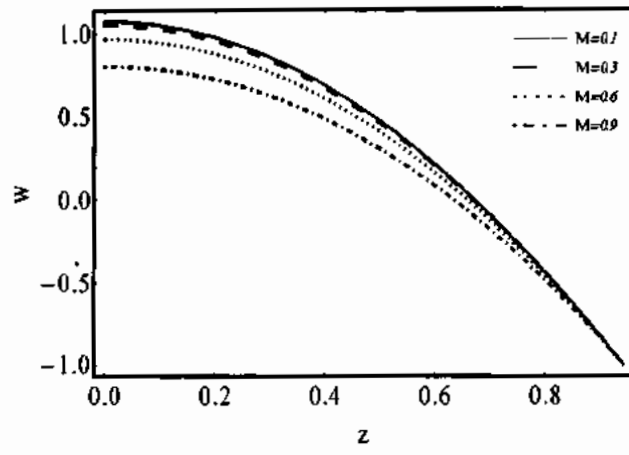


Fig 9.2. Velocity curves for several values of M

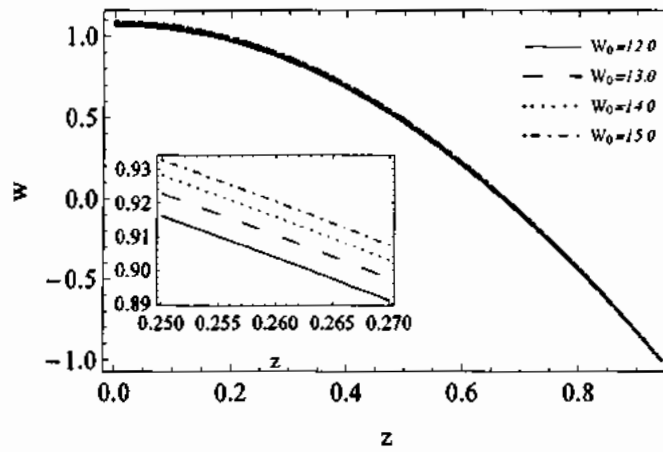


Fig 9.3. Velocity curves for several values of W_0 .

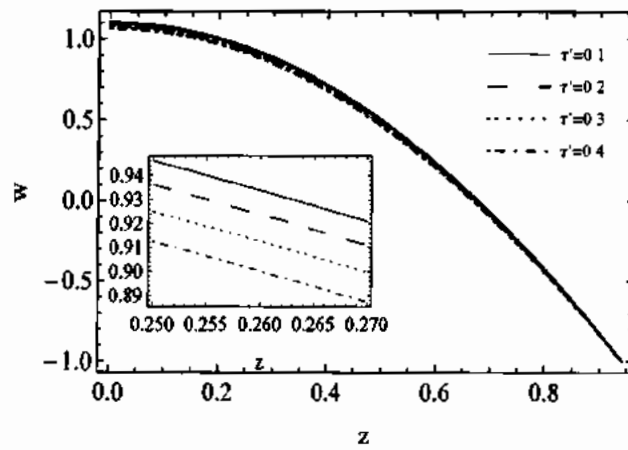


Fig 9.4. Velocity curves for several values of τ' .

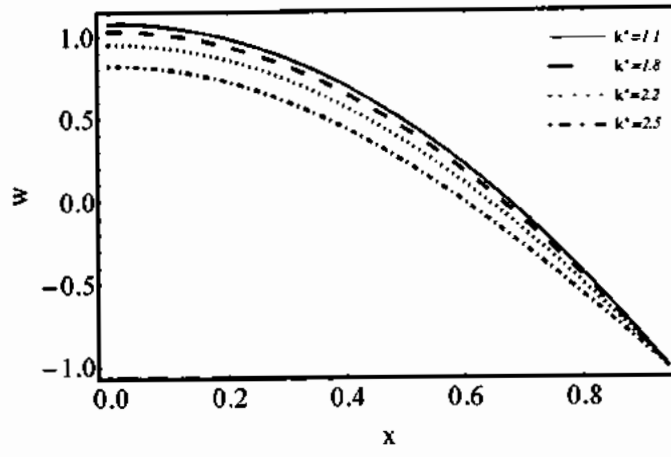


Fig 9.5. Velocity curves for several values of $k^* > 1$.

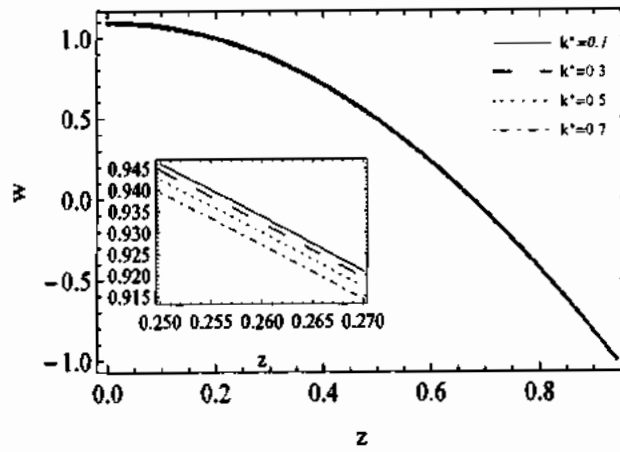


Fig 9.6. Velocity curves for several values of $k^* < 1$.

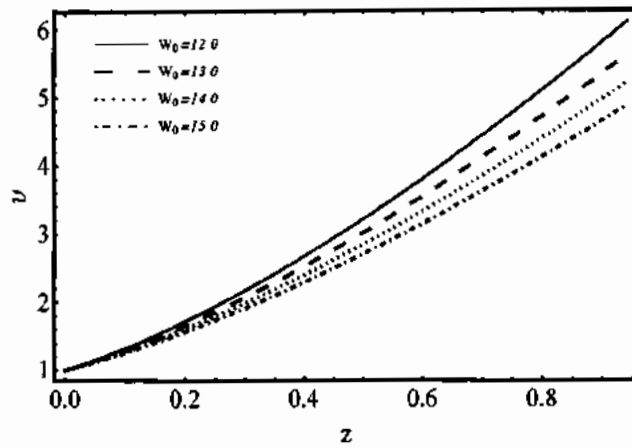


Fig 9.7. Volume of void curves for several values of W_0 .

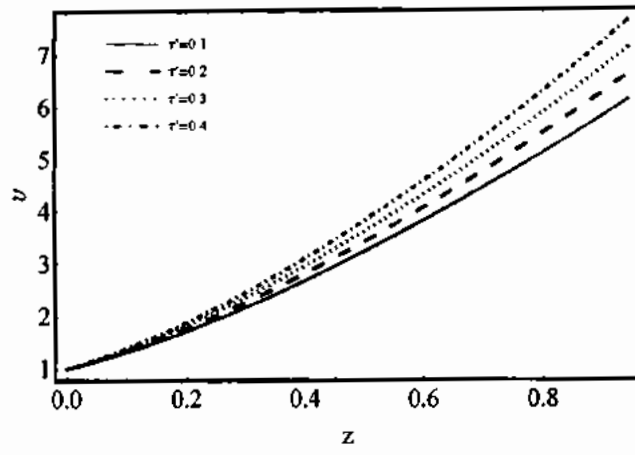


Fig 9.8. Volume of void curves for several values of τ' .

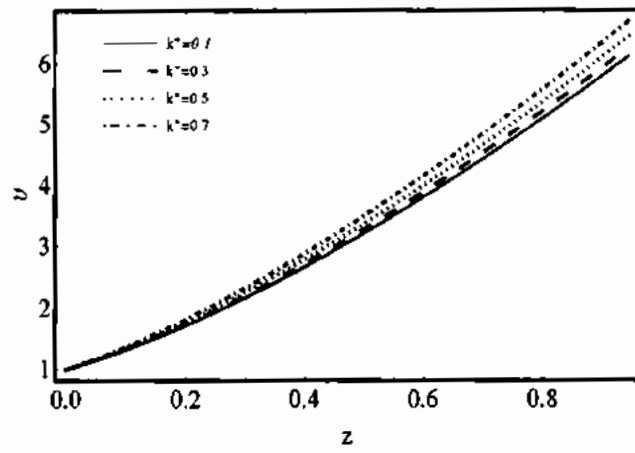


Fig 9.9. Volume of void curves for several values of k^* .

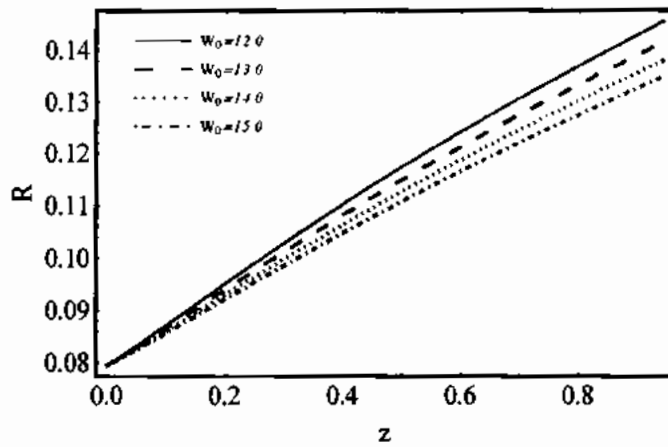


Fig 9.10. Radius of the bubble curves for several values of W_0 .

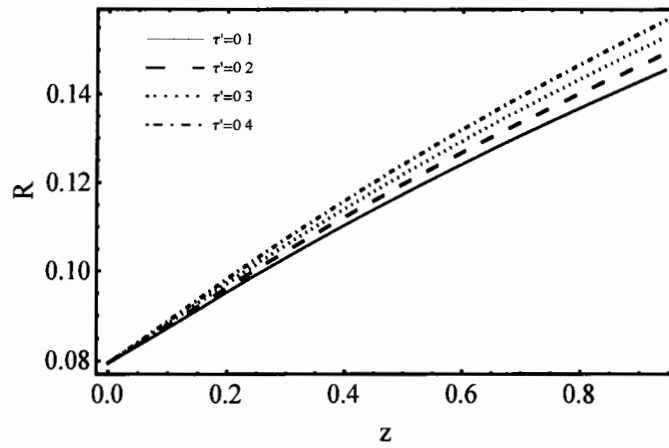


Fig 9.11. Radius of the bubble curves for several values of τ' .

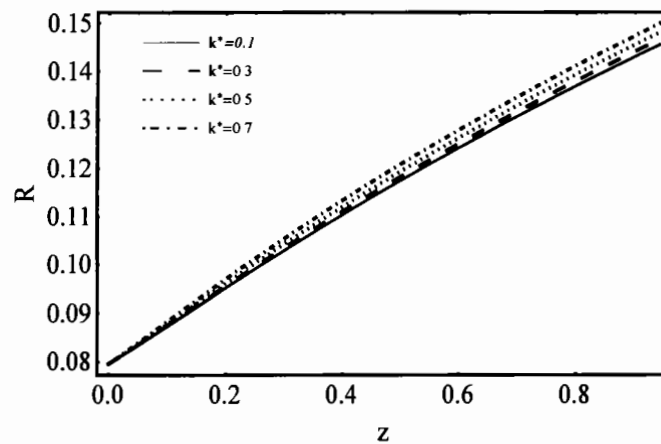


Fig 9.12. Radius of the bubble curves for several values of k^* .

9.5 Concluding remarks

In this chapter, we analyzed the formulation of the bubbly flow model with peristaltic motion only. Excluded real flow of other non-equilibrium factors such as thermal dependence between the density distribution and phases. The present study is the result obtained for the flow behavior for the radius of the bubble and void fraction with different parameters. It is observed that

- A decrease in fluid velocity is observed when increasing value of Hartmann number, Weber number, Cavitation number and behavior index.

- Void fraction tends to reduce with increasing value of Weber number, but increase with Cavitation number and behavior index.
- The flow evaporates due to the quasi-statically unstable, mean the void fraction bubbles rapidly approaches to unity.

References

1. K.S. Mekheimer, Peristaltic flow of blood under effect of a magnetic field in a non-uniform channels, *Appl. Math. Comput.* 153 (3) (2004) 763–777.
2. M.H. Haroun, Non-linear peristaltic flow of a fourth grade fluid in an inclined asymmetric channel, *Comput. Mater. Sci.* 39 (2) (2007) 324–333.
3. T. Hayat, M. Khan, A.M. Siddiqui, S. Asghar, Non-linear peristaltic flow of a non-Newtonian fluid under effect of a magnetic field in a planar channel, *Commun. Nonlinear Sci. Numer. Simul.* 12 (6) (2007) 910–919.
4. N.S. Akbar, S. Nadeem, Z.H. Khan, Numerical simulation of peristaltic flow of a Carreau nanofluid in an asymmetric channel, *Alex. Eng. J.* 53 (1) (2014) 191–197.
5. A. Afsar Khan, R. Ellahi, K. Vafai, Peristaltic transport of a Jeffrey fluid with variable viscosity through a porous medium in an asymmetric channel, *Adv. Math. Phys.* (2012).
6. E.N. Maraj, N.S. Akbar, S. Nadeem, Mathematical study for peristaltic flow of Williamson fluid in a curved channel, *Int. J. Biomath.* 8 (01) (2015) 1550005.
7. H. Enwald, E. Peirano, A.E. Almstedt, Eulerian two-phase flow theory applied to fluidization, *Int. J. Multiphase Flow* 22 (1996) 21–66.
8. K.S. Mekheimer, M.E. Kot, Suspension model for blood flow through arterial catheterization, *Chem. Eng. Commun.* 197 (9) (2010) 1195–1214.
9. P. Matousek, M.D. Morris, *Biological and Medical Physics*, Biomed. Eng, Springer, (2010).
10. J.K. Beddow, *Particle Characterization in Technology: Applications and Microanalysis*, vol. 1, Crc, 1984.

11. J. Yao, K. Tao, Z. Huang, Flow of particulate-fluid suspension in a channel with porous walls, *Transp. Porous Media* 98 (1) (2013) 147–172.
12. K.S. Mekheimer, Y. Abd Elmaboud, Peristaltic transport of a particle–fluid suspension through a uniform and non-uniform annulus, *Appl. Bionics Biomech.* 5 (2) (2008) 47–57.
13. M.H. Kamel, I.M. Eldesoky, B.M. Maher, R.M. Abumandour, Slip effects on peristaltic transport of a particle-fluid suspension in a planar channel, *Appl. Bionics Biomech.* (2015).
14. M.M. Bhatti, A. Zeeshan, Analytic study of heat transfer with variable viscosity on solid particle motion in dusty Jeffery fluid, *Mod. Phys. Lett. B* 1650196 (2016).
15. M.M. Bhatti, A. Zeeshan, M.M. Rashidi, Influence of magnetohydrodynamics on metachronal wave of particle-fluid suspension due to cilia motion, *Eng. Sci. Technol.* (2016)<http://dx.doi.org/10.1016/j.jestch.2016.03.001>.
16. Javed, Maryyam, T. Hayat, M. Mustafa, and B. Ahmad. "Velocity and thermal slip effects on peristaltic motion of Walters-B fluid." *International Journal of Heat and Mass Transfer* 96 (2016): 210-217.
17. M. M. Bhatti, R. Ellahi, A. Zeeshan, Study of variable magnetic field on the peristaltic flow of Jeffrey fluid in a non-uniform rectangular duct having compliant walls, *J. Mol. Liq.* 222 (2016) 101-108.
18. R. Ellahi, M. M. Bhatti, C. Fetecau, K. Vafai, Peristaltic flow of couple stress fluid in a non-uniform rectangular duct having compliant walls, *Commun. Theor. Phys.* 65 (2016) 66-72.
19. R. Ellahi, A. Riaz, S. Nadeem, M. Ali, Peristaltic flow of Carreau fluid in a rectangular duct through a porous medium, *Math. Prob. Eng.* 2012 (2012).

20. M. Kothandapani, J. Prakash, S. Srinivas, Peristaltic transport of a MHD Carreau fluid in a tapered asymmetric channel with permeable walls, *Int. J. Biomath.* 8 (2015) 1550054.
21. M. M. Bhatti, A. Zeeshan, R. Ellahi. Endoscope analysis on peristaltic blood flow of Sisko fluid with Titanium magneto-nanoparticles, *Comp. Bio. Med.* 78 (2016) 29-41.
22. Kh S. Mekheimer, T. Hayat, Al-Arabi, Nonlinear peristaltic transport of MHD flow through a porous medium, *Internat. J. Math. Math. Sci.* 26 (2003) 1663-1682.
23. A. Medhavi, U. K. Singh, A two-layered suspension flow induced by peristaltic waves, *International Journal of Fluid Mechanics Research.* 35 (2008) 258-272.
24. S. Nadeem, S. Akram, Peristaltic flow of a Jeffrey fluid in a rectangular duct, *Nonlinear Anal Real World Appl.* 11 (2010) 4238-4247.
25. Bhatti, M. M., R. Ellahi, and A. Zeeshan. "Study of variable magnetic field on the peristaltic flow of Jeffrey fluid in a non-uniform rectangular duct having compliant walls." *Journal of Molecular Liquids* 222 (2016): 101-108.
26. Bhatti, Muhammad Mubashir, A. Zeeshan, and R. Ellahi. "Heat transfer analysis on peristaltically induced motion of particle-fluid suspension with variable viscosity: clot blood model." *Computer methods and programs in biomedicine* 137 (2016): 115-124.
27. Bhatti, Muhammad Mubashir, A. Zeeshan, and R. Ellahi. "Endoscope analysis on peristaltic blood flow of Sisko fluid with Titanium magneto-nanoparticles." *Computers in biology and medicine* 78 (2016): 29-41.
28. Mekheimer, Kh S. "Peristaltic flow of blood under effect of a magnetic field in a non-uniform channels." *Applied Mathematics and Computation* 153, no. 3 (2004): 763-777.

29. Bhatti, M. M., A. Zeeshan, and R. Ellahi. "Simultaneous effects of coagulation and variable magnetic field on peristaltically induced motion of Jeffrey nanofluid containing gyrotactic microorganism." *Microvascular research* 110 (2017): 32-42.
30. Bhatti, Muhammad Mubashir, and Ahmed Zeeshan. "Study of variable magnetic field and endoscope on peristaltic blood flow of particle-fluid suspension through an annulus." *Biomedical Engineering Letters* 6, no. 4 (2016): 242-249.
31. S.Z.A. Zaidi, S.T. Mohyud-Din, Convective heat transfer and MHD effects on two dimensional wall jet flow of a nanofluid with passive control model, *Aerosp. Sci. Technol.* 49 (2016) 225–230.
32. U. Khan, N. Ahmed, S.T. Mohyud-Din, Thermo-diffusion and diffusion-thermo effects on flow of second grade fluid between two inclined plane walls, *J. Mol. Liq.* 227 (2016) 1074–1082.
33. M.M. Bhatti, A. Zeeshan, N. Ijaz, O.A. Bég, A. Kadir, Mathematical modelling of nonlinear thermal radiation effects on EMHD peristaltic pumping of viscoelastic dusty fluid through a porous medium duct, *Eng. Sci. Technol.* (2016) <http://dx.doi.org/10.1016/j.jestch.2016.11.003>.
34. Y. Jian, L. Chang, Electromagnetohydrodynamic (EMHD) micropumps under a spatially non-uniform magnetic field, *AIP Adv.* 5 (5) (2015) 057121.
35. M.M. Bhatti, S.R. Mishra, T. Abbas, M.M. Rashidi, A mathematical model of MHD nanofluid flow having gyrotactic microorganisms with thermal radiation and chemical reaction effects, *Neural Comput. & Applic.* (2016) 1–13, <http://dx.doi.org/10.1007/s00521-016-2768-8>.
36. M.M. Bhatti, T. Abbas, M.M. Rashidi, Effects of thermal radiation and electromagnetohydrodynamic on viscous nanofluid through a rigid plate, *Multidiscip. Model. Mater. Struct.* 12 (4) (2016) 605–618.

37. M.M. Bhatti, A. Zeeshan, R. Ellahi, Simultaneous effects of coagulation and variable magnetic field on peristaltically induced motion of Jeffrey nanofluid containing gyrotactic microorganism, *Microvasc. Res.* 110 (2017) 32–42.
38. M.M. Bhatti, M.A. Abbas, Simultaneous effects of slip and MHD on peristaltic blood flow of Jeffrey fluid model through a porous medium, *Alex. Eng. J.* 55 (2) (2016) 1017–1023.
39. M.M. Bhatti, A. Zeeshan, R. Ellahi, Heat transfer analysis on peristaltically induced motion of particle-fluid suspension with variable viscosity: clot blood model, *Comput. Methods Prog. Biomed.* 137 (2016) 115–124.
40. J.G. Smits, Piezoelectric micropump with three valves working peristaltically, *Sens. Actuators A* 21 (1) (1990) 203–206.
41. Fetecau, Corina, M. Athar, and Constantin Fetecau. "Unsteady flow of a generalized Maxwell fluid with fractional derivative due to a constantly accelerating plate." *Computers & Mathematics with Applications* 57, no. 4 (2009): 596-603.
42. Fetecau, Constantin, Corina Fetecau, M. Kamran, and D. Vieru. "Exact solutions for the flow of a generalized Oldroyd-B fluid induced by a constantly accelerating plate between two side walls perpendicular to the plate." *Journal of Non-Newtonian Fluid Mechanics* 156, no. 3 (2009): 189-201.
43. Fetecau, Constantin, Corina Fetecau, M. Kamran, and D. Vieru. "Exact solutions for the flow of a generalized Oldroyd-B fluid induced by a constantly accelerating plate between two side walls perpendicular to the plate." *Journal of Non-Newtonian Fluid Mechanics* 156, no. 3 (2009): 189-201.
44. Khalique, C. Masood, and Anjan Biswas. "A Lie symmetry approach to nonlinear Schrödinger's equation with non-Kerr law nonlinearity." *Communications in Nonlinear Science and Numerical Simulation* 14, no. 12 (2009): 4033-4040.

45. Khalique, Chaudry Masood, and K. R. Adem. "Exact solutions of the (2+ 1)-dimensional Zakharov–Kuznetsov modified equal width equation using Lie group analysis." *Mathematical and Computer Modelling* 54, no. 1 (2011): 184-189.
46. Khalique, C. M., and P. Ntsime. "Exact solutions of the Lane–Emden-type equation." *New Astronomy* 13, no. 7 (2008): 476-480.
47. Ünal, Gazanfer. "Symmetries of Itô and Stratonovich dynamical systems and their conserved quantities." *Nonlinear Dynamics* 32, no. 4 (2003): 417-426.
48. Ünal, Gazanfer, and Jian-Qiao Sun. "Symmetries and conserved quantities of stochastic dynamical control systems." *Nonlinear Dynamics* 36, no. 1 (2004): 107-122.
49. Nazar, Roslinda, Norsarahaida Amin, Diana Filip, and Ioan Pop. "Stagnation point flow of a micropolar fluid towards a stretching sheet." *International Journal of Non-Linear Mechanics* 39, no. 7 (2004): 1227-1235.
50. Nazar, Roslinda, Norsarahaida Amin, Diana Filip, and Ioan Pop. "Unsteady boundary layer flow in the region of the stagnation point on a stretching sheet." *International Journal of Engineering Science* 42, no. 11 (2004): 1241-1253.
51. Nazar, Roslinda, Norsarahaida Amin, and Ioan Pop. "Unsteady boundary layer flow due to a stretching surface in a rotating fluid." *Mechanics Research Communications* 31, no. 1 (2004): 121-128.
52. Ishak, Anuar, Roslinda Nazar, and Ioan Pop. "Boundary layer flow and heat transfer over an unsteady stretching vertical surface." *Meccanica* 44, no. 4 (2009): 369-375.

53. Ishak, Anuar, Roslinda Nazar, and Ioan Pop. "Heat transfer over a stretching surface with variable heat flux in micropolar fluids." *Physics Letters A* 372, no. 5 (2008): 559-561.
54. Ishak, Anuar, Roslinda Nazar, and Ioan Pop. "Heat transfer over a stretching surface with variable heat flux in micropolar fluids." *Physics Letters A* 372, no. 5 (2008): 559-561.
55. Turkyilmazoglu, M., and N. Uygun. "Direct spatial resonance in the compressible boundary layer on a rotating-disk." *Theoretical and Computational Fluid Dynamics* 20, no. 3 (2006): 145-162.
56. Türkyilmazoğlu, Mustafa. "Exact Solutions for the Incompressible Viscous Fluid of a Rotating Disk Flow." *Progress in Applied Mathematics* 1, no. 1 (2011): 90-97.
57. Vieru, D., Corina Fetecau, and Constantin Fetecau. "Flow of a viscoelastic fluid with the fractional Maxwell model between two side walls perpendicular to a plate." *Applied Mathematics and Computation* 200, no. 1 (2008): 459-464.
58. Nazar, M., Corina Fetecau, D. Vieru, and C. Fetecau. "New exact solutions corresponding to the second problem of Stokes for second grade fluids." *Nonlinear Analysis: Real World Applications* 11, no. 1 (2010): 584-591.
59. Kothandapani, M., and S. Srinivas. "Peristaltic transport of a Jeffrey fluid under the effect of magnetic field in an asymmetric channel." *International Journal of Non-Linear Mechanics* 43, no. 9 (2008): 915-924.
60. L.M. Srivastava, and V.P. Srivastava. "Peristaltic transport of blood: Casson model-II." *Journal of Biomechanics* 17, no. 11 (1984): 821-829.

61. Latham, T.W., 1966. Fluid motions in a peristaltic pump (Doctoral dissertation, Massachusetts Institute of Technology).
62. Brennen, C., 1978. Bubbly flow model for the dynamic characteristics of cavitating pumps. *Journal of Fluid Mechanics*, 89(2), pp.223-240.
63. Ali, N., M. Sajid, T. Javed, and Z. Abbas. "Peristalsis in a rotating fluid." *Scientific Research and Essays* 7, no. 32 (2012): 2891-2897.